

APPLICATION OF RADIAL BASIS FUNCTIONS METHOD TO
ADVECTION-DIFFUSION AND VISCOELASTIC FLOW PROBLEMS

by

Yusuf Tunçay

B.S., in M.E., Dokuz Eylül University, 2005

Submitted to the Institute for Graduate Studies in
Science and Engineering in partial fulfillment of
the requirements for the degree of
Master of Science

Graduate Program in Mechanical Engineering

Boğaziçi University

2009

ACKNOWLEDGEMENTS

I am very grateful to many people who have helped me in the study and preparation of this thesis.

First of all, I believe that I am lucky for the subject which was offered by my supervisor Assoc. Prof. Kunt Atalık. I am thankful to him for his patience and support during preparation of the thesis. His guidance has provided me to complete the study properly. Another person that I am really thankful for his wide knowledge, notes and extra documentations about the subject is Assoc. Prof. Osman Breki. When I was stucked somewhere he has immediately solved my problems. His cheerful attitude has always motivated me to step forward.

In addition to my supervisors, graduate assistants from Civil Engineering department, Yavuz Tokmak and Ufuk Őahin have provided great support at the beginning about the problems and coding.

Finally, I am definitely grateful to my family. They have provided essential encouragement and patience for those years. Their love and support made me complete the study and continue this period of graduate degree. I would like to thank and express my deep gratitude to my best friends Serhat Terece and Necati Soydemir for their valuable friendship. Aykut, Altuĝ, Hakan, mer and Uygur are my party friends, we enjoy a lot on hard times. I have overcome those hard times with their amazing characters, love and friendship. Thank you for all.

ABSTRACT

APPLICATION OF RADIAL BASIS FUNCTIONS METHOD TO ADVECTION-DIFFUSION AND VISCOELASTIC FLOW PROBLEMS

The objective of the thesis is to demonstrate an application of radial basis functions method to linear and nonlinear advection-diffusion and viscoelastic flow problems. As far as the radial basis functions method is considered, multiquadrics and thin-plate splines types of functions are used in the study. Firstly, the study is handling the linear advection-diffusion type of equation in one and two dimensional cases with specific examples in order to compare with the analytical and the numerical solutions existing in the literature. Then, one and two dimensional Burgers' equations and nonlinear advection-diffusion equation are solved to demonstrate the efficiency of the method. In addition to that, two models of viscoelastic flow in one dimension, Upper-Convected Maxwell and Oldroyd-B fluid models for mode one are investigated using radial basis functions collocation method considering start-up flow between parallel plates. Especially, for multiquadric radial basis functions solutions, the shape parameter effect is investigated and shape parameter optimization is carried out with the known exact solutions. It can be claimed from all implementations that this meshless radial basis functions collocation method is very easy to code, flexible with respect to high-dimensional geometries and efficient in comparison with the other methods.

ÖZET

RADYAL BAZLI FONKSİYONLAR METODUNUN ADVEKSİYON-DİFÜZYON VE VİSKOELASTİK AKIŞ PROBLEMLERİNE UYGULAMASI

Tezin amacı radyal bazlı fonksiyonlar ağırsız nümerik çözüm metodunun adveksiyon-difüzyon denklem tipine ve viskoelastik akış problemlerine bir uygulamasını göstermektir. Radyal bazlı fonksiyonlar metodu dikkate alındığında, çalışmada multiquadrics ve spline özellikte fonksiyon tipleri kullanılmıştır. İlk olarak, çalışmada bir ve iki boyutlu doğrusal adveksiyon-difüzyon denklem tipleri çözümü literatürdeki analitik ve başka nümerik çözümlerle karşılaştırılmak üzere ele alınmaktadır. Daha sonra bir ve iki boyutta Burgers denklemleri ve doğrusal olmayan adveksiyon-difüzyon denklemi metodun verimliliğini göstermek için çözülmüştür. Bunlara ilave olarak bir boyutta, viskoelastik akışın iki modeli olan, bir modlu Üst-Taşınımlı Maxwell ve bir modlu Oldroyd-B akışkan modellerinin, iki paralel plaka arasındaki akışı dikkate alınarak radyal bazlı fonksiyonlar metodu ile çözülmüştür. Özellikle, multiquadric radyal bazlı fonksiyon çözümlerinin şekil parametre etkileri incelenmiş ve her bir soru için bilinen kesin ve nümerik çözümler kullanılarak şekil parametresi optimizasyonu yapılmıştır. Tüm uygulamalardan yola çıkılarak, bu ağırsız radyal bazlı nümerik yöntemin kodlaması çok kolay, iki ve üç boyutlu uygulamalar için oldukça esnek ve diğer metotlara göre daha verimli olduğu söylenebilir.

TABLE OF CONTENTS

ABSTRACT.....	iv
ÖZET	v
LIST OF CONTENTS	vi
LIST OF FIGURES	viii
LIST OF TABLES.....	xi
LIST OF SYMBOLS/ABBREVIATIONS.....	xii
1. INTRODUCTION	1
1.1. Some Comments on Numeric: Mesh-Based/Mesh-Free Methods and RBFs.....	1
1.2. Literature Survey	2
1.3. Objective of the thesis.....	13
2. MESHLESS METHODS	14
2.1. From Mesh-Based Methods to Mesh-Free Methods	14
2.2. Categorization of Meshless Methods.....	20
2.3. Numerics for time-marching.....	23
2.3.1. First Order Time Integration.....	23
2.3.1.1. Runge-Kutta Method of Order Four	23
2.3.2. Second Order Time Integration	25
2.3.2.1. Houbolt Method	25
3. RADIAL BASIS FUNCTIONS METHOD	26
3.1. General Information about RBFs	26
3.2. Types of RBFs	30
3.2.1. Some Properties of RBFs	34
3.2.2. The Advantages using Meshless MQs and TPS-RBFs	35
3.2.3. Shape Parameter Effect	36
3.3. RMS Error Calculation	37
3.4. Reducing the Ill-Conditioning	38
3.4.1. Augmented Approximation	41
3.4.2. Adaptive Meshless Method	43
3.4.3. Symmetric Collocation Method	44
3.5. RBFs in the study	45

4. DEFINITION OF THE PROBLEMS	49
4.1. The Advection-Diffusion Equation in 1-D	49
4.2. Time Dependent Burgers' Equation in 1-D	53
4.3. The Nonlinear Advection-Diffusion Problem in 1-D	54
4.4. Viscoelastic Flow Problems	57
5. RESULTS AND DISCUSSION	66
5.1. The Advection-Diffusion Equation in 1-D	66
5.2. Time Dependent Burgers' Equation in 1-D	73
5.3. The Nonlinear Advection-Diffusion Problem in 1-D	80
5.4. Viscoelastic Flow Problems (UCM and Oldroyd-B fluid models).....	83
6. CONCLUSION	88
APPENDIX A: Solution Procedure	92
APPENDIX B: Derivation of the Governing Equations for Viscoelastic Flow Problem ..	99
APPENDIX C: ADDITIONAL PROBLEMS in 2-D	108
REFERENCES	116

LIST OF FIGURES

Figure 2.1. An example of finite element mesh	15
Figure 2.2. A mesh distortion example in FEM	15
Figure 2.3. An example of FDM grid for an irregular shape of geometry	17
Figure 2.4. FEM mesh for contact computation	18
Figure 2.5. Computation model for meshless method	18
Figure 2.6. Solution procedure of FEM and MLM	19
Figure 4.1. Source given at location $x = 0$, $u(x=0,t)=t^\beta$, $\beta = 0$	56
Figure 4.2. Source given at location $x = 0$, $u(x=0,t)=t^\beta$, $\beta = -1/4$	56
Figure 4.3. Source given at location $x = 0$, $u(x=0,t)=t^\beta$, $\beta = 1/10$	57
Figure 4.4. Numerical Solution Procedure of Viscoelastic Fluid Equations	59
Figure 4.5. Domain for the Viscoelastic Problem	63
Figure 5.1. MQ-RBF Solution, $c = 14.6$, $N = 51$, $dt = 0.1$, $t = 40$ s, $rms = 8.4087e-04$..	67
Figure 5.2. RMS vs. "c" vary, $N = 51$, $dt = 0.1$, $t = 40$ s	67
Figure 5.3. MQ-RBF Solution, $c = 0.8$, $N = 201$, $dt = 0.1$, $t = 40$ s, $rms = 3.8667e-04$	68
Figure 5.4. RMS vs. "c" vary, $N = 201$, $dt = 0.1$, $t = 40$ s	68

Figure 5.5. Numerical Solution, MQ-RBF, $c = 7$, $N = 101$, $dt = 0.1$	69
Figure 5.6. TPS-RBF, $m = 4$, $dt = 0.01$, $t = 40$ s, $rms = 6.5059e-05$	70
Figure 5.7. TPS-RBF Solution, RMS vs. N , $m = 4$, $dt = 0.1$, $t = 40$ s	70
Figure 5.8. MQ-RBF, $N = 81$, $dt = 0.0001$, $c = 0.07$, $t = 1.1$ s, $rms = 5.2135e-04$	74
Figure 5.9. RMS vs. "c" vary, $N = 81$, $dt = 0.0001$, $t = 1.1$ s	74
Figure 5.10. MQ-RBF, $N = 201$, $dt = 0.0001$, $t = 1.1$ s, $c = 0.01$, $rms = 2.2391e-04$	75
Figure 5.11. Numerical Solution, $N = 81$, $dt = 0.01$, $c = 0.004$, $rms = 9.3000e-03$	75
Figure 5.12. TPS-RBF, $m = 4$, $N = 51$, $dt = 0.0001$, $t = 1.1$ s, $rms = 8.9000e-03$	76
Figure 5.13. TPS-RBF, $m = 4$, $N = 101$, $dt = 0.0001$, $t = 1.1$ s, $rms = 7.0384e-03$	76
Figure 5.14. TPS-RBF, $m = 4$, $N = 201$, $dt = 0.0001$, $t = 1.1$ s, $rms = 1.8529e-04$	77
Figure 5.15. TPS-RBF, RMS and N vary, $m = 4$, $dt = 0.0001$, $t = 1.1$ s	77
Figure 5.16. MQ-RBF Solution, for $\beta = 0$, $dx = 0.5$, $N = 264$, $dt = 0.04$, $c = 1$	81
Figure 5.17. Time and spatial evolution of u , $\beta = 0$	81
Figure 5.18. MQ-RBF, for $\beta = -1/4$, $dx = 0.5$, $N = 264$, $dt = 0.04$, $c = 1$	82
Figure 5.19. Time and spatial evolution of u , $\beta = -1/4$	82
Figure 5.20. MQ-RBF, for $\beta = 1/10$, $dx = 0.2$, $N = 656$, $dt = 0.005$, $c = 0.2$	83
Figure 5.21. UCM Fluid, MQ-RBF Solution, $N = 101$, $dt = 0.001$, $c = 0.02$, $E = 1$	84

Figure 5.22. UCM Fluid, TPS-RBF (Aug.), $N = 51$, $y = 0.5$, $dt = 0.001$, $m = 4$, $E = 1$	85
Figure 5.23. Time and spatial evolution of u , $N = 101$, $c = 0.02$	85
Figure 5.24. Oldroyd-B Fluid, TPS-RBF, $N = 101$, $dt = 0.001$, $m = 4$, $E = 1$	86
Figure 5.25. Time and spatial evolution of u , $N = 101$, $m = 4$	86
Figure A.1. One Dimensional Domain - Space and Time	96

LIST OF TABLES

Table 3.1. Piecewise Smooth RBFs	31
Table 3.2. Infinitely Smooth RBFs	31
Table 3.3. Wendland's positive definite functions with compact support	32
Table 4.1. Rheology Concept	58
Table 5.1. MQ-RBF Solution of Problem 1, RMS errors	71
Table 5.2. TPS-RBF Solution of Problem 1, RMS errors	72
Table 5.3. MQ-RBF Solution of Problem 2, RMS errors	78
Table 5.4. TPS-RBF Solution of Problem 2, RMS errors	79
Table 6.1. CPU times of the problems	91
Table C.1. MQ-RBF Solution of Problem C.1, RMS errors	110
Table C.2. TPS-RBF Solution of Problem C.1, RMS errors	111
Table C.3. MQ-RBF Solution of Problem C.2, RMS errors	114
Table C.4. TPS-RBF Solution of Problem C.2, RMS errors	115

LIST OF SYMBOLS / ABBREVIATIONS

A	Coefficient Matrix
a	Acceleration
b	Time step
B	Boundary condition operator
c	Shape parameter
d	Spatial Dimension
E	Elasticity Number
f	Body forces per unit volume
f	Known function of a problem
g	Known function of a problem
h	Node density
i, j	Node number
L	Linear differential operator
N	Total number of nodes
p	Hydrostatic pressure
Re	Reynolds Number
t	Time space
\mathbf{T}	Total stress tensor
u	Approximation function
x	Vector position
We	Weissenberg Number
ϕ_{ij}	Radial Basis Function
r_{ij}	Radial distance between nodes
λ_j	Unknown coefficients to be determined
β	Order of the RBF
$\eta(r)$	Decay Function
$p(x)$	Polynomial Function
κ	Diffusion coefficient

v	Advection coefficient or velocity vector
∇	Gradient operator
ρ	Density
$\dot{\gamma}$	Shear rate
θ	Temperature variable
η	Kinematic viscosity function
Δt	Time difference
$\ \cdot\ $	Eucledian Norm
Ω	Domain of a problem
$\partial\Omega$	Boundary of a problem
1-D	One Dimensional
2-D	Two Dimensional
3-D	Three Dimensional
ALE	Arbitrary Lagrangian Eulerian formulation
BEM	Boundary Element Method
BVP	Boundary Value Problem
DDM	Domain Decomposition Method
DEM	Diffuse Element Method
DPD	Dissipative Particle Dynamics
DRM	Dual Reciprocity Method
EFG	Element Free Galerkin
FDM	Finite Difference Method
FEM	Finite Element Method
FPM	Finite Point Method
GBMM	Galerkin Based Meshless Method
MFS	Method of Fundamental Solution
MKM	Modified Kansa Method
MLM	Meshless Methods
MQ	Multiquadrics
NEM	Natural Element Method
PCM	Point Collocation Method

PGM	Petrov-Galerkin Method
PIM	Point Interpolation Method
RBF	Radial Basis Function
RBFCM	Radial Basis Function Collocation Method
RPCM	Radial Point Collocation Method
SPH	Smooth Particle Hyrdodynamics
TPS	Thin-Plate Splines
UCMM	Upper-Convected Maxwell Model

1. INTRODUCTION

1.1. Some Comments on Numerics : Mesh-Based & Mesh-Free Methods and RBFs

Many problems in science and engineering are reduced to a set of differential equations through a process of mathematical modeling. It is not easy to obtain their exact solutions, so numerical methods must be resorted to. There are a lot of techniques available such as the finite difference method and the finite element method. These methods require the definition of a mesh (domain discretization) where the functions are approximated locally. The construction of a mesh in two or more dimensions is a nontrivial problem. Usually, in practice, only low-order approximations are employed resulting in a continuous approximation of the function across the mesh but not its partial derivatives. The discontinuity of the approximation of the derivative can adversely affect the stability of the solution. While higher-order schemes are necessary for more accurate approximation of the spatial derivatives, they usually involve additional computational cost. To increase the accuracy of the low-order schemes, it is required that the computational mesh must be refined with a higher density of elements in the regions near the contours. This, however, is also achieved at the expense of increased computational costs [1]. Even though, significant advances have been made in the area of grid generation over the last few decades, it still remains a complex and time consuming process, particularly for complex three dimensional (3D) geometries. This problem has motivated the development of so-called meshfree or meshless methods that try to circumvent the cumbersome issue of grid generation [2].

In the last decade, there has been great interest in using meshless methods to find the numerical solution of partial differential equations [3]. Various types of meshless methods have been developed in last recent two decades. A brief discussion of these methods will be given in the following chapters.

One of the meshless methods is due to the pioneering effort of Kansa, who solved PDEs by collocation employing radial basis functions. His work was motivated by advances in the field of function approximation. This method is known as the unsymmetric

RBF collocation method where the unknown function is expanded in terms of radial basis functions (RBFs). Many studies have shown that the RBFs method can be numerically more accurate than FDM and FEMs. Additionally, RBFs have an advantage of being easily applicable to high dimensional problems. This method has been successfully applied to a number of areas including tissue engineering problems [4], heat transfer [5], convection-diffusion problems [6], nonlinear problems [7, 8, 9] and free boundary problems [10]. The unsymmetric RBF collocation method generates full, unsymmetric coefficient matrices. A symmetric variant of the unsymmetric RBF method was propounded by Fasshauer [11], wherein the coefficient matrices formed are symmetric and dense [5]. Li [12] have formulated a particular case where the coefficient matrix for the unsymmetric RBF method turns out to be singular. Theoretical proofs for the invertibility of the resultant coefficient matrices exist in the literature for the symmetric collocation method [13]; however, for Kansa's unsymmetric method, the proofs are still elusive. But implementation of symmetric version is much more complex (especially for variable coefficient equation and nonlinear systems) than the unsymmetric version due to the use of adjoint differential operators [14].

In the study, the advection-diffusion and the viscoelastic flow problems have been considered. There are few studies on advection-diffusion type and viscoelastic problems using RBF method in the literature. Then it will be demonstrated that there are lots of advantages in using radial basis function meshless method over traditional methods. Literature survey includes overviews of studies and papers prepared related to the subject. Papers put forward concern with the advection - diffusion and viscoelastic flow that deal with the problems using different methods. This will be explained in the literature survey section.

1.2. Literature Survey

Radial Basis Functions Method has been under intensive research as a technique for multivariate data and function interpolation in the past decades. Since its easy implementation on linear and non-linear partial differential equations for numerical solution and also in multi-dimensional applications, this method has currently become more applicable in various areas in science and engineering. Many papers and publications

demonstrate that the radial basis functions method is of great importance as a powerful tool in numerical approximation. Their crucial structure of having exceptional rates of convergence and infinite differentiability feature also widen their applications in the world of science. The function u is approximated with global radial basis functions as;

$$u_i^b = \phi_{ij} \lambda_j^b \quad (1.1)$$

$$u_i^b(\mathbf{x}, t) = \sum_{j=1}^N \phi(r_{ij}) \lambda_j^b = \sum_{j=1}^N \phi(\|x_i - x_j\|) \lambda_j^b \quad (1.2)$$

where i denotes the node / point on the domain, and b is the time step.

Some commonly used radial basis functions are multiquadrics, thin-plate splines, Gaussians and Wendland's compactly supported functions which are grouped considering specific features in the chapter three. In the Equation 1.2, N refers to number of nodes defined on the domain, $\|\cdot\|$ denotes the common choice of Euclidian norm, therefore our approximation u is a linear combination of translates of a fixed function $x \rightarrow \phi(\|x\|)$ which is “radially symmetric” with respect to the given norm, in the sense that it clearly possesses the symmetries of the unit ball. We shall often say that the points $x_j, j = 1, 2, \dots, N$ are the *centres* of the radial basis function interpolant. Moreover, it is usual to refer to ϕ_{ij} as the radial basis function, if the norm is understood. So, here ϕ_{ij} is the given or arbitrarily chosen radial basis function, r is the distances between the nodes on the domain defined in Equation (1.3). Also λ_j s are the unknown coefficients to be calculated.

$$r_{ij} = \sqrt{(x_i - x_j)^2 + (y_i - y_j)^2 + (z_i - z_j)^2} \quad \text{in 3-D} \quad (1.3)$$

Let's call the elements of $\phi(\|x_i - x_j\|, c_j) = a_{ij}$ which are the elements of matrix A as shown in the following and, “ c ” is defined as shape parameter,

This study includes solution of advection-diffusion type of equation and viscoelastic fluid flow problem using radial basis functions method. Before that, if we review the papers about radial basis functions method applications to different kind of problems, I believe it will provide a wide insight for this meshless method. Then we will consider the papers review with the applications of radial basis functions to advection-diffusion type of equations and, this section will be concluded with a mention of studies related to applications of radial basis function to viscoelastic cases.

For example in the paper [5], Chantasiriwan used multiquadric type of radial basis function to solve the nonlinear time-dependent heat conduction problem having temperature dependent thermal properties and compares it with the solution of Kirchoff transformation. This method is tested using the heat conduction problem for which the exact solution is known. The natural convection problem in porous media has also been tested by Perko in [15]. Results are shown for different number of collocation points and compared with known finite volume method results. Kansa and Hon [16], devised an algorithm using the multiquadric radial basis function to solve the shallow water equations. This study shows that the method is robust and stable; the results are in good agreement with measured data. Also Singh [17] applied this meshless method in two dimensional fluid flow problems. He compared the results with exact solution and finite element method solutions. More promising results have been obtained for exponential functions than multiquadrics and Gaussians in this study.

Obviously, we can see that great contributions have been made in this area apart from scientists above mentioned. Shu *et.al.* [7] indicate that although some excellent results were obtained, all previous works related to application of RBFs for the numerical solution of PDEs are actually based on the function approximation instead of derivative approximation. In other words, these works directly substitute the expression of function approximation by RBFs into a PDE, then change the dependent variables into the coefficients of function approximation. For nonlinear problems, as mentioned in [7] some special techniques such as numerical continuation and bifurcation approach were proposed. These contributions take good effect about easy implementation of this method. In the Fasshauer's paper [11], it is claimed that the Kansa's method has not been validated yet to be well-posed because of some problems such as localization, preconditioning and fine

tuning of the shape parameter “ c ”. In addition, coefficient matrix of approximation function has a tendency to be singular. There an alternate approach is described based on Hermite basis functions which ensures well-posedness for other types of partial differential equation problems such as nonlinear elliptic PDEs, systems of elliptic PDEs, time dependent parabolic or hyperbolic PDEs. With Fasshauer’s Hermite interpolation, Chen [18] developed symmetric scheme to circumvent the ill-conditioning which will be cited in the following chapters. The accuracy and the efficiency of the symmetric matrix solution are numerically validated in 2-D and 3-D also for complicated geometries. Chen [18] in 1982 have actually applied the RBF concept to develop the currently popular Dual Reciprocity Boundary Element Method (DR-BEM) without the notion of “RBF” and they use related advances in multivariate scattered data processing. Only after Kansa’s pioneering work [19] in 1990, has the research on the RBF method for PDEs become very active.

It is very common to utilize different forms of methods including radial basis functions in order to increase the accuracy of approximation. These methods will be handled in the following chapter shortly with their ways of application. For example, Karur and Ramachandran [20] applied augmented thin plate spline type of radial basis function in dual reciprocity method which involves the approximation of the non-homogeneous term by a set of RBF and transferring the resultant domain integral to an equivalent boundary integral. This work claimed that the augmented form of radial basis function approximation method shows superior results to frequently used linear RBF, and the comparison of the DRM implementation with augmented and unaugmented form of approximation is also provided in the paper. Augmented form of approximation, say, combining radial and polynomial basis functions is also called a Point Interpolation Method (PIM) in the literature. It is implemented by Wang and Liu [21] to curve/surface fittings and solid mechanics problems. Involvement of radial basis functions overcomes possible singularity associated with the meshless methods based on only the polynomial basis. This non-singularity is useful in constructing well-performed shape functions. In addition, the partial derivatives of shape functions are easily obtained, thus improving computational efficiency.

Another form of approximation to partial differential equations is to use adaptive radial basis functions method. This is used to choose the location of the collocation points. Sarra [8] takes advantage of the grid free property of the methods and arbitrary defined collocation points. The RBFs method produce results similar to the well known analyzed spectral methods, but while allowing greater flexibility in the choice of grid point locations. It is demonstrated that the adaptive RBF methods are more successful when the basis functions are chosen so that the PDE solution can be approximated well with a small number of the basis functions. In the paper [22], Munoz-Gomez *et. al.* use the local refinement technique just as similar to above-mentioned adaptive algorithm for Kansa's unsymmetric collocation approach. The proposed scheme is based on a cell by cell data structure, which by using the former local error estimator, iteratively refines the node density in regions with insufficient accuracy. They found that the node refinement lets them to reduce the approximation error and that the node insertion is only performed in regions where the analytical solution shows a high spatial variation. Heryudono and Driscoll [23] give some examples to depict the efficiency of adaptive radial basis functions method including Runge function, Poisson equation, time independent and time dependent Burgers' equations and Buckley-Leverett equation. Furthermore, this algorithm has been tried on live-object handling applications by Li [12] in a dissertation proposed in 2007. It has been shown that increasing the node density around the contact area improves the accuracy significantly. Considerable effort has been devoted to developing good adaptive algorithms for contact problems where important variations and fluctuations are being encountered. In addition, Iske and Martin [24] applied adaptive meshfree method to a well-established model problem in petroleum reservoir simulation. The numerical results and subsequent numerical comparisons with two leading commercial reservoir simulators, ECLIPSE and FrontSim, show the good performance of their adaptive meshfree advection scheme.

One of the problems encountered in radial basis function interpolation is ill-conditioning of the coefficient matrix. It occurs when the coefficient matrix is singular or very close to singular. Because singular matrices have no inversion, the unknown weighted coefficients can not be determined. In Kansa's method, also known as the unsymmetric collocation method, it is possible to see singularity if radial or combined polynomial basis functions aren't adjusted as well as they should be. To circumvent this bad condition,

many methods have been developed in the last decade. A symmetric variant of the unsymmetric RBF method was propounded by Wu and Fasshauer [11], wherein the coefficient matrices formed are symmetric and dense. However, in most of the cases the unsymmetric matrix is invertible, in some particular cases the coefficient matrix for the unsymmetric radial basis function collocation method may turn out to be singular [2]. In terms of efficiency and stability, symmetry is widely considered as a merit in the numerical solution of PDE's. For example, memory requirements are reduced by a half. Chen [18] has studied the Boundary Knot Method (BKM) with the purpose of developing a novel BKM scheme, which holds symmetric interpolation matrix merit for mixed boundary problems without loss of any advantages of the original BKM. He tested symmetric BKM on some 2D and 3D Helmholtz and diffusion-reaction problems under complicated geometry. It is expected that compared with other numerical techniques, the BKM may become more efficient for higher dimensional complex shape problems since the general solutions of high-dimensional operators are simpler and the radial basis function is independent of dimensionality and geometric complexity.

As mentioned, the coefficient matrix for Kansa's method is generally ill-conditioned, nonsymmetrical and dense, which constrains its applicability to solve large scale problems. As a remedy, the Domain Decomposition Method (DDM) can provide a way to reduce the computational time and the ill-conditioning of the matrix. Gomez *et.al.* have carried out a study [3], where they have investigated the overlapping domain decomposition method applied to time dependent partial differential equations with unsymmetrical radial basis function collocation method using as an example the linear advection equation. They have investigated how the number affects the computational effort and the accuracy of the numerical solution. They observed a drastic time reduction of the computational effort. In addition, Chinchapatnam *et.al.* [2] present meshless overlapping Schwarz additive and multiplicative domain decomposition schemes for time dependent problems using radial basis functions. The proposed schemes are compared with the global radial basis function collocation method and an explicit multizone domain decomposition method by solving an unsteady convection-diffusion problem for various Peclet numbers. Numerical results show that the ill-conditioning problem of global radial basis functions collocation method is reduced by proposed Schwarz schemes. Also with an increase in the number of

subdomains the efficiency of the Schwarz schemes increases with a slight loss in the accuracy.

This present study aims to handle the approximation of partial differential equations governing advection-diffusion type of problem and viscoelastic fluid flow problem. There exist lots of papers studying the problems from different perspectives.

In Li and Chen's paper [14], the time independent advection-diffusion problem is considered. They investigate the unsymmetric radial basis function collocation method for solving advection-diffusion problem with high Peclet numbers. They found that this method can still solve high Peclet number problems reasonably well by using more nodes and domain decomposition techniques. Apart from this study, in most cases the time dependent advection-diffusion problems are more common in the literature. Boztosun *et. al.* [6] have carried out a numerical solution of advection-diffusion equation based on thin plate spline radial basis function. The efficiency of the method in terms of computational processing time, accuracy and stability is discussed and they obtained excellent results compared to the results of the finite difference method. For different values of κ and ν , the diffusion and advection coefficients respectively, various solutions are obtained to observe the dominance of advection or diffusivity. Another paper of Boztosun and Charafi [25] compares the results with the findings from the dual reciprocity boundary element and finite difference methods as well as with the analytical solution. There, 2-D advection-diffusion problem is also investigated with given exact solution. Zerroukat *et.al.* [26], the linear advection-diffusion problem is developed and validated. Unlike the above-mentioned paper of Charafi, this time the scheme uses well distributed quasi-random points and approximates the solution using global radial basis functions. This allows the computation of problems with complex-shaped boundaries in higher dimensions with no need for complex mesh/grid structure and with no extra implementation difficulties. Solutions of the equation for 1-D and 2-D cases are approximated with an additional polynomial. The augmented form is used in this solution to reduce the error of numerical approximation.

The one dimensional groundwater contaminant transport modeling can also be described by the advection-diffusion equation. Li *et.al.* [27] and David [28] have

developed a meshless method for modeling groundwater contaminant transport using method with radial basis functions. They investigated five cases; pure diffusion, advection and dispersion for continuous source, advection and dispersion for instantaneous source for 1-D and 2-D, advection and dispersion for patch source. The results claim that the method is very simple and accurate.

In the literature, there are many approaches to the solution of advection-diffusion type of problems. Thiffeault [29] shows that the advection-diffusion equation in Lagrangian coordinates can be reduced to the one dimensional diffusion equation along the stable manifold of the flow (the direction along which fluid elements are compressed). Physical interpretation of the equation and break down of the approximation eventually has been shown and explained. Chantasiriwan [30] suggests that the solution of the advection-diffusion equation with the cartesian grid method (CGM) by collocation using radial basis functions combines the global radial basis functions and fundamental solutions and yields more accurate solutions that are less sensitive to the shape parameter of multiquadrics and node arrangement. Additional collocation appears to improve the quality of solutions. Hernandez [31] uses a high-order finite volume method based on piecewise interpolant polynomials to discretize spatially the one-dimensional and two-dimensional advection-diffusion equation. The mathematical difficulty of the advection-diffusion equation arises when the diffusion is very small. Many grid points are necessary to obtain reliable solutions to avoid this limitation and high-order methods must be considered to solve this equation. While Wan *et.al.* [32] use stochastic approximation for the two dimensional advection-diffusion equation with random transport theory, they use generalized polynomial chaos expansion to discretize the equation in random space while the spectral/*hp* element method is used for spatial discretization. Zhang [33] has prepared a master thesis comparing the results from Runge-Kutta-Chebyshev methods for advection-diffusion-reaction problems with the MATLAB solvers. She finds more satisfactory results than those using traditional solvers of matlab due to the additional Chebyshev polynomials used in the method. Other advection-diffusion-reaction type problems can be found in the paper [34] by Hundsdorfer. Time accurate solutions with the help of time discretization performed before the spatial discretization by introducing second and third order accurate generalization of the standard time stepping schemes by Taylor series expansion in time is carried out by Mehra and Kumar [35, 36] for the numerical solution of advection-diffusion

equation. Lastdrager *et.al.* [37] have investigated the efficiency of the sparse-grid combination technique for time dependent advection-diffusion problem employing a third-order Rosenbrock scheme for time discretization with adaptive step size control and approximate matrix factorization. They proved that the combination technique is more efficient than a single grid approach for a linear problem. Advection-diffusion problem is solved using the domain decomposition method by Lesnic [38].

An essential approach is due to James [39], where he provides a solution of advection-diffusion problem for radial flow using the cylindrical coordinates formulation. Describing the dimensionless variables, analytical solution is also given in the paper with appropriate initial and boundary conditions. Hon and Chen [40] solve the advection-diffusion equation is solved using Boundary Knot Method (BKM) under complicated geometry. The purpose of this paper is to extend the BKM to solve convection-diffusion problems under rather complicated irregular geometry. Numerical experiments validate that the BKM can produce highly accurate solutions using relatively small number of knots. The Radial Point Collocation Method (RPCM or PIM) is simply implemented to advection-diffusion equation as well as in the papers by Xin [41]. The main feature of this approach is to use the interpolation schemes in local supported domains based on radial basis functions. As a result, this method is local and hence the system matrix is banded which is very attractive for practical engineering problems.

All the papers above were reviewed to see what has been done for the solution of advection-diffusion type of problems. We can easily observe that the application of radial basis function collocation method is presently gaining attention. Due to its simple implementation and its advantage of being independent of dimension it has become very popular as a numerical method. The following paragraphs cover important sources related to the studies of viscoelastic fluid flow.

There are various studies about viscoelastic fluid flow problems in the literature. A few studies can be found for the application of the radial basis functions to viscoelastic fluid flow. Ellak *et. al.* [60] tried to simulate viscoelastic flow with Dissipative Particle Dynamics (DPD) meshless method instead of grids concept as finite difference or similar methods. They see that the advantage of the method is that many of the numerical

instabilities of conventional methods can be avoided, and that the model gives clear physical insight into the origins of many viscoelastic flow instabilities. Tran-Cong and Mai-Duy [61] propose a BEM-RBF approach for viscoelastic flow analysis. The solution of the Newtonian part of the equation is achieved by BEM, while the non-Newtonian viscous effect acting as a pseudo-body force is handled by approximating in terms of suitable radial basis functions. Ellero and Tanner [47] attempt to present a numerical framework called Smoothed Particle Hydrodynamics (SPH) which is used for the simulation of transient viscoelastic flows at low Reynolds number. An important reference due to Damasky [54] is "A note on start-up and large amplitude oscillatory shear flow of multi-mode viscoelastic fluids". This study analyzes analytical or semi-analytical procedures using the Laplace transformation of the models for Upper-Convected Maxwell and Oldroyd-B fluids defined with different type of PDEs.

Furthermore, Doa and Pinho [53] have investigated a criterion for fully-developed pipe and planar of multi-mode viscoelastic models based on the Phan-Thien Tanner (PPT) and Giesekus Equations. Berauda and Fortin [52] have developed a quasi-Newton method for a fluid obeying a multi-mode Phan-Thien Tanner and Tanner constitutive equations in spite of the difficulties of differential constitutive equations for numerical computation of viscoelastic fluid flows. They compare the results for two dimensional or axisymmetric flows to experimental results. Based on a modified Darcy's law for a viscoelastic fluid, Stoke's first problem was extended to that for an Oldroyd-B fluid in a porous half space and, Tan and Masuoka [62] obtained the exact solutions with limitations and for special cases by using Fourier sine transform. Hosseini *et.al.* [63] present a fully explicit Smoothed Particle Hydrodynamics (SPH) method to solve non-Newtonian fluid flow problems described in Lagrangian framework. Three constitutive laws including power-law, Bingham plastic and Herschel-Bulkley models are studied in this work. The results have shown that the proposed SPH algorithm are in close agreement with the available experimental and/or numerical data. A study of viscoelastic flow using neural networks and stochastic simulation is given by Tran-Canh and Tran-Cong [64]. This method uses a "universal approximator" based on neural network methodology in combination with the kinetic theory of a polymeric liquid in which the stress is computed from the molecular configuration rather than from closed form constitutive equations. As an illustration of the method, the time development of the planar Couette flow is studied for two molecular

kinetic models with finite extensibility, namely the Finitely Extensible Nonlinear Elastic (FENE) model.

1.3. Objective of the Thesis

We choose the radial basis functions method due to its wide application in the area of solution of partial differential equations. Being dimension independent and a meshless property it reduces the computational costs, time and coding difficulties. In addition, efficiency and accuracy increase by a considerable amount.

As seen from the literature survey, numerous kinds of approximation techniques and numerical studies have been carried out to solve both the advection-diffusion problem and the constitutive equations of viscoelastic models. Although only a few studies using the radial basis function collocation method exists for viscoelastic models, there are considerably more studies done on the numerical solution of advection-diffusion problem using this technique.

In the thesis, it is demonstrated that the radial basis functions collocation method cannot be underestimated due to its many advantages in solving partial differential equations. It is shown that this method gives good agreement with the analytical results and is at least as accurate as traditional methods given in the related papers. Two types of radial basis functions are also compared in the study in terms of error norms.

For the Multiquadric-RBF (MQ-RBF), the shape parameter effect is investigated and shape parameter optimization is shown using a curve for each problem. The optimum shape parameter " c " is determined considering the minimum RMS error, and specified in the tables for the solution with different number of nodes and time step sizes. First to fourth order Thin-Plate Splines (TPS-RBF) are used. It is observed when number of nodes are increased, the RMS error decreases. Thin-Plate Splines are much more sensitive to collocation points or number of nodes on the domain.

2. MESHLESS METHODS

2.1. From Mesh-Based Methods to Meshless Methods

Numerical methods that are more reliable, general and stable have become increasingly popular in industry and also its application in science is unavoidable. The most widely applied engineering computational methods are Finite Element Method (FEM), Finite Volume Method (FVM), and Finite Difference Method (FDM) [12]. Especially, since computers have made numerical simulations a daily activity for engineering science, most numerical simulations are carried out with the help of the Finite Element Method (FEM) [21]. The essence of the FEM is that a problem domain can be divided into small non-overlapping elements. It means the FEM has difficulty solving certain problems where its mesh has to be modified during the computation.

The popularity of FEM is mainly due to its generality and robustness. Unlike other methods such as FDM and BEM, the analysis procedures in FEM (which normally consist of pre-process, solve and post-process) are standard routines, and need almost no additional formulation for the computation in general. This feature helps to reduce the cost and time spent on learning the method. In addition, as the human involvement in the analysis is reduced, the error due to human mistake can be minimized. After more than half a century of development, FEM packages have become so easy to use that an engineer with little knowledge of FEM theory can easily perform some basic FEM analyses. Even with such a success, there is room for improving FEM. Among the issues, one of the essential tasks in a FEM analysis is the generation of a FEM mesh. The FEM mesh, which can be various shapes such as triangular or rectangular, is used to discretize the physical geometry [12], Figure 2.1 shows one FEM mesh example. Any field function is approximated within each element through simple interpolation functions. If the element is heavily distorted as shown in Figure 2.2, shape functions for this element are of poor quality and thus the numerical results may not be acceptable. One scheme to solve element distortions is to re-mesh the local domain and to develop adaptive techniques [21].

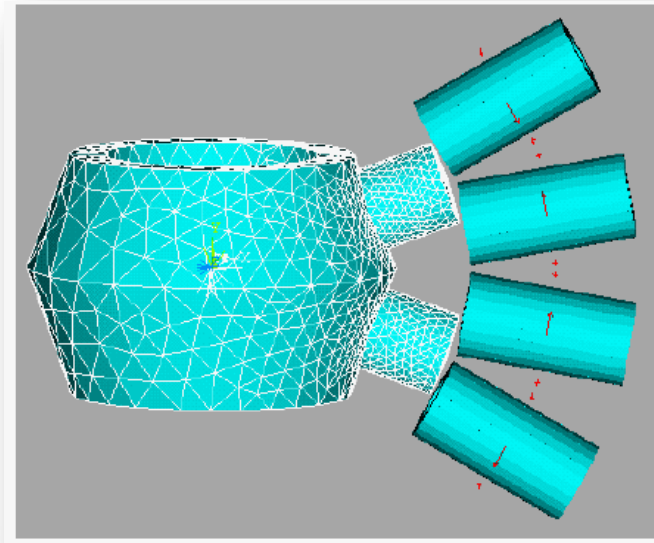


Figure 2.1. An example of finite element mesh [12]

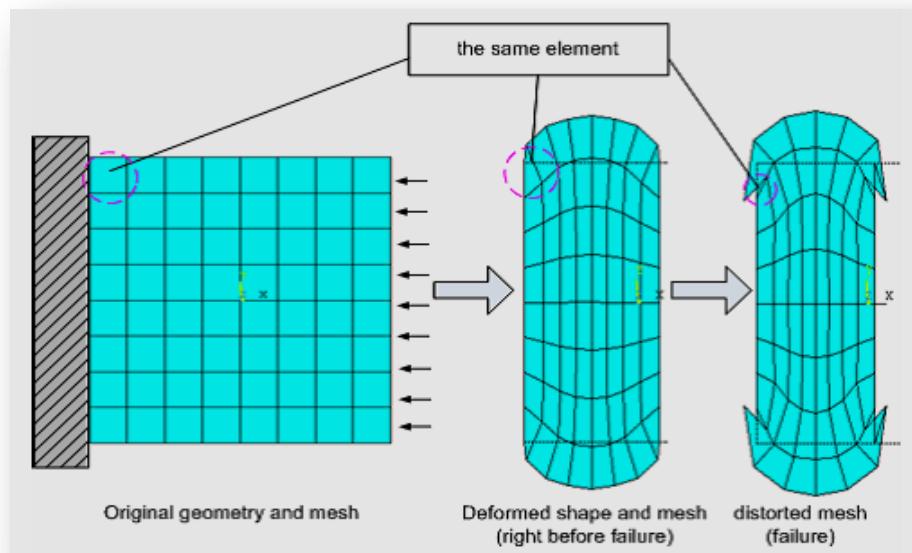


Figure 2.2. A mesh distortion example in FEM [21]

The driving force behind the scene is that the mesh-based methods such as the standard FEM and BEM often require prohibitive computational effort to mesh or remesh in handling high dimensional, moving boundary and complex-shaped boundary problems [18]. For such problems, it has become necessary to find the methods, which may be somewhat more expensive from the viewpoint of computer time but require less time in the preparation of data [17]. Even though considerable effort has been devoted to improving the design of the mesh and the algorithm to generate it, generation of the proper element structure remains a significant challenge; human involvement is still unavoidable for most engineering analyses with FEM [12].

Since FEM discretizes the whole physical domain into small elements, its computation could fail catastrophically due to the singularity of elemental Jacobian matrix when the element experiences large deformation. In order to alleviate this problem, Arbitrary Lagrangian Eulerian (ALE) formulation was proposed. The basic idea of ALE formulation is to make FEM mesh relatively independent of the material so that the mesh distortion can be minimized.

FDM also discretizes the governing PDE directly using their strong form. Although it is the most straight forward way to obtain the discrete system equations, it is difficult to handle boundary conditions with FDM. For a problem domain with complex geometry, the discretization of the geometry and the application of the natural and essential boundary conditions can seldom be done automatically by a computer program with no human involvement. As an example, Figure 2.3 shows a FDM grid for simulating the manufacturing process to draw an optical fiber. For a complicated geometry like this, additional efforts have to be spent on deriving a customized curvilinear coordinate to transform the geometry to a regular shape.

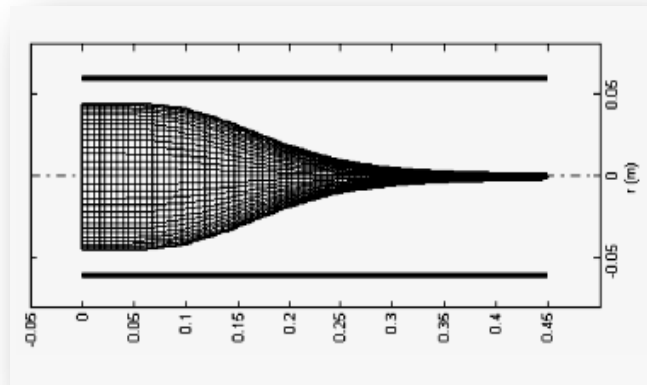


Figure 2.3. An example of FDM grid for an irregular shape of geometry [26]

Being different from element-based techniques or mesh-based methods, recently, a class of new methods, known as meshless methods, has been developed, which are also referred to in the literature as meshfree, element-free, gridless, cloud methods [26]. The aim of meshless methods is to eliminate at least the structure of the mesh and approximate the solution entirely using the nodes/points as a quasi-random set of points rather than nodes of an element/grid-based discretization. Meshless methods approximate field functions within an influence domain instead of an element [42, 21]. Meshless methods rely only on a group of scattered points, which means not only that the burdensome work of mesh generation is avoided, but also more accurate description of irregular complex geometries can be achieved. Furthermore, the meshless approximation has higher smoothness, and no additional postprocessing is needed [4].

Meshless Methods (MLM) that inherit many advantages of FEM have emerged and yet, they need no explicit mesh structure to discretize geometry. As a result, it greatly reduces the difficulty associated with FEM meshes. Since MLM does not need the element structure to discretize the geometry, the mesh generation algorithm only needs to deal with nodes rather than elements. This important feature makes MLM an attractive alternative for solving engineering problems (such as large deformation contact and fracture mechanics) where the adaptive meshes are often needed.

Recently, considerable research has been devoted to the development of meshless methods (MLM) for solving boundary value problems (BVP). As compared to its counterparts such as FEM, MLM has some advantages.

- It discretizes the physical domain into a scattered set of points and uses shape functions to interpolate the field variables at a global level.
- The fact that MLM does not need explicit meshes greatly reduces the dependency on a mesh generation program.
- In addition, computed results using MLM are generally smooth; therefore, it requires no post-processing as often needed in FEM.

We can give another example [15] to depict the complexity of generating mesh in FEM and comparison for the method in terms of node distribution of meshless methods in Figures 2.4 and 2.5.

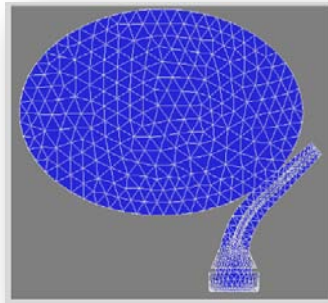


Figure 2.4. FEM mesh for contact computation [15]

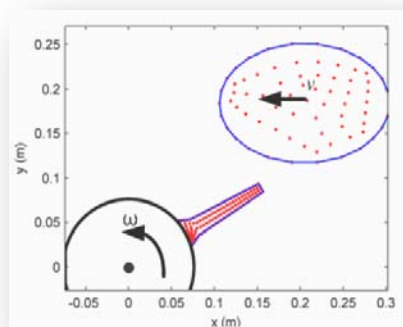


Figure 2.5. Computation model for meshless method [15]

The Figures 2.4 and 2.5 above demonstrate the ability for easy computation of analysis using nodes on the domain even for a complicated geometry over mesh generated methods. Computational points and their relation existing in the basis function simplify the implementation of this method to various areas of science and engineering.

As shown in Figure 2.6, in the solution procedure of the MLM, the ML basis function must be constructed after the nodes are generated. Without relying on elements, the construction of the basis function in MLM is solely based on the relationship among nodes. The methods for constructing basis functions are very important in the sense that they have direct effects on the efficiency and accuracy of the solution.

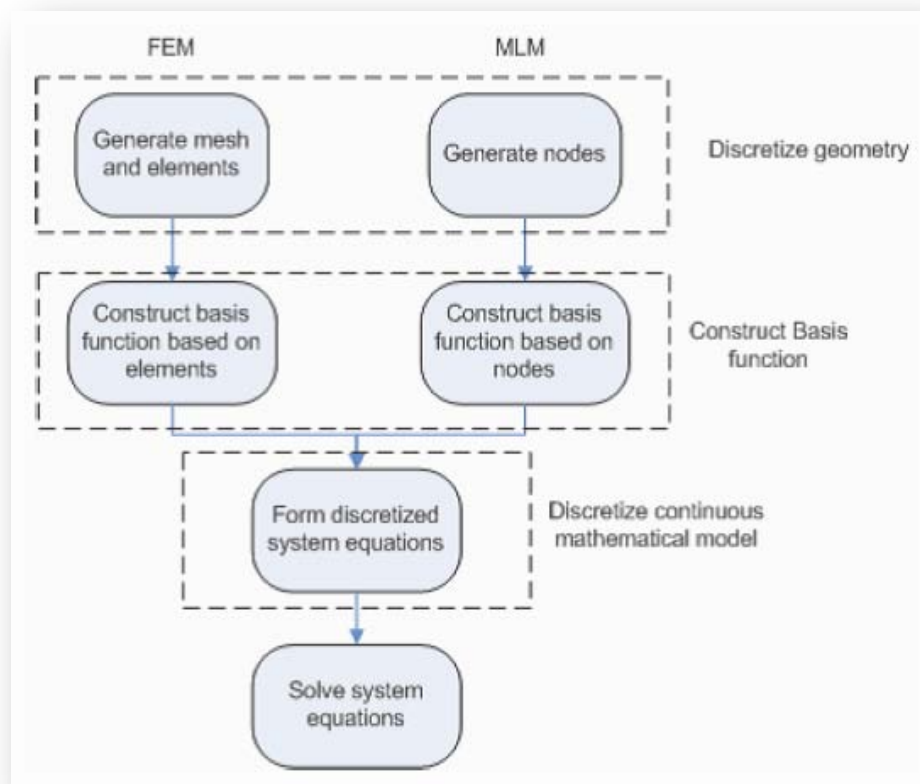


Figure 2.6. Solution procedure of FEM and MLM [21]

2.2. Categorization of Meshless Methods

The first meshless method, known as the Smooth Particle Hydrodynamics method (SPH), was developed in the late 1970's, but it did not attract much attention until the 1990's. Nayroles developed the Diffuse Element Method (DEM) for structural analysis, and it was later improved leading to a relatively complete Element-Free Galerkin method (EFG). After that, many meshless methods were proposed, such as the Reproducing Kernel Particle Method (RKPM), the Natural Element Method (NEM), the free-mesh method, the finite spheres method, the local Petrov-Galerkin method and the h-p cloud method. On the basis of these proposed methods and the theoretical development, meshless method has been applied to many engineering areas, such as fracture mechanics, fluid mechanics, microelectromechanical systems (MEMs), and electromagnetic computation [12]. These methods aim to eliminate the structure of the mesh and approximate the solution using a set of quasi-random points rather than points from a grid discretization [6].

All the above meshless methods can be categorized into two groups according to their discretization scheme. The first group is Galerkin-Based Meshless Methods (GBMMs), of which the Element Free Galerkin Method (EFG) proposed by Belytschko in 1994 is a famous representative [4]. Most of the current meshless methods applications have been based on the Galerkin formulation, which uses the weak form formulation of the original partial differential equation. Galerkin Based MLM is similar to FEM in that they both require numerical integration to form the discretized system equations. The accuracy of GBMMs is high, and good stability can always be obtained. The main shortcoming of GBMMs is that the integrals in the weak form must be evaluated properly. One way of evaluating integrals is to use a background mesh, which makes the method not truly meshless; another is to use nodal integration, which results in significant errors because the divergence theorem used in the establishment of the weak form demands accurate integration. In addition, because meshless shape functions are too complex to be expressed in closed form, a delicate background mesh and a large number of quadrature points are always employed, which decreases the efficiency seriously. As a consequence, GBMMs are much more computationally expensive than the FEM. However, unlike FEM where the basis functions are simple piecewise polynomials, the basis functions used for MLM are

often highly nonlinear and not in closed form, as they must satisfy a number of stringent requirements [15].

Some commonly used methods for generating the basis functions include the Moving Least Squares method (MLS), and Diffuse Element Method (DEM) was the first meshless method to employ Moving Least Squares approximation (MLS) in constructing their shape functions over scattered nodes instead of an element. The MLS was originally proposed by Lancaster and Salkauskas [55] for surface fitting. Belytschko *et.al.* [56] extended the DEM to more solid foundation within the framework of Galerkin weak form and developed an Element-Free Galerkin (EFG) method. Also the Reproducing Kernel Particle method (RKPM), Point Interpolation Method (PIM) and the Natural Element Method (NEM) were developed. In general, Galerkin Based MLM requires higher-order numerical integration and a background mesh (unlike the mesh in FEM, it is independent of the nodes) for the global integration, which tends to increase the computational cost. In addition, most of the basis functions in MLM do not have interpolation property, which often makes direct application of the essential boundary conditions difficult. More recently, the Petrov-Galerkin Method (PGM) has attracted some interest as the formulation uses a local integration scheme (local weak form) requiring no background mesh. However, the drawback of the Petrov-Galerkin Method is the difficulty in handling of the numerical integration near the boundary and the asymmetry of the discretized system matrix.

An alternative to eliminate the difficulty of handling boundary conditions at the interface and to avoid numerical integration in deriving the discretized system equations for MLM is to use another formulation – the strong form of the governing equation. This other group of meshless methods is built on collocation schemes. Several MLMs are formulated using the strong form of governing equation have been successfully applied to analyzing mechanics problems; notably, Finite Point Method (FPM) and the Point Collocation Formulation (PCF). More recently, the point collocation method has been proposed for electromagnetic field analysis. Unlike the Galerkin formulation, PCF uses the strong form of the governing equations to directly obtain a system of discretized equations without numerical integration. For linear problems, PCF appears simpler and requires less computational time. Additionally, it is easy to add nodes to improve computational accuracy at any desired local area. Finite Point Method (FPM), Dual Reciprocity Method

(DRM), Least-Square Collocation Meshless Method (LSCMM), and Radial Basis Function Collocation Methods (RBF-CM) all belong to this group. These methods are very efficient and easy to program, but they usually suffer from being full and unsymmetric coefficient matrix, and the accuracy often goes down near the boundary. Radial Basis Functions based methods are being developed in the present. Although the meshless methods based on the MLS have been successfully applied in computational mechanics, two major technical issues are still not well solved: (i) Difficulties in the implementation of essential boundary conditions. This is because its shape functions are short of delta function properties, (ii) complexity in numerical algorithms for computing shape functions and their derivatives. For the first issue, many schemes have been proposed such as Lagrangian, penalty and collocation. For the second issue, some useful algorithms have been proposed such as analytical integration, recursive method and parallel computing [21]. In a different view, RBF based methods can be divided into two groups; domain type and boundary type meshless methods. The Radial Basis Function method was first used by Hardy [57] for the interpolation of geographical scattered data, and later used by Kansa for the solution of partial differential equations (PDEs) [43]. Kansa's method or known as unsymmetric radial basis function collocation method is domain type meshless method, DRM-BEM or Method of Fundamental Solutions (MFS) is based on boundary type meshless methods.

Due to advances in computational technologies in past two decades, many numerical simulation tasks, which were once considered computationally formidable or could be addressed only by a supercomputer, can now be carried out by a desktop computer. Encouraged by this trend, more and more research effort has been devoted to developing numerical tools to facilitate the design or analysis of engineering systems. These efforts, in turn, have led to more reliable, more powerful and faster software packages for numerical simulation. In engineering designs, numerical methods along with high-fidelity mathematical models are able to predict the behavior of an engineering system before the physical system has been built. This drastically reduces the number of different configurations for experimental investigation and thus saves the cost and time in design. In many situations, numerical simulation can effectively reduce or replace expensive experimental studies as a primary investigation tool for engineers. In addition to that, radial basis function based meshless methods have considerably been attracting attention in last decade. Especially, solving partial differential equations numerically using RBFs has

become very popular due to its easy implementation and independence of problem dimension.

In the following part, some fundamental numerical methods in order to discretize time marching processes are presented. Apart from space discretization, these methods are very useful and found to be attractive and efficient in most cases.

2.3. Numerics For Time Marching

Differential Equations are used to model problems in science and engineering that involve the change of some variable with respect to another. Most of these problems require the solution to an Initial Value Problem (IVP), that is, the solution to a differential equation that satisfies a given initial condition. Progression in time requires raising an initial condition to a given problem, so time procedure can begin to reflect the phenomenon which is easy to compare with the experiments after obtaining numerical simulation results. Some essential first and second order time integration methods are explained in the following parts.

2.3.1. First Order Time Integration

2.3.1.1. Runge-Kutta 4th Order

The known Taylor methods have the desirable property of high-order local truncation error, but the disadvantage of requiring the computation and evaluation of the derivatives of $f(t,u)$. This is a complicated and time-consuming procedure for most problems, so the Taylor methods are seldom used in practice.

There are a number of self starting (single step) schemes for initial value problems such as the Euler method, the modified Euler method, the Heun method, Runge-Kutta methods, and the Taylor polynomial method as well as multi-step methods such as Adams-Basforth method and Adams-Moulton method. However, since the predictor-corrector type equations use past information they lack the ability to start initial value problems.

As a time integration method, fourth order Runge-Kutta method is used in this study because it is known to work well for smooth problems. Moreover, it is a self starting method so that the initial input will be sufficient to proceed in time. It involves four evaluations per time step and the local truncation error is fourth order. Also, since the expected results are smooth, adaptive step size control is not deemed necessary.

Approximating to the solution of initial value problem, let's assume the model occurs as the following in general,

$$\frac{\partial u}{\partial t} = f(t, x, y, u, u_x, u_y, \dots), \quad a \leq t \leq c \quad (2.2)$$

where $t_1 = a$ is the initial time, and assumed to be $u(t_1) = \alpha$ then Runge-Kutta Order Four reduces to,

$$u(t_1) = u_1 = \alpha$$

$$k_1 = hf(t_b, u_b)$$

$$k_2 = hf\left(t_b + \frac{h}{2}, u_b + \frac{1}{2}k_1\right)$$

$$k_3 = hf\left(t_b + \frac{h}{2}, u_b + \frac{1}{2}k_2\right)$$

$$k_4 = hf(t_b + h, u_b + k_3)$$

$$u_{i+1} = u_i + \frac{1}{6}(k_1 + 2k_2 + 2k_3 + k_4) \quad (2.3)$$

where $t_{b+1} = t_b + \Delta t$, Δt is the time step size for each $b = 1, 2, 3, \dots, (T-1)$, here T refers to total time steps. This method has local truncation error $O(h^4)$, provided the solution $u(t)$ has

five continuous derivatives. These values of k_1 , k_2 , k_3 and k_4 are the steps between the each time steps in equal size. It reduces the error while approximating to solution.

2.3.2. Second Order Time Integration

2.3.2.1. Houbolt Integration

For second order time integration, Houbolt method [10] is common in application. Apart from the other methods for the second order time integration, this method is very easy to implement and practical. In the study, the viscoelastic flow problem involves second order time derivative, it seems that this method will provide good results in approximation.

Houbolt method depends on the first three time steps for the next fourth step, say, the first three step values should be evaluated firstly, then it will continue to march. In the problem, only the initial values are known. The next two steps must be found by reducing the governing equation with the help of backward or forward finite difference discretization to shape the procedure using only the initial values. After the first three time steps values are evaluated, Houbolt method takes over. The Houbolt integration method involving 2nd order time derivatives can be given as,

$$\left(\frac{\partial^2 u}{\partial t^2}\right)^{b+1} = \frac{1}{(\Delta t)^2} (2u^{b+1} - 5u^b + 4u^{b-1} - u^{b-2}) \quad (2.4)$$

$$\left(\frac{\partial u}{\partial t}\right)^{b+1} = \frac{1}{6\Delta t} (11u^{b+1} - 18u^b + 9u^{b-1} - 2u^{b-2}) \quad (2.5)$$

where b is the time step. The original Houbolt method does not uniquely define the response; by considering the original Houbolt method as the analysis tool, one cannot talk about specific and unique responses computed by the integration process. Lack of a specific starting procedure also prevents / complicates the implementation of the Houbolt method in problems involved in nonlinearity, adaptive time stepping,... etc. We directly use the above-mentioned procedure for marching the time steps.

3. RADIAL BASIS FUNCTIONS METHOD

3.1. General Information about RBFs

Many of the important concepts of analysis and computation have their origins in the study of physical problems leading to the partial differential equation (PDE) systems. The currently ubiquitous Fourier series and transform came from Fourier's original exploration of the solution of a bar heat transmission problem in the early 1800s. What Fourier proposed due to this quest is that an arbitrary 1D function $f(x)$ over a bounded interval, even if not differentiable, can be represented by an infinite sum of sinusoids,

$$f(x) = \sum_{k=1}^{\infty} c_k \sin \frac{k\pi}{a} x \quad (3.1)$$

where sinusoids are the eigenfunctions of any PDE problem. Despite a lack of rigorous proof, Fourier was quite confident of the basic truth of his assertion for obvious physical and geometric grounds. Nevertheless, the implications of this discovery go well beyond Fourier's wildest imaginations. The unanswered mathematical points forcefully gave birth to many more new problems and consequently motivated the development of many important mathematic concepts and techniques such as Riemann Integration, Sturm-Liouville eigenvalue problem, Set Theory, Laplace Transform, Lebesgue Integration, Green's function and distribution theory, functional analysis, and most recently, wavelets theory as well as enormous applications in numerous ramifications of science and engineering.

Despite the widespread applicability, the Fourier analysis approach suffers some drawbacks. Most noticeably, for more than one-dimension problems, the direct use of the Fourier series becomes very mathematically complicated and is only feasible for such regular geometry as rectangular, circle, sphere, cylindrical domains,... etc., where we can separate the space variables (in Cartesian, polar, or some other coordinate systems). Otherwise the tensor product approach, very costly in high dimensions, must be applied.

However, when the scattered data are involved, the tensor product Fourier analysis also immediately fails.

Because of the great success of the polynomials, splines, and tensor product methods, mathematician and engineers alike grow accustomed to expressing a function in terms of coordinate variables. To majority of scientific and engineering community, the Radial Basis Function (RBF), which uses the one-dimensional distance variable irrespective of dimensionality, has become a quite brand-new and exotic concept. In high dimensional scattered data cases, the RBF approach, however, is the method of the choice. It is also found that the RBF is very efficient in handling lower-dimensional problems.

Since the pioneering works of Frankle, Michaelli and Kansa, the research into the RBF theory and its applications have grown. In parallel, Daubechies' break through orthogonal compact wavelets lead revolutionary advances in multiscale analysis. The RBF is well known for its striking effectiveness in multivariate scattered data approximation [36]. The Radial Basis Function method was first used by Hardy [57] for the interpolation of geographical scattered data, and later used by Kansa for the numerical solution of partial differential equations (PDEs) [19].

In 1990, Kansa introduces a new approach for this kind of problems, where the true solution is approximated for a linear combination of radial basis functions. This method has shown to be more efficient than the traditional methods like, Finite Differences Methods and Finite Element Methods. Owing to the independence of the dimension of radial basis functions, this strategy is very attractive to resolve high dimensional problems. The Kansa's approach is truly meshless and does not demand any connectivity requirements as needed with the traditional techniques like Finite Differences Methods, Finite Elements Methods and Boundary Element Methods [3].

Presently, RBFs have many applications in engineering problems apart from using as interpolation functions [22],

- Applications in Machine Learning, for example: datamining, knowledge discovering, object recognition in computer vision and game playing.

- In the scope of static modelling, the RBF networks are used to build models, generally the activation functions employed are the Gaussian function and the inverse multiquadric function.
- Also, the RBFs are used in the field of pattern analysis.

As expressed in the previous chapter, radial basis function meshless method exists in the group that is categorized according to collocation scheme of meshless methods. One of the domain type collocation meshless methods is obtained by simply applying the radial basis functions as a direct collocation, which was proved to be effective in solving complicated physical problems with irregular domains. More recently, a boundary type collocation scheme that combines the Method of Fundamental Solutions (MFS) and Dual Reciprocity Method (DRM) with the RBFs has been developed [20].

The Radial Basis Function method also called Kansa's method is based on Kansa's unsymmetric domain type collocation. Basis functions are infinitely differentiable, smooth and they have continuous derivatives in the defined interval. Basis functions use collocation nodes instead of elements or meshes which makes the method easy to implement.

The ideal numerical method for PDE problems should be high-order accurate, flexible with respect to the geometry, computationally efficient, and easy to implement. The methods that are commonly used, usually fulfill one or two of the criteria, but not all. Finite Difference Methods can be made high-order accurate, but require a structured grid (or a collection of structured grids). Spectral methods are even more accurate, but have severe restrictions on the geometry and, in the Fourier case, also require periodic boundary conditions. Finite Element Methods are highly flexible, but it is hard to achieve high-order accuracy, and both coding and mesh generation become increasingly difficult when the number of space dimensions increases [44]. So finally, Radial Basis Function (RBF) methods have been praised for their simplicity and ease of implementation in multivariate scattered data approximation, and they are becoming a viable choice as a method for the numerical solution of partial differential equations (PDEs) [23].

Fortunately, there is a theoretical justification for this method in Buchmann's essential book [58]. Fasshauer proposed an alternative approach based on the theory of Hermite–Birkhoff interpolation [21]. This is the so-called symmetric RBF collocation method since the coefficient matrix obtained is symmetric. Existence of numerical solution and a convergence analysis are given in references. But implementation of symmetric version is much more complex (especially for variable coefficient equation and nonlinear systems) than the unsymmetric version due to the use of adjoint differential operators [14].

Application of this radial basis collocation method is widespread in the world of science and engineering, the following problems also frequently appear in the literature: electrical, magnetic, thermal, gravitational, vibration, hydrodynamics, acoustics problems [36]. Its popularity has been regularly growing in the implementation into partial differential equations as we see in lots of academic papers or simulations.

In the literature, some papers are available which deal with the methods developed using radial basis functions. A few novel RBF-based numerical schemes discretizing partial differential equations are now popular and combination of so-called methods are ready to increase the efficiency and stability.

A boundary type meshless method was developed by combining the method of Method of Fundamental Solution (MFS) and the Dual Reciprocity Method (DRM) with the RBFs. The DRM method is a class of BEMs to solve non-homogeneous term of partial differential equations [20]. Being meshless of course, fast convergent and extensible to high dimensional problems make the MFS very attractive in solving problems with complex geometry as we mentioned several times. The MFS is also known as an indirect boundary method or regular BEM in the engineering literature [20].

Especially as boundary-type methods, Chen [18] derives the indirect and direct symmetric Boundary Knot Methods (BKM). The resulting interpolation matrix of both is always symmetric irrespective of boundary geometry and conditions. In particular, the direct BKM applies the practical physical variables rather than expansion coefficients and becomes very competitive to the Boundary Element Method (BEM). On the other hand, based on the multiple reciprocity principle, it has been found that the RBF-based boundary

particle method (BPM) for general inhomogeneous problems does not use inner nodes. The direct and symmetric BPM schemes can also be developed.

For domain-type RBF discretization schemes, by using the Green integral Chen [18] develop a new Hermite RBF scheme called as the Modified Kansa Method (MKM), which differs from the symmetric Hermite RBF scheme in that the MKM discretizes both governing equation and boundary conditions on the same boundary nodes. The local spline version of the MKM is named as the Finite Knot Method (FKM). Both MKM and FKM significantly reduce calculation errors at nodes adjacent to boundary. In addition, the nonsingular high-order fundamental or general solution is strongly recommended as the RBF in the domain-type methods and dual reciprocity method approximation of particular solution relating to the BKM [18].

Now, we need to have a look over the types of RBFs which are popular for solving different kinds of linear or nonlinear partial differential equations in the literature. The most common type of RBFs are multiquadrics, thin-plate splines and compactly supported radial basis functions. In the study, the multiquadrics and thin-plate splines will be cited in detail. And shape parameter effects of MQs will be discussed and some methods reducing the ill-conditioning of the coefficient matrix will be available in the work.

3.2. Types of RBFs

The most common radial basis functions can be categorized into three main groups according to their differentiability and supported features which are shown in the Tables 3.1, 3.2 and 3.3. Some of the functions include free-parameter and some of them are parameter-free. The choice of suitable radial basis functions can vary in terms of the problem types. The present study also explores the effectiveness of the most common radial basis functions while implementing these functions to advection-diffusion and viscoelastic type of problems.

Common choices of $\phi(r)$ are [23, 44, 45];

- Piecewise smooth functions and parameter-free in Table 3.1,
- Infinitely smooth functions with a free parameter in Table 3.2,
- Compacty supported piecewise polynomials with free parameter for adjusting the support: Wendland functions in Table 3.3.

Tables for Fourier transforms and convergences rates of some radial basis functions can be found in [46].

Table 3.1. Piecewise Smooth RBFs

Piecewise Smooth RBFs	$\phi(r)$
Piecewise Polynomials (R_β)	r^β $\beta > 0, \beta \in 2N+1$
Thin Plate Splines (TPS_β)	$r^\beta \ln r$ $\beta > 0, \beta \in 2N$

Table 3.2. Infinitely Smooth RBFs

Infinitely Smooth RBFs	$\phi(r)$
Multiquadrics (MQs)	$(r^2 + c^2)^{\beta/2}$ $\beta > 0, \beta \in 2N+1$
Inverse Multiquadrics (IMQs)	$(r^2 + c^2)^{-\beta/2}$ $\beta > 0, \beta \in 2N+1$
Inverse Quadratics (IQs)	$\left(\frac{1}{r^2 + c^2}\right)^{\beta/2}$ $\beta > 0, \beta \in 2N$
Gaussian (GS)	$\exp(-c^2 r^2)$

3.3. Wendland's positive definite functions with compact support

Dimension	$\phi(r)$	Smoothness
$d = 1$	$\phi_{1,0} = (1-r)_+$	C^0
	$\phi_{1,1} = (1-r)_+^3(3r+1)$	C^2
	$\phi_{1,2} = (1-r)_+^5(8r^2+5r+1)$	C^4
$d \leq 3$	$\phi_{3,0} = (1-r)_+^2$	C^0
	$\phi_{3,1} = (1-r)_+^4(4r+1)$	C^2
	$\phi_{3,2} = (1-r)_+^6(35r^2+18r+3)$	C^4
	$\phi_{3,3} = (1-r)_+^8(32r^3+25r^2+8r)$	C^6
$d \leq 5$	$\phi_{5,0} = (1-r)_+^3$	C^0
	$\phi_{5,1} = (1-r)_+^5(5r+1)$	C^2
	$\phi_{5,2} = (1-r)_+^7(16r^2+7r+1)$	C^4

In Table 3.1 and 3.2 N refers to natural numbers 0, 1, 2, ...; and in Table 3.3 $(\)_+$ operator is used to express $\phi(r)$ as a univariate polynomial $p(r)$ or 0 depending on the values of r . Clearly [47],

$$\phi(r) = \begin{cases} p(r) & , \text{ if } 0 \leq r < 1 \\ 0 & , \text{ if } r \geq 1 \end{cases} \quad (3.2)$$

A key feature of an RBF method is that it does not require a grid. The only geometric properties that are used in an RBF approximation are the pairwise distances between points. Distances are easy to compute in any number of space dimensions, so working in higher dimensions does not increase the difficulty. The method works with points scattered throughout the domain of interest, and the RBF interpolant is a linear combination of RBFs centered at the scattered points x_j , in other words, using N distinct locations $x_1, \dots, x_N \in$

\mathcal{R}^n at which the values u_1, \dots, u_N are defined, one can construct a linear combination as given in the Equation (1.2) [44]. There $u(x)$ is the dependent variable in the partial differential equation say, in governing equation it will be denoted as $u(x,c)$ which refers to “ c ” shape parameter related function of x and c is the interpolation or approximation function which will approximate the function to be calculated over the defined domain using linear combination of radially assigned basis functions. In the Equation 1.3, “ r ” is the distance also means the Euclidian distance shown $\|\cdot\|$ between two nodes given by in 3-D, λ_j s are the coefficients to be found and those are most functions of time. Given scalar function values $u_i = u(x_i)$, the expansion coefficients λ_j are obtained by solving a system of linear equation as given in (1.5) where the interpolation matrix satisfies $a_{ij} = \phi(\|x_i - x_j\|, c)$.

If we show this linear system of equations in terms of time, in general the system of equations become as follows in (3.3), here b denotes the time steps, at each time step the coefficient matrix remains constant, so it means while λ changes the u values change [23].

$$\begin{bmatrix} \phi_{11} & \phi_{12} & \cdot & \cdot & \phi_{1N} \\ \phi_{21} & \phi_{22} & \cdot & \cdot & \phi_{2N} \\ \phi_{31} & & & & \\ \cdot & & & & \\ \cdot & & & & \\ \phi_{N1} & \cdot & \cdot & & \phi_{NN} \end{bmatrix} \begin{bmatrix} \lambda_1^b \\ \lambda_2^b \\ \cdot \\ \cdot \\ \cdot \\ \lambda_N^b \end{bmatrix} = \begin{bmatrix} u_1^b \\ u_2^b \\ \cdot \\ \cdot \\ \cdot \\ u_N^b \end{bmatrix} \quad (3.3)$$

Even though Franke as mentioned in [48] demonstrated that global RBF methods were superior to the commonly used, compactly supported interpolation schemes, the debate still continues whether it is better to use compactly supported approximations or globally supported RBFs for large scale computations. The main impetus behind this debate is the problem with full ill-conditioned matrices. Matrix sparsity, however, is not the entire remedy because FEM using compactly supported basis functions still can give rise to poorly conditioned matrices. Also there has been developed another type of multiquadric radial basis function called Truncated-MQs. The evidence finds the range of significant influence to yield matrices with finite, rather than full band-widths. Its structure

consists of a construction transcendental functions which are infinitely differentiable as shown in the following,

$$\phi(\|x - x_j\|, c) = \begin{cases} \sqrt{\|x - x_j\| + c_j^2} & , \text{ if } r \leq r_{cutoff} \\ \eta(r) \sqrt{\|x - x_j\| + c_j^2} & , \text{ if } r > r_{cutoff} \end{cases} \quad (3.4)$$

where,

$$\eta(r) = \frac{(r + r_{cutoff})}{2r_{cutoff}} \exp(-k_3 |r - r_{cutoff}|) \quad (3.5)$$

Here the decay function, $\eta(r)$ is set to zero if its magnitude is less than 0.001 in the exercise presented in [48], yielding zero matrix coefficient elements and k_3 is assumed the decay constant. The cutoff distance should have been lowered to a certain constant value in order to prevent divergence. Then, the RMS error is reduced further by optimizing the shape parameter. As seen in the present study, the shape parameters "c" are optimized to obtain the lowest possible RMS error.

3.2.1. Some Properties of RBFs

As mentioned before, RBFs can be a) globally supported, b) infinitely differentiable, and c) contain a free parameter, c, called the shape parameter [8]. In all the interpolation methods for scattered data sets, RBFs outperforms all the other methods regarding

- accuracy,
- stability,
- efficiency,
- memory requirement,
- simplicity of the implementation.

When the problems to be solved are different, the choice of the optimal RBFs will change. So the network performance is decided not only by the number of the nodes, but also by the RBFs' type [1].

If we look at piecewise smooth versus infinitely smooth RBFs, it can be found that for PDE applications with smooth solutions, the infinitely smooth RBFs are preferable, mainly because they lead to higher accuracy. In a comparison of RBF-based methods against two standard techniques (a second-order finite difference method and a pseudospectral method), the former gives a much superior accuracy. When infinitely smooth RBFs are used, the approximations feature spectral convergence as the points get denser. This has been proven strictly only for some special cases, although numerical evidence strongly suggests that it is true in much more general settings. Furthermore, implementation of an RBF method is straightforward [44].

Under certain conditions, the infinitely smooth radial basis functions exhibit exponential or spectral convergence as a function of center spacing, while the piecewise smooth types give algebraic convergence. In addition, the appeal of compactly supported radial basis function is that lead naturally to banded interpolation matrices. Experience has shown that these matrices need to be large for good accuracy [23]. It is unavoidable to repeat the most essential property of radial basis function collocation, that is they lead to a truly mesh-free algorithm, and they are space dimension independent in the sense that the convergence order is of $O(h^{d+1})$ where h is the density of the collocation points and d is the spatial dimension [48].

3.2.2. The Advantages using Meshless MQs and TPS-RBFs

Basis functions may have global or compact support and may have varying degrees of smoothness. It was found in [8], numerical results that the “best” choice of basis function for a particular problem was one in which the shapes of the basis functions best matched the shapes or features of the PDE solution. This allowed the solution to be approximated well with a small number of basis function.

In addition, it is shown that the multiquadric collocation method is more accurate as grid spacing and time step decrease, a random arrangement of nodes does not affect the accuracy of the method significantly. This study will also try to show that the multiquadric collocation method has the potential to be an acceptable alternative numerical method for solving general partial differential equations [5].

As far as the thin plate radial basis function method is considered for the numerical solution of PDEs, it has also the same advantages like using MQs as basis functions.

The radial basis functions method with its simple implementation, generates excellent results and speeds up the computational processing time, independent of the shape of the domain and irrespective of the dimension of the problem.

3.2.3. Shape Parameter Effect

It is well known that the accuracy of the multiquadric radial basis functions collocation method is sensitive to the shape parameter, which may be chosen to optimize the performance of multiquadrics as an interpolating function. Although a variable shape parameter has been suggested, there is evidence that using a variable shape parameter does not always lead to a more accurate solution than using a constant shape parameter. In order to investigate effects of the shape parameter on the solution by the proposed method, variations with time of average error may be calculated for several values of the shape parameter [5]. Or as it has been done in our study, the effect of shape parameter can also be observed according to final time of the time interval.

The shape parameter affects both the accuracy of the approximation and the conditioning of the interpolation matrix. In general, for a fixed number of centers N , smaller shape parameters produce the more accurate approximations. The condition number also grows with N for fixed values of the shape parameter c . In practice, the shape parameter must be adjusted with the number of centers in order to produce a interpolation matrix which is well conditioned enough to be inverted in finite precision arithmetic. The optimal choice of the shape parameter is still an open question [8]. Numerical studies also

show that the ill-conditioning problem of global radial basis function collocation method is reduced by the Schwarz schemes for many problems [2].

As far as the shape parameter is considered, the value of the shape parameter for the MQ directly affects the approximation. If $c^2 \gg r_{\max}^2$, then all u using ϕ computed from (1.2) will more or less have the same value – in the limit as the shape parameter becomes extremely large, the ϕ -matrix becomes singular. On the other hand the approximation loses its smoothness as $c^2 \rightarrow 0$. Although a number studies have been conducted to determine the optimum value of the shape parameter, there is still no conclusive answer. There are however some expressions that provide starting values for a trial and error procedure to find a good c^2 value. For example, a suggestion due to Hardy [57] is

$$c = 0.815 r_{\text{av}} \quad (3.6)$$

where r_{av} is the average distance between each node and its nearest neighbor. Experience shows that the value obtained from this expression is conservative; that is, on the small side of possible c 's. In their study on the tide induced flows in Tolo Harbor, Hong Kong, Hon et al [40] state that satisfactory results were obtained for c between $5r_{\text{av}}$ and $8r_{\text{av}}$. Another suggestion for c given by Wu and Hon in 2003 is

$$c = 4 r_{\text{min}} \quad (3.7)$$

where r_{min} is the smallest distance between nodes [45].

3.3. RMS Error Calculation

The RMS error is defined as;

$$RMS = \sqrt{\frac{1}{N} \sum_{i=1}^N \left(\frac{u^i_{\text{numerical}} - u^i_{\text{exact}}}{u^i_{\text{exact}}} \right)^2} \quad (3.8)$$

where N denotes the total number of nodes including the nodes both interior and boundary. In some parts of the numerical solution the error amount can drastically change according to instant or large variations. The RMS error evaluates the average error that is distributed to all part of the so-called numerical solution at a certain time. The MQs and TPS-RBFs have provided satisfactory results in many papers proposed. Regular or random node distribution on the domain can affect the RMS error and we have to consider also shape parameter effect in numerical solution of partial differential equation [48]. Instead of using that calculation given in 3.8, the following expression may be a good choice where the units of RMS error will be the same as those of u values.

$$RMS = \sqrt{\frac{1}{N} \sum_{i=1}^N (u^i_{numerical} - u^i_{exact})^2} \quad (3.9)$$

3.4. Reducing the Ill-Conditioning

In addition to the advantages of meshless radial basis function collocation method mentioned in the previous section, sometimes RBF methods may have negative drawbacks. As the number of centers or nodes on the domain grows, the method needs to solve a relatively large algebraic system. Moreover, ill-conditioning of the interpolation matrix $[A]=\phi_j$ defined in Equation 1.2 causes instability that makes spectral convergence difficult to achieve [23]. On the other hand, a big obstacle for radial basis function collocation method has emerged that the companion matrix is generally ill-conditioned, nonsymmetric and full dense matrix, which constrains the applicability of RBFs method to solve large scale problems [3].

This behavior is manifested as a classic accuracy and stability trade-off, for instance, the condition number of $[A]$ grows exponentially with N . For small N , it is possible to compute the coefficient vector λ accurately, using complex contour integration, but the robustness of this method for large N is not yet tested. If ones wishes to use an iterative method to solve for the interpolation coefficients, ill-conditioning can also create a serious convergence issue. In such cases basically good preconditioners [23] are needed. Moreover than preconditioners, domain decomposition method can also provide a way to reduce the

computational time and the ill-conditioning of the matrix which will not be cited in this study in detail, only augmented approximation, adaptive method and symmetric collocation methods will be briefly overviewed at the end of this section.

Also in most studies, researchers have implemented the method for infinitely smooth RBFs, and then compared them across the full range of values for the shape parameter “ c ” for which RBF includes this parameter. This was made possible by a recently discovered numerical procedure that bypasses the ill-conditioning, which has previously limited the range that could be used for this parameter. We have to find the optimum value for the approximation.

Several different strategies have been somewhat successful in reducing the ill-conditioning problem when using RBF methods in PDE problems [8]. The strategies include [8, 48] :

- variable “ c_j ” shape parameters, variable MQ shape parameters based upon the local radius of curvature of the function being solved,
- domain decomposition technique or method (DDT / DDM) ,
- preconditioning the interpolation matrix by using matrix preconditioners,
- optimizing the center locations or knot adaptivity that minimizes the total number of knots required in a simulation problem, say adaptive collocation method,
- augmented approximation by adding a polynomial term to approximation function,
- replacement of global solvers by block partitioning, LU decomposition schemes,
- a truncated MQ (T-MQ) basis function having a finite, rather than a full bandwidth.

The hybrid combination of these methods contribute to very accurate solutions. Often, more than one of these strategies (hybrid) can be used together [8] .

Even though FEM gives rise to sparse coefficient matrices, these matrices in practice can become very ill-conditioned. Spectral methods typically require the construction of a tensor-product mesh using the zeros of a higher-order polynomial such as the Chebyshev polynomial. However, the primary disadvantages of such schemes are that the domain

must be regular to obtain the tensor product mesh, and the knots are restricted to the loci of the zeros of these polynomials. Whether FDM, FEM, FVM or spectral methods are used, they all suffer from the problem of dimensionality.

It is unavoidable to dismiss global RBF scheme as MQ, because there are alternate methods that within a hybrid scheme could circumvent the problem of global matrices and ill-conditioning [48]. Some comments regarding a few of these methods are provided in the following.

- Simple preconditioners improve the condition number of large matrices. A preconditioner should be simple, easily calculated approximation to the inverse of the matrix. This is still an unresolved issue that requires more research. Symmetric collocation method includes a kind of so-called technique that conditions the coefficient matrix of the interpolation problem will be cited in the following part.
- A variable MQ shape parameter recipe based upon the local radius of curvature yields better conditioned matrices and more accurate solutions than a constant shape parameter MQ scheme. The condition numbers of both the global and partitioned blocks are smaller because the rows of the matrix elements are more distinct, but the RMS errors can be one to two orders of magnitude less than the accepted constant shape parameter MQ scheme.
- Transforming the global MQ basis function into a truncated basis function is another way to reduce the ill-conditioning of the coefficient matrix. By multiplication by an exponentially decaying function, the resulting matrix has a finite, rather than a full band-width. The T-MQ-RBF that was constructed from transcendental functions is continuously differentiable. A balance between efficiency and accuracy will require optimization.
- Optimization of knot location requires many fewer knots and better conditioned matrices, and yields superior accuracy. Sarra [8] showed that how an adaptive

algorithm (adjusting the knots to follow the peaks of the function curvature) has gained extremely excellent results.

3.4.1. Augmented Approximation

The interpolant given in equation (1.2) may also be augmented by using polynomials $p_k(x)$ of order M_a , that is

$$u_i^b = u^b(x_i) = \sum_{j=1}^N \phi(\|x_i - x_j\|, c) \lambda_j^b + \sum_{k=1}^{M_a} \beta_k^b p_k(x_i) \quad (3.10)$$

The form given in equation (3.9) has now $N+M_a$ coefficients to be determined, “ b ” denotes the time step, and so the system of equation becomes $(N+M_a) \times (N+M_a)$ system as shown in the following matrix (3.11), and $i=1, 2, 3, \dots, N$ total number of nodes.

The polynomial term is an extra requirement that guarantees the unique approximation. Following constraint is usually imposed in order to eliminate extra polynomial terms,

$$\sum_{i=1}^N p_k(x_i) \lambda_i = 0 \quad , \quad k = 1, 2, 3, \dots, M_a \quad (3.11)$$

$$\begin{bmatrix} \phi_{11} & \phi_{12} & \phi_{13} & \cdot & \cdot & \phi_{1N} & p_1(x_1) & p_2(x_1) & \cdot & p_M(x_1) \\ \phi_{21} & \phi_{22} & \cdot & \cdot & \cdot & \phi_{2N} & p_1(x_2) & \cdot & \cdot & p_M(x_2) \\ \phi_{31} & \phi_{32} & & & & \cdot & p_1(x_3) & \cdot & \cdot & \cdot \\ \cdot & & & & & \cdot & \cdot & & & \cdot \\ \cdot & & & & & \cdot & \cdot & & & \cdot \\ \phi_{N1} & \cdot & \cdot & \cdot & \cdot & \phi_{NN} & p_1(x_N) & p_2(x_N) & \cdot & p_M(x_N) \\ p_1(x_1) & p_1(x_2) & \cdot & \cdot & \cdot & p_1(x_N) & 0 & 0 & 0 & 0 \\ p_2(x_1) & \cdot & & & & \cdot & 0 & 0 & 0 & 0 \\ \cdot & \cdot & & & & \cdot & 0 & 0 & 0 & 0 \\ p_M(x_1) & p_M(x_1) & & & & p_M(x_N) & 0 & 0 & 0 & 0 \end{bmatrix} \quad (3.12)$$

growth towards infinity. Examples are thin plate splines and multiquadrics. Moreover, the polynomial in Equation 3.9 is added for a special proof technique of nonsingularity of the extended interpolation system. A comprehensive study of RBF interpolation can be found in the book of Buhmann [58].

3.4.2. Adaptive Meshless Method

Using an adaptive algorithm to choose the location of the collocation points is of great advantage in order to increase accuracy. The RBF methods produce results similar to the more well-known and analyzed spectral methods, but while allowing greater flexibility in the choice of grid point locations as demonstrated in [8]. The adaptive RBF methods are most successful when the basis functions are chosen so that the PDE solution can be approximated well with a small number of the basis functions.

It has generally been accepted, at least for problems in one space dimension, that adaptive grid methods are capable of resolving PDE solutions that contain regions of rapid variation with acceptable accuracy and without using an excessive number of grid points. Adaptive grid methods and applications in one space dimension, have been extensively studied. Many one-dimensional adaptive grid algorithms for time-dependent PDEs in the context of finite difference, finite element, and pseudospectral methods have been described in [8].

The adaptive RBF methods are used to maintain an overall high order of accuracy. The algorithm prepared is simple and computationally inexpensive in that it is not necessary to transform the original PDE into a new coordinate system, nor is it necessary to solve an additional companion PDE to choose the coordinate system and node distribution. Other algorithms may result in different, and possibly “better” grids, but for our purposes, we wish to examine the features of the RBF methods will remain very similar, regardless of the particular adaptive algorithm used.

Adaptive grid algorithms might be implemented to the nodes on the boundary and maybe some nodes in the domain where a fluctuation possibility may occur. It depends on the modeler who has an insight for any difficulties. Studies [8, 22, 23, 24] give very good

examples for adaptive grid algorithm and adaptive meshless methods using radial basis functions.

An exciting node distribution for different time steps can be seen in [24]. It has been claimed that it facilitates the approximation in order to get high accuracy numerical solutions of the problems.

3.4.3. Symmetric Collocation Method

A variation of the RBFCM that leads to a symmetric coefficient matrix was derived by Wu mentioned in [44]; see also Fasshauer's [11]. It has been shown for this method that the symmetry assures a non-singular system of equations.

The idea is to modify the basis functions in the interpolant by using the operator in the partial differential equation that is being studied. For each node, we look at what the operator is and then apply it to the basis function centered in that point.

Let us consider a general linear time-dependent equation of the form,

$$\frac{\partial u}{\partial t} + Lu(x,t) = f(x,t), \quad x \in \Omega \in R^d \quad (3.14)$$

$$Bu(x,t) = g(x,t), \quad x \in \partial\Omega \in R^d \quad (3.15)$$

where Ω denotes a closed physical domain over which the PDE is to be solved, $\partial\Omega$ denotes its boundary and d is the dimension of the problem. Here, L is a linear differential operator and B is an operator which imposes the boundary conditions. “ $u(x, t)$ ” is the desired field solution and $f(x,t)$, $g(x,t)$ are prescribed functions.

For collocation, we use nodal points distributed both along the boundary (x_j ; $j = 1, 2, \dots, N_B$), and over the interior (x_j ; $j = N_B + 1, \dots, N_B + N_I = N$). In general with “c” shape parameter,

MQ-RBFs are,

$$\phi(r) = (r^2 + c^2)^{\beta/2}, \quad \beta > 0 \text{ and } \beta \in 2N+1 \quad (3.20)$$

TPS-RBFs are,

$$\phi(r) = r^\beta \ln r, \quad \beta > 0 \text{ and } \beta \in 2N \quad (3.21)$$

where N refers to set of natural numbers. In matrix element formulation, in most cases we use 2-D implementation, for MQs β is taken 1, and for thin-plate splines β will be tested from first order to fourth order of function, say $\beta = 2, 4, 6, 8$. The following radial basis functions express the multiquadrics (3.21) and thin-plate splines (3.26) explicitly in terms of space variables.

MQ-RBFs and its first order and second order derivatives can be written as in 2-D,

$$\phi(\mathbf{x}_i, \mathbf{x}_j) = \left[\left(\sqrt{(x_i - x_j)^2 + (y_i - y_j)^2} \right)^2 + c^2 \right]^{1/2} \quad (3.22)$$

$$\phi^x(\mathbf{x}_i, \mathbf{x}_j) = \frac{x_i - x_j}{\phi(\mathbf{x}_i, \mathbf{x}_j)} \quad (3.23)$$

$$\phi^y(\mathbf{x}_i, \mathbf{x}_j) = \frac{y_i - y_j}{\phi(\mathbf{x}_i, \mathbf{x}_j)} \quad (3.24)$$

$$\phi^{xx}(\mathbf{x}_i, \mathbf{x}_j) = \frac{1}{\phi(\mathbf{x}_i, \mathbf{x}_j)} - \frac{(x_i - x_j)}{\phi^3(\mathbf{x}_i, \mathbf{x}_j)} \quad (3.25)$$

$$\phi^{yy}(\mathbf{x}_i, \mathbf{x}_j) = \frac{1}{\phi(\mathbf{x}_i, \mathbf{x}_j)} - \frac{(y_i - y_j)}{\phi^3(\mathbf{x}_i, \mathbf{x}_j)} \quad (3.26)$$

TPS-RBFs and its first order and second order derivatives can be written as in 2-D,

$$\phi(\mathbf{x}_i, \mathbf{x}_j) = \left[\sqrt{(x_i - x_j)^2 + (y_j - y_j)^2} \right]^\beta \ln \left[\sqrt{(x_i - x_j)^2 + (y_i - y_j)^2} \right] \quad (3.27)$$

$$\phi^x(\mathbf{x}_i, \mathbf{x}_j) = (x_i - x_j) r_{ij}^{\beta-2} (\beta \ln r_{ij} + 1) \quad (3.28)$$

$$\phi^y(\mathbf{x}_i, \mathbf{x}_j) = (y_i - y_j) r_{ij}^{\beta-2} (\beta \ln r_{ij} + 1) \quad (3.29)$$

$$\phi^{xx}(\mathbf{x}_i, \mathbf{x}_j) = r_{ij}^{\beta-2} (\beta \ln r_{ij} + 1) + (x_i - x_j)^2 r_{ij}^{\beta-4} \{2(\beta - 1) + \beta(\beta - 2) \ln r_{ij}\} \quad (3.30)$$

$$\phi^{yy}(\mathbf{x}_i, \mathbf{x}_j) = r_{ij}^{\beta-2} (\beta \ln r_{ij} + 1) + (y_i - y_j)^2 r_{ij}^{\beta-4} \{2(\beta - 1) + \beta(\beta - 2) \ln r_{ij}\} \quad (3.31)$$

The MQ-RBF has the property of being continuously differentiable which allows for the approximation of higher order derivatives. The MQ-RBF, which is positive definite, can be used by itself in approximation. However, the TPS-RBF is only conditionally positive definite and must be augmented by a global function in general .

In all of our test cases and problems, β is taken 1 for MQ-RBF approximation, and Thin-Plate Splines are investigated from the first-order to the fourth order of approximation function. In most of the studies, $r^2 \ln r$ and $r^8 \ln r$ yield almost no solution or have singularity problem due to nature of the radial basis function at most time, it is again tested to verify these judgements. If your problem has no exact solution or any experimental data to compare with, start numerical solution using MQ-RBF with a convenient shape parameter, as a suggestion by Wu and Hon it is supposed to be valid $c = 4r_{\min}$, tune up and down the parameter, and carefully observe what is happening. You will sense the suitable solution for your problem which is out of the region including large fluctuating absurd results.

The RMS error is computed at the end, it is evaluated for the final time of the time interval when the solution becomes stable and then the shape parameter optimization curves are obtained. All the curves have similar characteristics. Finally, the shape

parameters are determined for different time step sizes. Time step has a little effect on RMS error. But range is very important for the convergence. It is expressed clearly on each table and figure.

4. DEFINITION OF THE PROBLEMS

4.1. The Linear Advection-Diffusion Problem

The solution of the advection-diffusion equation is a long standing problem and many numerical methods have been introduced to model accurately the interaction between advective and diffusive processes. This modelling is the most challenging task in the numerical approximation of the partial differential equations and the available numerical solutions are very sophisticated in order to avoid two undesirable features: oscillatory behavior and numerical diffusion, which are mainly due to the advection term when it dominates [1].

The numerical solution of this equation is a difficult task because of two reasons; Firstly, the nature of the governing equation, which includes first-order and second-order partial derivatives in space. According to the value of κ (diffusion coefficient) and v (advection coefficient), the equation becomes parabolic for diffusion dominated processes or hyperbolic for advection dominated processes. Traditional finite difference methods are generally accurate for solving the former but not the latter, in which case oscillations and smoothing of the wave front are introduced. This can be interpreted as the artificial diffusion intrinsic to these methods [1].

The advection-diffusion equation is the basis of many physical and chemical phenomena [20]. A large number of problems in physics, chemistry and other branches of science can be modeled by the advection-diffusion equation. Especially, advection-diffusion processes occur in many evolutionary problems, such as fluid dynamics, transport of pollutants, heat and mass transfer,... etc [23]. For example,

- the steady-state distribution of a passive substance dissolved in water and transported by the flow as in the paper including groundwater contaminant
- transport modeling [49], transport of multiple reacting chemicals,
- the dispersion of atmospheric tracers or the far-field transport of decaying radio nuclides through a porous medium,

can all be described by the advection-diffusion equation. And its use has also spread into economics, financial forecasting and other fields. Industrial problems involving the solution of the advection-diffusion equations range from the solution of fluid dynamic problems such as,

- the galvanization of steel sheets and alloy solidification,
- heat transfer applications such as the temperature increase in current carrying wires, the water jet cooling of a moving hot rolled steel strip,
- financial applications such as the variation of asset prices in stock-market [1].

The mathematical difficulty of the advection–diffusion equation arises when the diffusion is very small. Solutions may present boundary layers together with long diffusive lengths that make difficult to approximate them. When the diffusion is very small and classical second-order methods are considered, many grid points are necessary to obtain reliable solutions [23]. It is well known that finite difference and finite element solutions of the advection-diffusion equation present numerical problems of oscillations and damping [20]. In order to avoid such limitations, the radial basis functions method application has demonstrated that this meshless method has great advantages in approximating over traditional methods.

In general the advection-diffusion problem is defined in the following form,

$$\frac{\partial u(\mathbf{x},t)}{\partial t} = \kappa \nabla^2 u(\mathbf{x},t) + v \cdot \nabla u(\mathbf{x},t), \quad x \in \Omega \subset R^d, \quad t > 0 \quad (4.1)$$

Together with the general boundary and initial conditions,

$$c_1 u(\mathbf{x},t) + c_2 \cdot \nabla u(\mathbf{x},t) = f(\mathbf{x},t), \quad x \in \partial\Omega, \quad t > 0 \quad (4.2)$$

$$u(\mathbf{x},t) = u_0(\mathbf{x}), \quad t = 0 \quad (4.3)$$

where $u(\mathbf{x}, t)$ is the temperature or any other passive scalar at the position \mathbf{x} at the time t , $\mathbf{x} = (x_1, x_2, \dots, x_d)$ is the vector position, d is the dimension of the problem, ∇ the gradient differential operator, Ω is the bounded domain in \mathbf{R}^d , $\partial\Omega$ the boundary on Ω , κ is the diffusion coefficient, $\mathbf{v} = [v_x, v_y, v_z]^T$ the advection coefficient or advective velocity vector, c_1 is a known constant and c_2 is a known advective velocity vector, and $u_0(\mathbf{x})$ is a known function. The advective velocity field is assumed to be divergence free, say $\nabla \cdot \mathbf{v} = 0$ in both the continuous and discrete sense. For the ensuing the analysis, both the advective and diffusion coefficients are constant [1]. The rate of advection of a flow to its rate of diffusion is often called Peclet number. At low Peclet numbers were studied in the thesis. ($Pe = v / \kappa$)

Many problems were solved for different coefficient of advection and diffusion in the literature. You may review the papers to observe how the differences occur when either advection or diffusion coefficients are dominated [1, 8, 20, 49].

The linear advection-diffusion problem with a constant advection and diffusion coefficient in 1-D will be handled. Then a test problem will be solved to exemplify an application of radial basis functions method to nonlinear case using time dependent Burgers' equation in 1-D. After that, the nonlinear advection-diffusion problem in 1-D will be evaluated for different sources at a given location on the domain. Burgers' equation and the linear advection-diffusion equation in 2-D are available in the Appendix C.

From [27], we have a linear advection-diffusion problem in one dimension. In this case, we consider a column initially free of solute and subjected to a continuous source u_0 at the inlet. The following is the governing equation for advection-diffusion reduced to one-dimensional case,

$$\frac{\partial u}{\partial t} = \kappa_x \frac{\partial^2 u}{\partial x^2} + v_x \frac{\partial u}{\partial x} \quad (4.4)$$

The domain of the problem is in 1-D, the independent space variable x interval is $0 \leq x \leq 100$ and N is the total number of nodes on the defined domain. The nodes are $x_1, x_2, x_3, \dots, x_N$.

The initial condition is,

$$u(x, t) = u(x, 0) = 0, \quad x > 0, \quad t = 0 \quad (4.5)$$

The boundary conditions are,

$$u(x_1, t) = u_0 \quad u(x_N, t) = 0 \quad t > 0 \quad (4.6)$$

The exact solution is given as,

$$u(x, t) = \frac{u_0}{2} \left[\operatorname{erfc} \left(\frac{x + v_x t}{2\sqrt{\kappa_x t}} \right) + \exp \left(\frac{-v_x x}{\kappa_x} \right) \operatorname{erfc} \left(\frac{x - v_x t}{2\sqrt{\kappa_x t}} \right) \right] \quad (4.7)$$

The constants are $u_0 = 1$, $\kappa_x = 0.5$, $v_x = -1$ and $Pe = -2$ for uniformly distributed nodes on domain. A total of $nt = 401$ time steps were used with $\Delta t = 0.1$ given in the tables.

4.2. Time Dependent Burgers' Equation in 1-D

To further assess the robustness of the radial basis functions method, a nonlinear test case, the popular time dependent Burgers' equation in 1-D was solved. This nonlinear equation is taken into account in many studies and solved using numerical methods. The time dependent Burgers' equation in 1-D can be given,

$$\frac{\partial u}{\partial t} = \kappa_x \frac{\partial^2 u}{\partial x^2} + u \frac{\partial u}{\partial x} \quad (4.8)$$

The domain in 1-D and the time interval in seconds are,

$$-1 \leq x \leq 1 \quad , \quad 0 \leq t \leq 1.1 \quad (4.9)$$

The analytical solution is given as below for the governing equation,

$$u(x,t) = \frac{0.1e^a + 0.5e^b + e^c}{e^a + e^b + e^c} \quad (4.10)$$

where a , b and c are functions of x and t given as,

$$a = -\frac{(x + 0.5 + 4.95t)}{20\kappa_x}, \quad b = -\frac{(x + 0.5 + 0.75t)}{4\kappa_x}, \quad c = -\frac{(x + 0.625)}{2\kappa_x} \quad (4.11)$$

where $\kappa_x = 0.0035$ and the problem is evaluated in the time interval defined above.

The initial and the boundary conditions should be specified from analytical solution. The nonlinear term might be discretized properly to determine the u values easily. Surely, “ u ” vector in nonlinear term must be in a square matrix.

4.3. The Nonlinear Advection-Diffusion Problem in 1-D

As defined in [9], the spreading of a localized monolayer of dilute, insoluble surfactant, discharged from a point source that moves at constant speed over a thin liquid film coating a planar substrate, is described according to lubrication theory by a pair of coupled nonlinear evolution equations for the monolayer concentration u , and the film depth “ l ”. A single nonlinear advection-diffusion equation involving u alone is used here to show the extent and structure of such spreading asymmetric monolayer. Gravity generates horizontal pressure gradients that ensure that “ l ” remains approximately uniform. So, in one dimensional planar geometry, film deformation generally has only a modest effect on the rate of spreading of a monolayer. The governing equation is written as,

$$\frac{\partial u}{\partial t} + \frac{\partial u}{\partial x} = \nabla \cdot (lu \nabla u) \quad (4.12)$$

An approximation to the surfactant concentration may be obtained by neglecting the effects of flow-induced film deformation by setting $l = 1$. The governing nonlinear advection-diffusion equation in 1-D can then be written as,

$$\frac{\partial u}{\partial t} + \frac{\partial u}{\partial x} = \frac{\partial}{\partial x} \left(u \frac{\partial u}{\partial x} \right) \quad (4.13)$$

If we write the equation explicitly, we obtain,

$$\frac{\partial u}{\partial t} + \frac{\partial u}{\partial x} = \left(\frac{\partial u}{\partial x} \right)^2 + u \frac{\partial^2 u}{\partial x^2} \quad (4.14)$$

Finally, the governing equation can be rearranged to read,

$$\frac{\partial u}{\partial t} = \left(\frac{\partial u}{\partial x} \right)^2 + u \frac{\partial^2 u}{\partial x^2} - \frac{\partial u}{\partial x} \quad (4.15)$$

A line source problem will be solved. The evolution will be for three different source strengths at a given location. This one dimensional version of the equation retains the symmetry-breaking effects of advection, but ignores transverse spreading. The domain of the problem in 1-D and the time interval are given as,

$$-10 \leq x \leq 130 \quad , \quad 1 \leq t \leq 101 \quad (4.16)$$

The time interval starts with the initial condition at $t = 1$. s and provides the conditions below for the left and the right extreme points,

$$u(0,t) = t^\beta \quad , \quad \text{when } |x| \rightarrow \infty \quad u \rightarrow u_\infty \quad (4.17)$$

with $u_\infty \rightarrow 0$ and $\beta < 1$. The equation is integrated numerically from $t = 1$ using the initial condition,

$$u(x,1) = \begin{cases} u_\infty + (1-u_\infty)\cos^2(x/u_w) & , \quad |x| < x_w \\ u_\infty & , \quad |x| \geq x_w \end{cases} \quad (4.18)$$

where $x_w = u_w\pi/2$ and $u_w = 0.41$ and the node intensity should be carefully adjusted according to these restrictions for the initial condition. Numerical solutions are obtained for $u_\infty = 0.01$ at times $t = 21, 41, 61, 81$ and 101 for different source strengths.

Different source strengths are employed to location where $x = 0$. Those figures below show the source schemes which one applied on the given location in the time interval $1 \leq t \leq 101$. Boundary condition on the left side of the domain, say at $x = -10$, will remain constant which shall be obtained from the initial condition. Other boundary conditions should be inserted to qualify variations in the vicinity of the center $x = 0$.

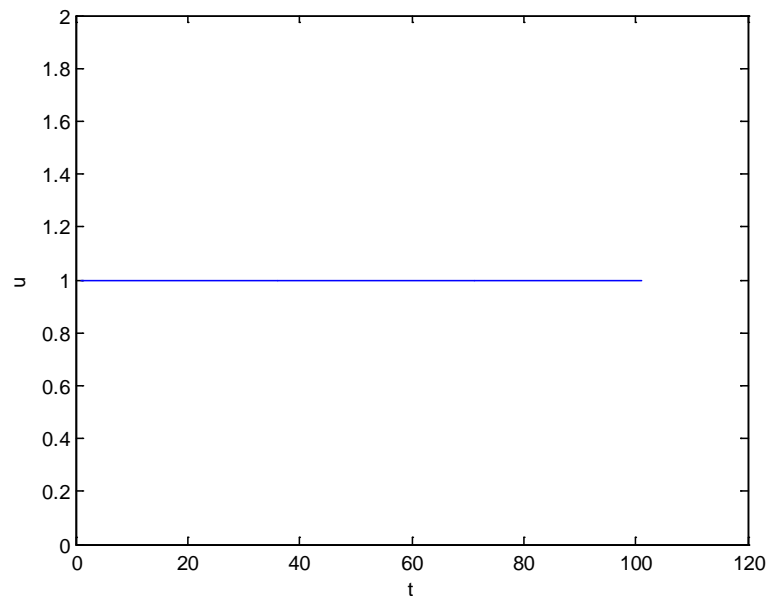


Figure 4.1. Time evolution of concentration “u” given at $x = 0$

$$u(x=0, t) = t^\beta, \beta = 0$$

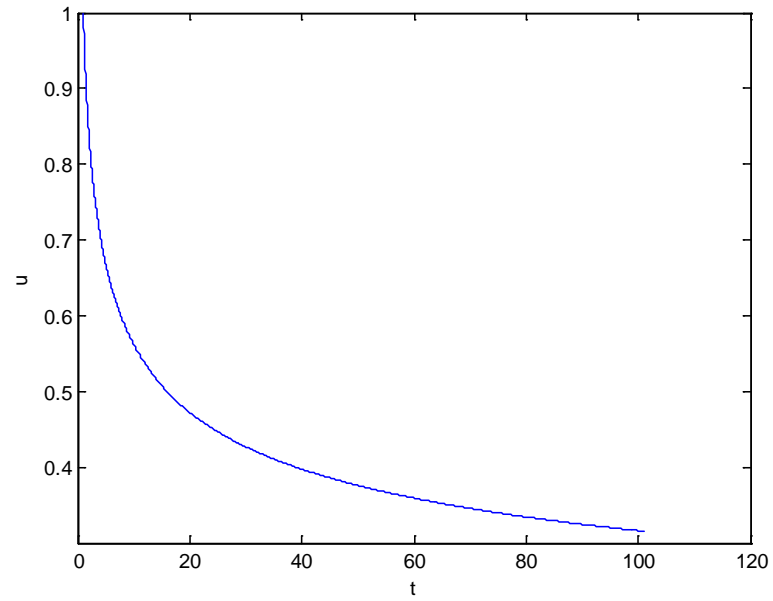


Figure 4.2. Time evolution of concentration “u” given at $x = 0$

$$u(x = 0, t) = t^\beta, \beta = -1/4$$

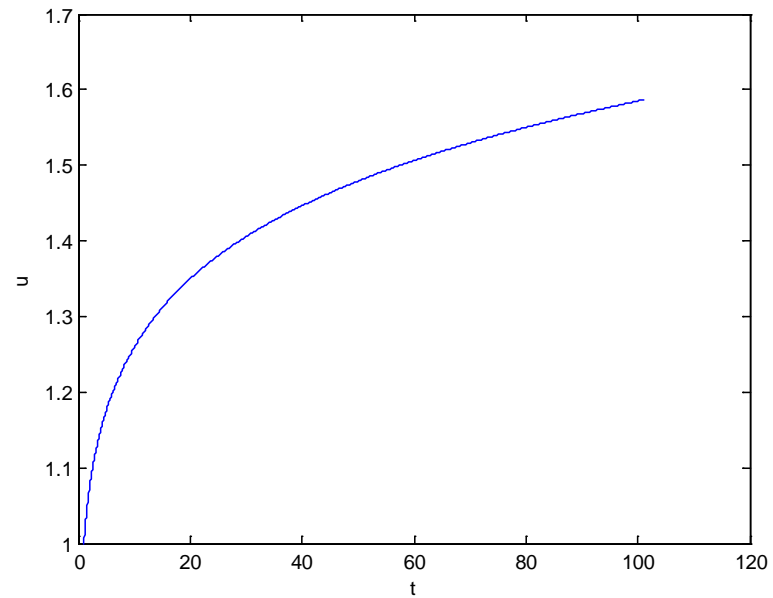


Figure 4.3. Time evolution of concentration “u” given at $x = 0$

$$u(x = 0, t) = t^\beta, \beta = 1/10$$

In the Equation 4.15, the term $(\partial u / \partial x)^2$ is linearized by using single term production. Then, one term of $(\partial u / \partial x)$ is referred to as new values of u , the other is called old values of u . After that assignment, iteration has been carried out. Finally, approximate u values have been found considering the convergence between the old and the new values by iteration process.

4.4. Viscoelastic Flow Problems

Fluid structure analysis varies according to different approaches. Continuum mechanics point of view or macroscale view is common in most part of the fluid science. Fluids are categorized whether they have suitable behaviour in consistency with Newtonian Law. Most of the fluids can not be grouped as Newtonian fluid. So, those so-called non-Newtonian fluids have different structure to be determined in microscale or molecular point of view apart from Newtonian fluids. It has brought up the rheology concept.

Rheology is the study of deformation and flow of matter: mainly liquids but also soft solids or solids under conditions in which they flow rather than deform elastically. One of the subareas of rheology is the development of constitutive equations (or rheological equations of state) that relate suitably defined stress and deformation variables. It is shown in the following Table 4.1 to define the concept clearly. It applies to substances which have a complex structure, including muds, sludges, suspensions, polymers, many foods, bodily fluids, and other biological materials. The flow of these substances cannot be characterized by a single value of viscosity (at a fixed temperature) instead the viscosity changes due to other factors as characterized in Newtonian fluids.

Table 4.1. Rheology Concept

Continuum Mechanics	Solid Mechanics or Strength of Materials	Elasticity	
		Plasticity	Rheology
	Fluid Mechanics	Non-Newtonian Fluids	
		Newtonian Fluids	

Many fluids exhibit a stress–strain relation which is not linear, as it is in the simple Newtonian case, and, in addition, stress can depend upon past strain history. These fluids are physically represented, for example, by polymer solutions, melts or fibre suspensions to mention but a few. The importance of such liquids for industrial applications is today well-established and, accordingly, potentially high is the impact that a full physical understanding of them could have on many manufacturing processes. Improvements and contributions in the area of the so-called “computational rheology” have been very impressive in recent years as evidenced by the vast literature appearing on specific journals and the appearance of an increasing number of general reviews on this topic [47].

Theoretical aspects of rheology are the relation of the flow/deformation behaviour of material and its internal structure (e.g. the orientation and elongation of polymer molecules), and the flow/deformation behaviour of materials that cannot be described by classical fluid mechanics or elasticity.

The rheological properties of materials are specified in general by their so-called constitutive equations. These equations determine the flow behavior of the respective materials in arbitrary types of motion. The simplest constitutive equation for a fluid is a Newtonian one. The departure from Newtonian behavior of many real fluids, especially those of high molecular weight, manifests itself in these materials in many ways. After much experimenting and theorizing it has been concluded that a new and non-linear constitutive equation for the stress is required [50].

The following Figure 4.4 illustrates the process for the solution of general viscoelastic fluid mechanics problems. In contrast to Newtonian fluid mechanics, non-Newtonian fluid mechanics has had to be concerned with the development of general constitutive equations for viscoelastic fluids. These constitutive equations should in principle lead to the definition of flow properties that need to be measured to define the viscoelastic fluid (rheometry) and to the development of the equivalent Navier Stokes equations for the solution of all possible boundary value problems. The process is completed by solution of the appropriate equations, where the methods of computational fluid mechanics have been required; analytical methods for complex flows of viscoelastic fluids are generally difficult to obtain.

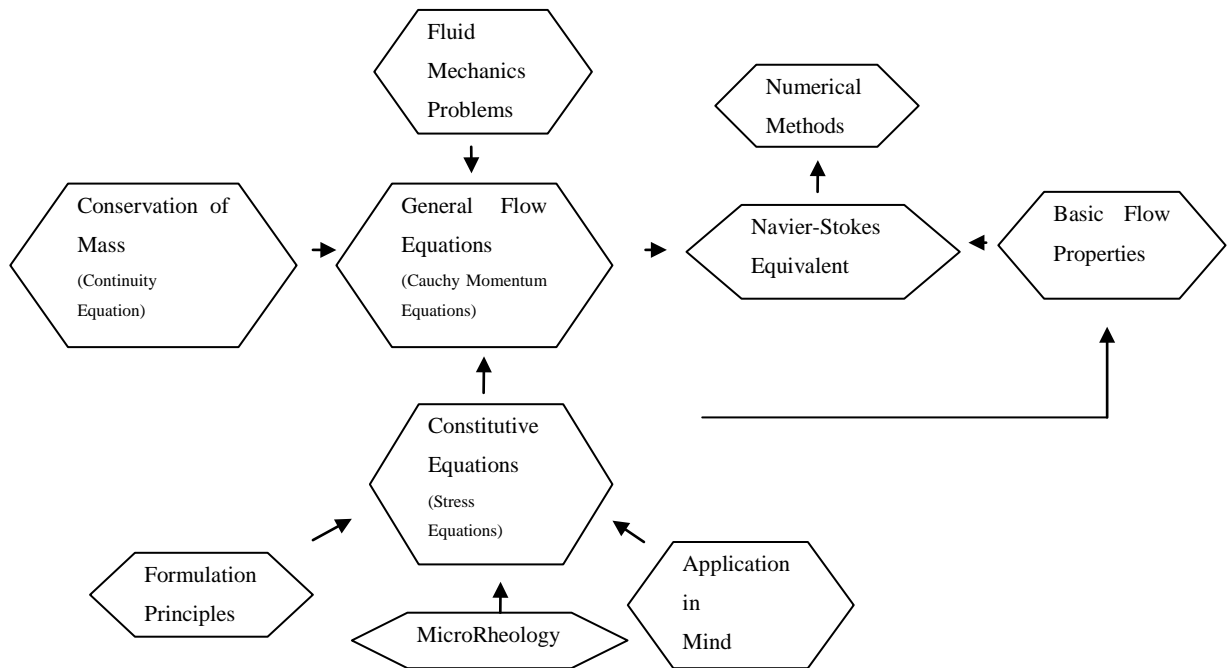


Figure 4.4. Numerical Solution Procedure of Viscoelastic Fluid Equations [51]

The viscoelastic models are categorized in three groups such as,

- Differential viscoelastic models
- Integral viscoelastic models
- Simplified viscoelastic models

The differential approach to modeling viscoelastic flow is appropriate for most practical applications. The numerical computation of viscoelastic fluid flows with differential constitutive equations presents various difficulties. The first one lies in the numerical convergence of the complex numerical scheme solving the nonlinear set of equations. Due to the hybrid type of these equations (elliptic and hyperbolic), geometrical singularities such as reentrant corner or die induce stress singularities and hence numerical problems. Another difficulty is the choice of an appropriate constitutive equation and the determination of rheological constants. For example the numerical simulation of polymer processing needs to take into account their complex viscoelastic rheological behavior. A large number of constitutive equations have been proposed and the selection of an adequate model is obviously a critical step in the simulation of viscoelastic flows.

Different criteria have to be considered but the constitutive equation should at least give satisfactory predictions in simple rheometrical flows. Furthermore, a numerical solution of the resulting governing set of equations must be possible [52].

Nonlinear differential constitutive equations are increasingly used to describe the rheology of viscoelastic fluids and in solving fluid mechanics problems of relevance to polymer melts and solutions. Analytical solutions of such problems provide strong insight and are also useful for validation and verification purposes. However, analytical solutions can only be obtained for simple constitutive models and/ or under simplifying flow conditions, such as flow symmetry and fully-developed flow conditions, which lead to integrable expressions. As a consequence, most of the studies in the literature concern single-mode models.

However, the complex rheology of viscoelastic polymer melts and polymer solutions usually requires the use of multimode models for an adequate description of the fluid behavior. The coupling between the various modes and the flow kinematics makes analytical solutions for multimode models a rather challenging task, so the tendency is to use computational rheology tools to obtain numerical solutions [53].

In this study, we deal with two models of viscoelastic fluids: Upper-Convected Maxwell and Oldroyd-B fluid ranking among the group of differential viscoelastic models. These models are different from each other in terms of the effect of retardation time.

As given in the paper [54], the multimode equations for UCM and Oldroyd-B fluids are reduced to one mode equations. The stress and the momentum equations are considered in one mode. In the reference section of that paper the assigned coefficients are included in the appendix up to mode of five. For simplicity, I applied the radial basis functions collocation method to UCM and Oldroyd-B model only for one mode equations. The efficiency of the method still remains acceptably well when applied to viscoelastic models.

Let's begin with the general fluid equations governing incompressible fluid flow. Then narrow the equations down to the viscoelastic models we study in the thesis. The following are the equations governing fluid flow,

- Mass conservation for an incompressible fluid gives,

$$\nabla \cdot \mathbf{U} = 0 \quad (4.19)$$

Where \mathbf{U} is the velocity and ∇ is the gradient operator and (\cdot) denotes the dot or scalar product,

- Momentum Conservation gives,

$$-\nabla p + \nabla \cdot \mathbf{T} + f = \rho \mathbf{a} \quad (4.20)$$

where ∇p is the gradient of hydrostatic or isotropic pressure p , \mathbf{T} is the total stress tensor, f represents the body forces per unit volume acting on the fluid such as gravity $f = mg$ or other fields of electromagnetic or centrifugal force, and \mathbf{a} is the acceleration.

The right side of the momentum equation above-mentioned is usually called inertia term of the equation. There, " \mathbf{a} " denotes the material derivative of velocity and it is defined as with material derivative operator $D(\)/Dt$,

$$\frac{D(\)}{Dt} = \frac{\partial(\)}{\partial t} + \mathbf{U} \cdot \nabla(\) \quad (4.21)$$

Then acceleration becomes,

$$\mathbf{a} = \frac{\partial \mathbf{U}}{\partial t} + \mathbf{U} \cdot \nabla \mathbf{U} \quad (4.22)$$

In the acceleration equation $\partial \mathbf{U} / \partial t$ is called unsteady acceleration term and the term $\mathbf{U} \cdot \nabla \mathbf{U}$ represents the convective acceleration.

The velocity equation is reduced as the following after requiring substitutions are done as in [54],

$$\left\{ \sum_{i=1}^{N+1} K_i \frac{\partial^{(i-1)}}{\partial t^{(i-1)}} \right\} \frac{\partial^2 U}{\partial y^2} - \rho \left\{ \sum_{i=0}^N \Lambda_i \frac{\partial^{(i+1)}}{\partial t^{(i+1)}} \right\} U = 0 \quad (4.23)$$

where the coefficients K_i and Λ_i are available in the appendix section of [54] and also the derivation of governing velocity equation is put into the Appendix B of the thesis. The boundary conditions for start-up flow are as follows,

$$U(0,t) = 0; \quad U(h,t) = V(t) \quad (4.24)$$

where h is the distance between the plates, $V(t) = V_0 H(t)$ or $V(t) = V_0(1 - \exp(-t/g))$ is the velocity of the upper plate, here $H(t)$ is the Heaviside step function and $g = 1$ [54]. The governing partial differential equation for velocity is reduced to the following equation.

$$\eta_1 \frac{\partial^2 U}{\partial y^2} + \eta_1 \lambda_{21} \frac{\partial}{\partial t} \left(\frac{\partial^2 U}{\partial y^2} \right) - \rho \frac{\partial U}{\partial t} - \rho \lambda_{11} \frac{\partial^2 U}{\partial t^2} = 0 \quad (4.25)$$

This is the general equation governing both the UCM and the Oldroyd-B fluid flow model. In this equation λ_{11} represents the relaxation time and λ_{21} is the retardation time for mode one. If we set to $\lambda_{21} = 0$ then UCM model is obtained otherwise the Oldroyd-B model is obtained.

We model the problem in one dimensional geometry. It is assumed as a unidirectional flow between two infinite plates. The lower plate is stationary constant and the upper plate is moved with a constant speed which is regarded as a start-up flow widely in the literature. The following figure is demonstrating the model considered with the given boundary conditions.

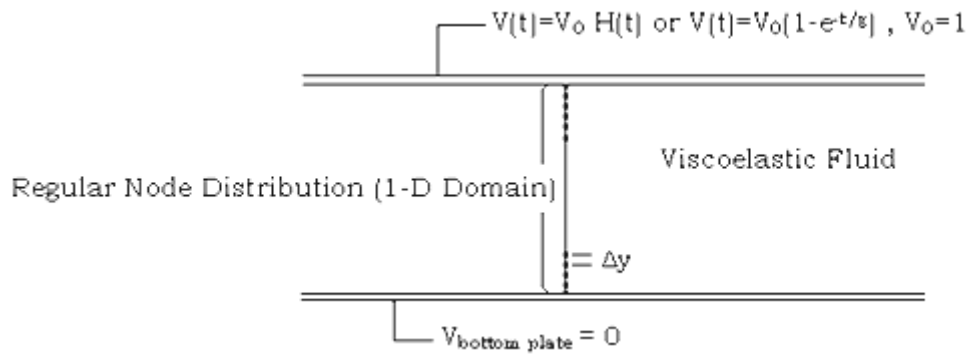


Figure 4.5. Domain for the Viscoelastic Problem

Time – marching for second order time integration is carried out using Houbolt method. For space discretization, the regular node distribution is done along the vertical path between two plates in one dimensional as shown in the figure.

The coefficient matrices are obtained using radial basis functions and Houbolt method together. Adjusting the initial vector for both UCM and the Oldroyd-B fluid to prevent shock input instabilities, we obtained good results in agreement with the results in the referenced paper using radial basis functions collocation method.

Upper-Convected Maxwell Viscoelastic Fluid Model :

The Governing Equation is given as,

$$\eta_1 \frac{\partial^2 U}{\partial y^2} - \rho \frac{\partial U}{\partial t} - \rho \lambda_{11} \frac{\partial^2 U}{\partial t^2} = 0 \quad (4.26)$$

After nondimensionalizing the equation above, we obtain the following equation.

$$E \frac{\partial^2 U}{\partial y^2} - We \frac{\partial U}{\partial t} - We^2 \frac{\partial^2 U}{\partial t^2} = 0 \quad (4.27)$$

In the Equation (4.27) "We" refers to Weissenberg Number which is a dimensionless number defined as the ratio of the relaxation time of the fluid and a specific process time. "Re" refers to Reynolds Number is a dimensionless number that gives a measure of the ratio of inertial forces to viscous forces. "E" is called Elasticity number, a dimensionless number which is a measure of the ratio of elastic forces to inertial forces on a viscoelastic fluid flowing, and is equal to the product of the fluid's relaxation time and its dynamic viscosity in general. It is given by,

$$E = \frac{We}{Re} \quad (4.28)$$

The dimensionless numbers are $We = 1$, $E = 1$, and $Re = 1$. The parameters used for the numerical solution of the viscoelastic cases are given in figures captions.

Oldroyd-B Viscoelastic Fluid Model :

Setting the retardation time $\lambda_{21} \neq 0$, we obtain the governing equation for Oldroyd-B fluid model as follows,

$$\eta_1 \frac{\partial^2 U}{\partial y^2} + \eta_1 \lambda_{21} \frac{\partial}{\partial t} \left(\frac{\partial^2 U}{\partial y^2} \right) - \rho \frac{\partial U}{\partial t} - \rho \lambda_{11} \frac{\partial^2 U}{\partial t^2} = 0 \quad (4.29)$$

and the equation becomes with the nondimensionalizing process as follows,

$$\frac{1}{Re} \frac{\partial^2 U}{\partial y^2} + 0.125E \frac{\partial}{\partial t} \left(\frac{\partial^2 U}{\partial y^2} \right) - \frac{\partial U}{\partial t} - 1.125We \frac{\partial^2 U}{\partial t^2} = 0 \quad (4.30)$$

The coefficients coming from the derivation for the governing equations can be found in the Appendix B of the thesis. The assigned constants are taken directly from the referenced paper [54]. The same boundary and the initial conditions are used for both models.

Boundary Conditions are given as,

$$U(x=0,t)=0 \quad \text{and} \quad U(x=h,t)=V(t) \quad (4.31)$$

Here $V(t)$ represents the Heaviside Step function or $V(t) = V_0(1-\exp(-t/g))$ and $V_0=1$ and the initial conditions must be adjusted for input velocities to prevent shock instabilities. Shock input causes divergence or bad-conditioned matrix in the numerical solution of the problem. Time difference should be maintained as small as possible for smooth and clear results.

5. RESULTS AND DISCUSSION OF THE PROBLEMS

5.1. The Linear Advection-Diffusion Problem

There are several applications of radial basis functions method to linear advection-diffusion equation with different approaches in the literature. In the study, the linear advection-diffusion problem is solved using radial basis functions meshless collocation method directly comparing the numerical solutions between multiquadrics, thin-plate splines and the given exact solution.

The governing Equation 4.3 is discretized using multiquadratic and thin-plate spline functions. The first and the second derivative of the dependent function are also discretized using radial basis functions. With the given boundary and the initial values, system matrix is constructed in order to evaluate the numerical solution.

The following figures are obtained using multiquadratic solutions with different number of nodes on the domain. Time step size effects are also investigated with error analysis. Error norm can be interpreted observing RMS errors which are inserted on the related tables.

In multiquadratic solutions, shape parameter optimization is carried out and optimum shape parameter is determined. Focusing on the final time of the time interval has provided to determine optimum shape parameter. The final time can be assumed the time at which solution of the problem becomes stable. RMS versus "c" shape parameter curves are plotted in order to verify how the shape parameter is determined. The minimum RMS error is observed to specify the optimum shape parameter.

In Matlab coding, to avoid from long computational time, large time shape parameter differences are used. The shape parameters determined on the tables can vary very little amount because of this reason.

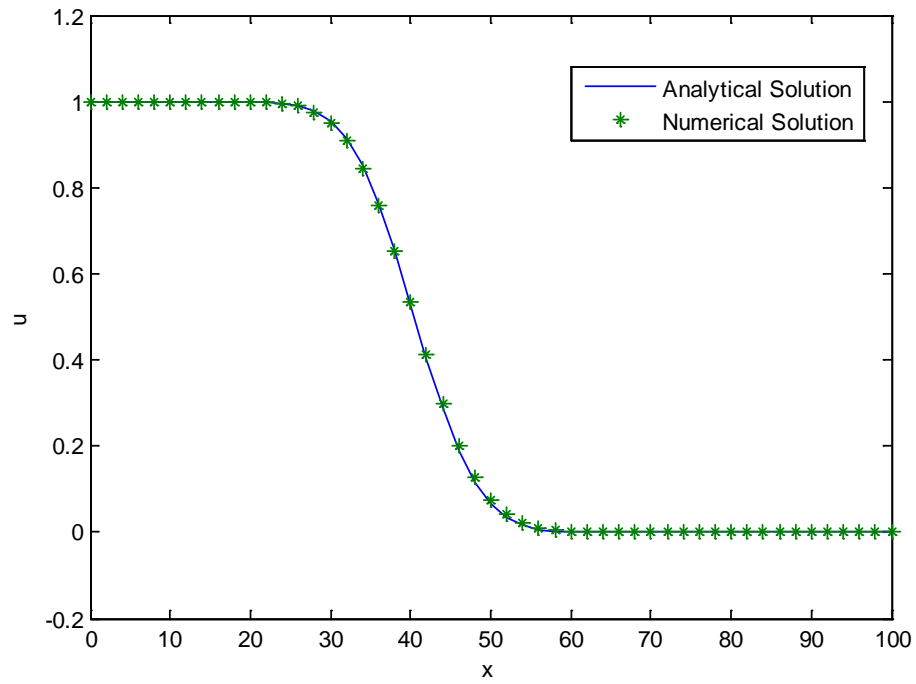


Figure 5.1. MQ-RBF Solution, $c = 14.6$, $N = 51$, $dt = 0.1$, $t = 40$ s, $RMS = 8.4087e-04$

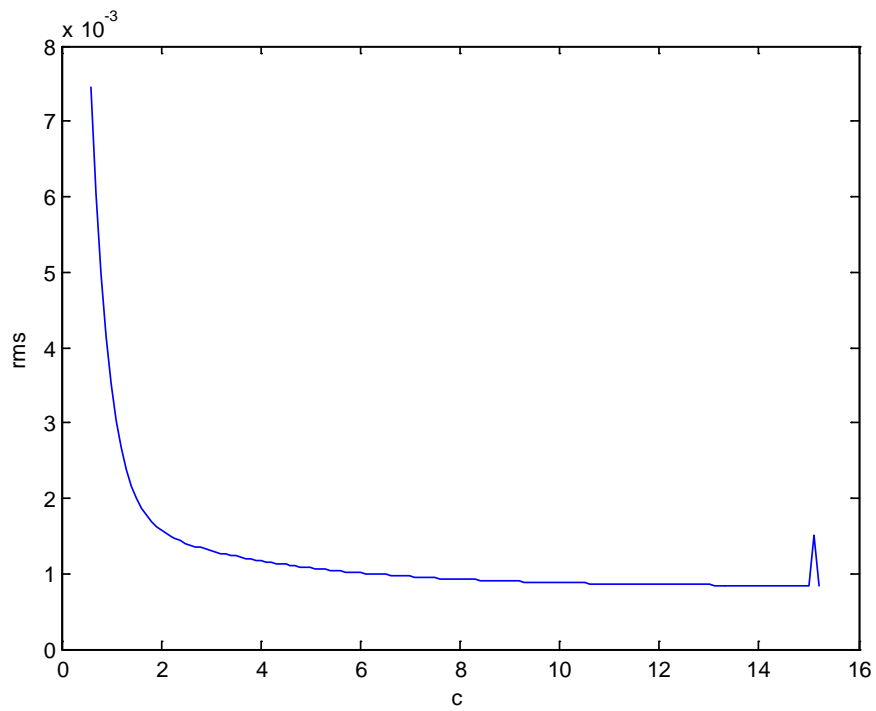


Figure 5.2. RMS and "c" vary, $N = 51$, $dt = 0.1$, $t = 40$ s

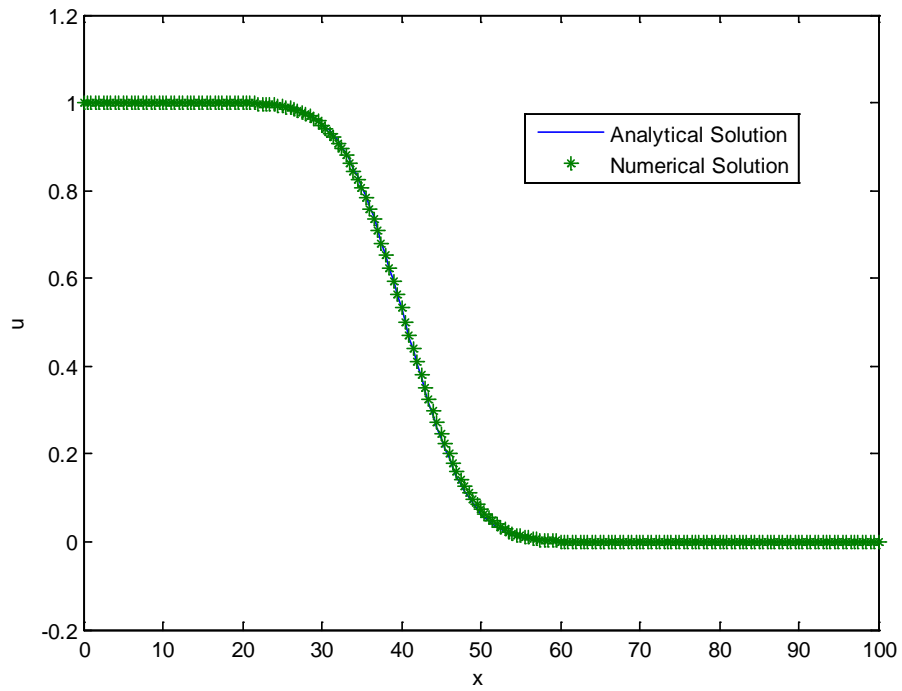


Figure 5.3. MQ-RBF Solution, $c = 0.8$, $N = 201$, $dt = 0.1$, $t = 40$ s, $RMS = 3.8667e-04$

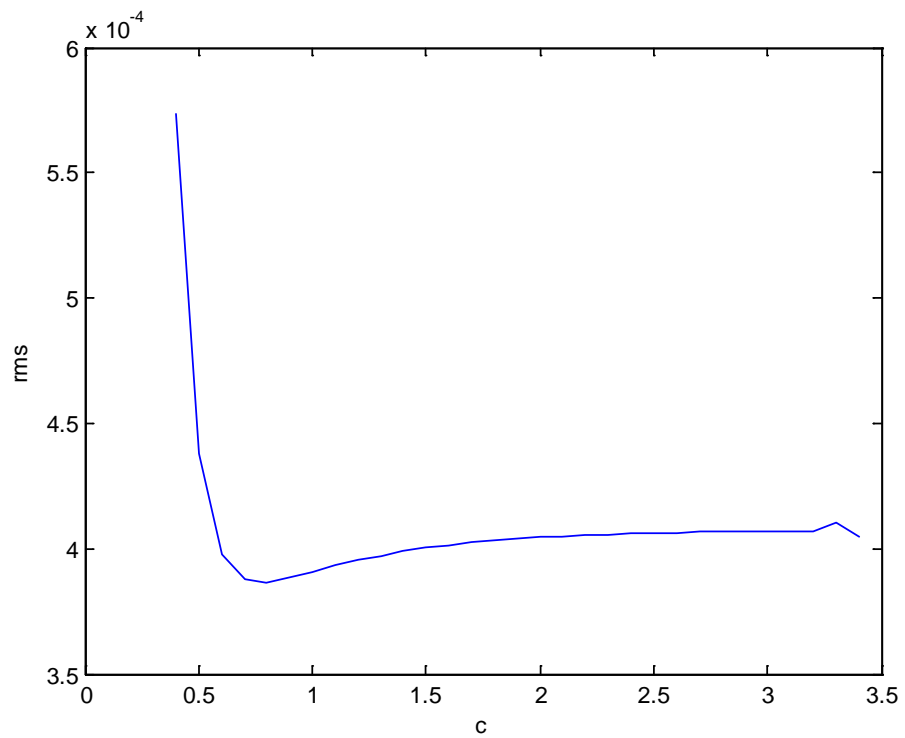


Figure 5.4. RMS and "c" vary, $N = 201$, $dt = 0.1$, $t = 40$ s

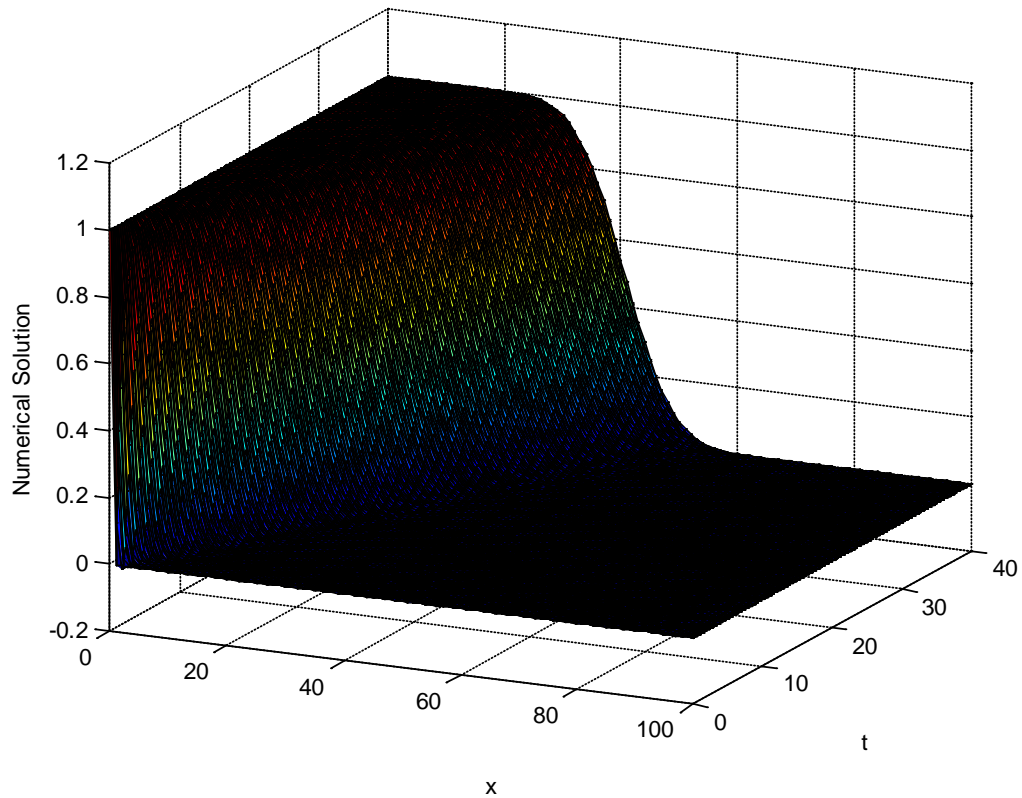


Figure 5.5. Numerical Solution, MQ-RBF, $c = 7$, $N = 101$, $dt = 0.1$

For the thin-plate splines, the spline functions from first order to fourth order were used. Only the unaugmented form of thin-plate spline functions are investigated. Due to the sensitivity of this type of function to number of nodes, for some situations we can not obtain any results because of the ill-conditioning of the coefficient matrix. The asterisk “ * ” in the table entries means no result has been found for the order of that function of splines. This can be explained as the coefficient matrix becoming singular or solution instability occurs. It may be overcome with the addition of polynomials to the approximation function.

RMS error decreases when the time step size has been lowered in the convergence range. It is deduced from the thin-plate splines approximation functions, the RMS error decreases as the number of nodes increases in a certain ranges. Figure 5.7 has been provided to demonstrate the decrease in error with increasing number of nodes.

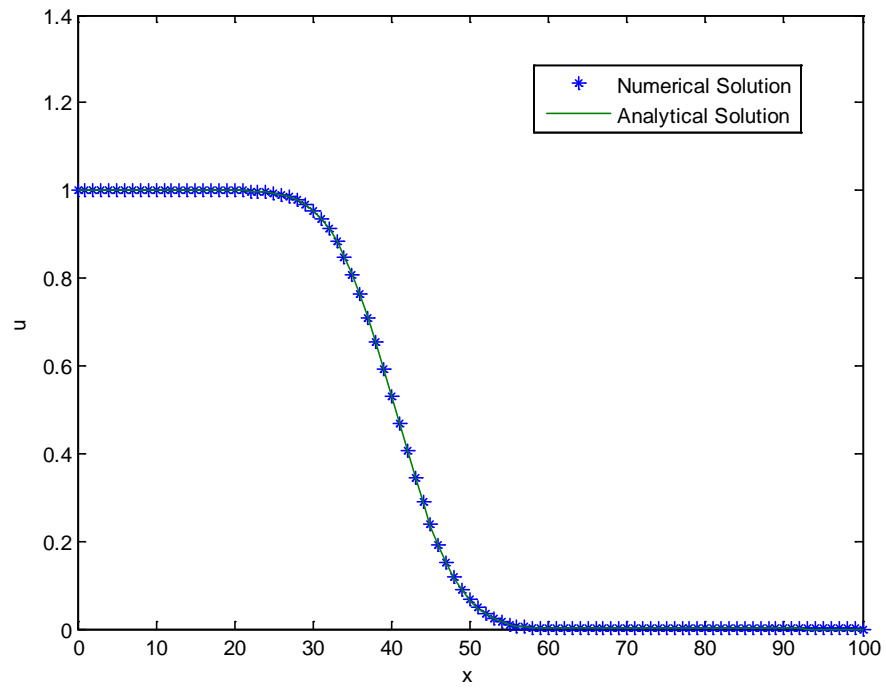


Figure 5.6. TPS-RBF solution, $m = 4$, $dt = 0.01$, $t = 40$ s, $RMS = 6.5059e-05$

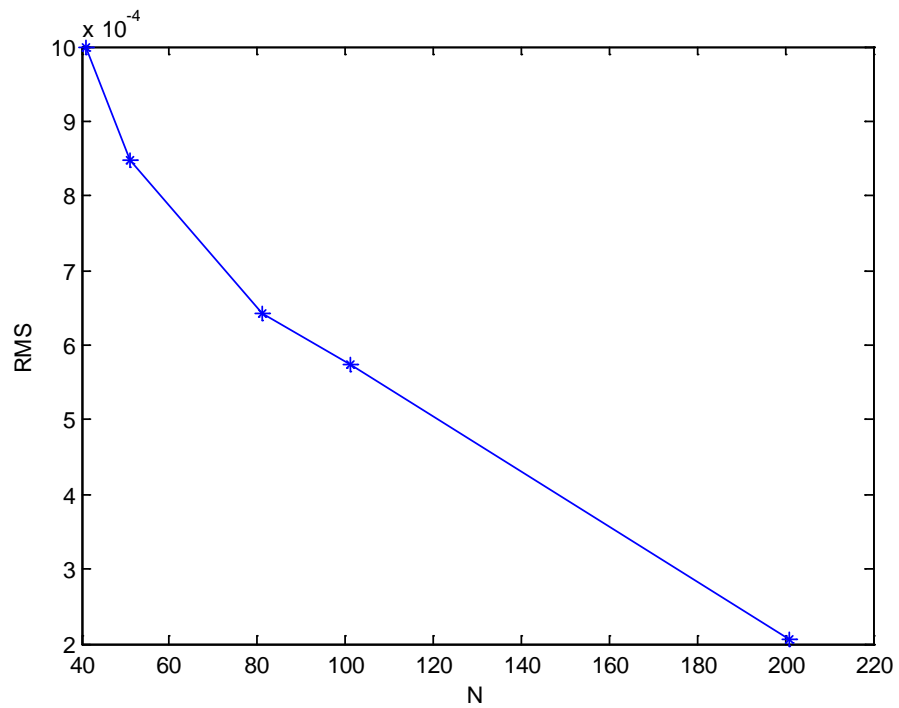


Figure 5.7. TPS-RBF solution, RMS vs. N , $m = 4$, $dt = 0.1$, $t = 40$ s

Table 5.1. MQ-RBF Solution of Problem 1, RMS errors

Problem 1					
RBF	Features of RBF optimum "c" or order of the TPS	Number of Nodes	Time Step	Time	RMS error
MQ	c = 19.1	41	0.1	t = 40 s	9,5163E-04
			0.01	t = 40 s	1,7902E-04
	c = 14.6	51	0.1	t = 40 s	8,4087E-04
	c = 14		0.01	t = 40 s	1,4528E-04
	c = 14		0.001	t = 40 s	8,5505E-05
	c = 9	81	0.1	t = 40 s	6,0678E-04
	c = 8.8		0.01	t = 40 s	7,8780E-05
	c = 8.5		0.001	t = 40 s	3,6258E-05
	c = 7	101	0.1	t = 40 s	5,7505E-04
			0.01	t = 40 s	5,6770E-04
	c = 0.8	201	0.1	t = 40 s	3,8667E-04
	c = 3.1		0.01	t = 40 s	4,4215E-05

Table 5.2. TPS-RBF Solution of Problem 1, RMS errors

Problem 1					
RBF	Features of RBF optimum "c" or order of the TPS	Number of Nodes	Time Step	Time	RMS error
TPS	m = 2	41	0.1	t = 40 s	2,5000E-03
	m = 4		0.1	t = 40 s	1,0000E-03
	m = 6		0.1	t = 40 s	8,1459E-04
	m = 8		0.1	t = 40 s	*
	m = 2	51	0.1	t = 40 s	1,6000E-03
	m = 4		0.1	t = 40 s	8,4664E-04
	m = 6		0.1	t = 40 s	7,6732E-04
	m = 2	81	0.1	t = 40 s	6,6438E-04
	m = 4		0.1	t = 40 s	6,4290E-04
			0.01	t = 40 s	8,3804E-05
			0.001	t = 40 s	4,4218E-05
	m = 2	101	0.1	t = 40 s	4,6079E-04
	m = 4		0.1	t = 40 s	5,7369E-04
			0.01	t = 40 s	6,5059E-05
			0.001	t = 40 s	2,2519E-05
	m = 2	201	0.1	t = 40 s	2,2733E-04
m = 4	0.05		t = 40 s	2,0547E-04	

5.2. Time Dependent Burgers' Equation in 1-D

As a test problem, the radial basis functions collocation method was used to solve Burgers' equation which is a nonlinear partial differential equation. The time dependent Burgers' equation in one dimension was chosen as a test case and satisfactory results were obtained.

The same approaches and approximation techniques for the solution of linear advection-diffusion equation were also used here. From the data given in the tables, after determining the optimum shape parameter it can be easily observed that the RMS error decreases as the number of nodes increases. Time difference has less impact on the RMS errors, but it cannot be ignored.

For multiquadric approximation, plots are given for number of nodes $N = 81$ and $N = 201$, then the shape parameter optimization is done. The plots are obtained using optimum shape parameter with an efficient time step.

For thin-plate spline solutions, the number of centers varies; $N = 51$, $N = 101$ and $N = 201$ were used. The plots show the essential information for this type of radial basis functions approximation. From Figure 5.12 and 5.13, the effect of the node number can easily be detected. Figure 5.15 once again demonstrates the thin-plate splines' sensitivity to nodes.

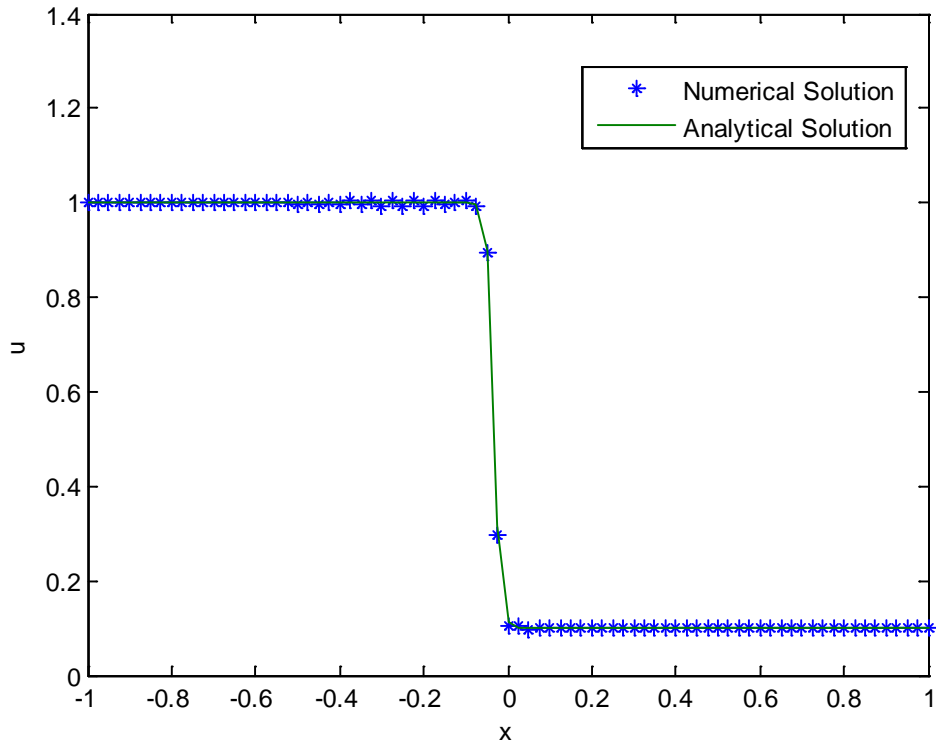


Figure 5.8. MQ-RBF, $N = 81$, $dt = 0.0001$, $c = 0.07$, $t = 1.1$ s, $RMS = 5.2135e-04$

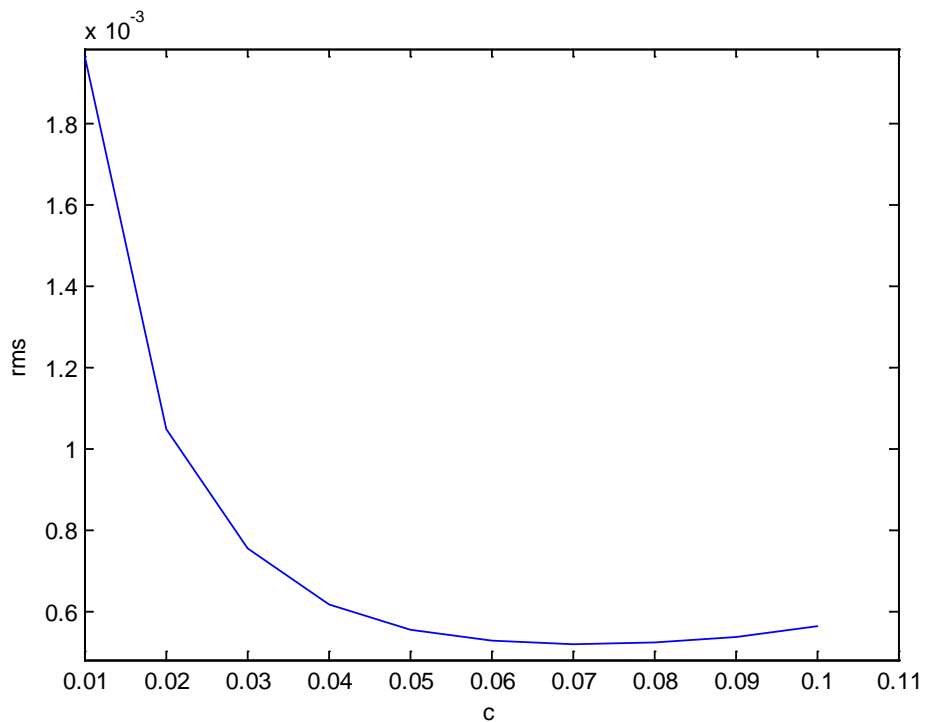


Figure 5.9. RMS and "c" vary, $N = 81$, $dt = 0.0001$, $t = 1.1$ s

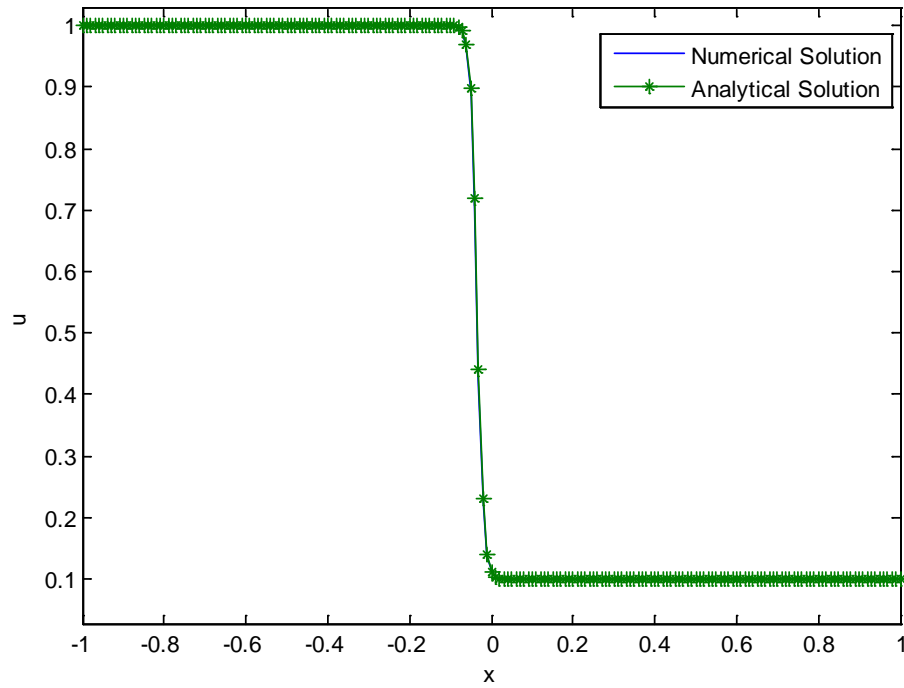


Figure 5.10. MQ-RBF , $N = 201$, $dt = 0.0001$, $t = 1.1$ s , $c = 0.01$, $RMS = 2.2391e-04$

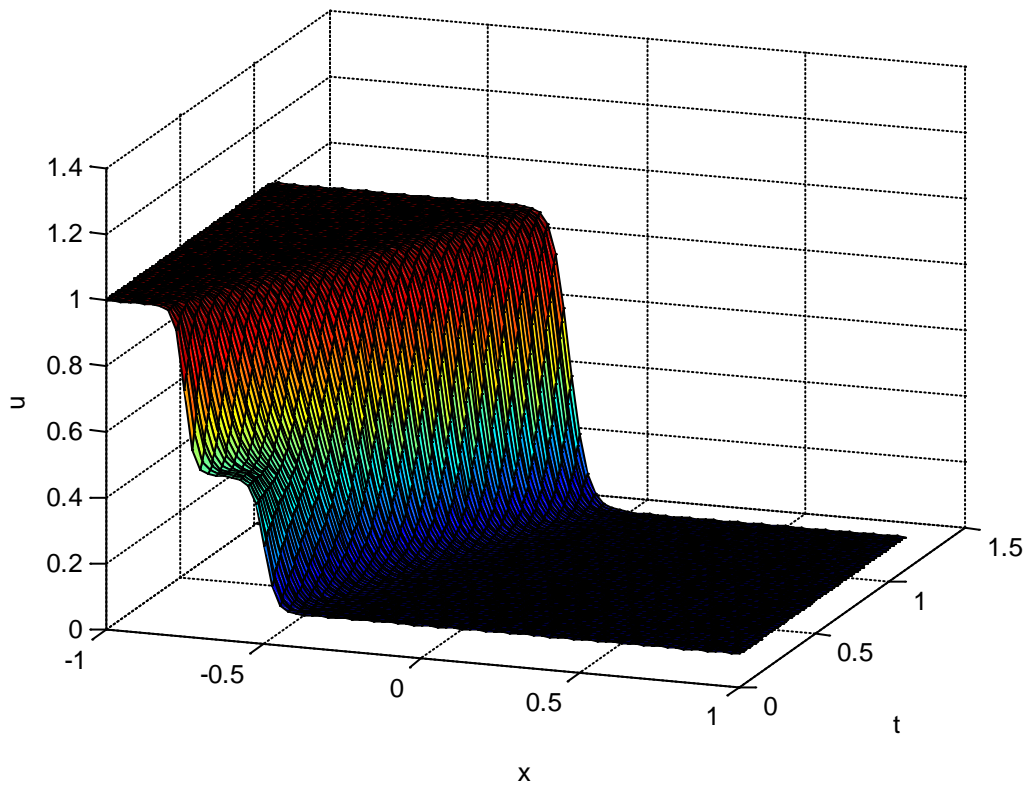


Figure 5.11. Numerical Solution, $N = 81$, $dt = 0.01$, $c = 0.004$, $RMS = 9.3000e-03$

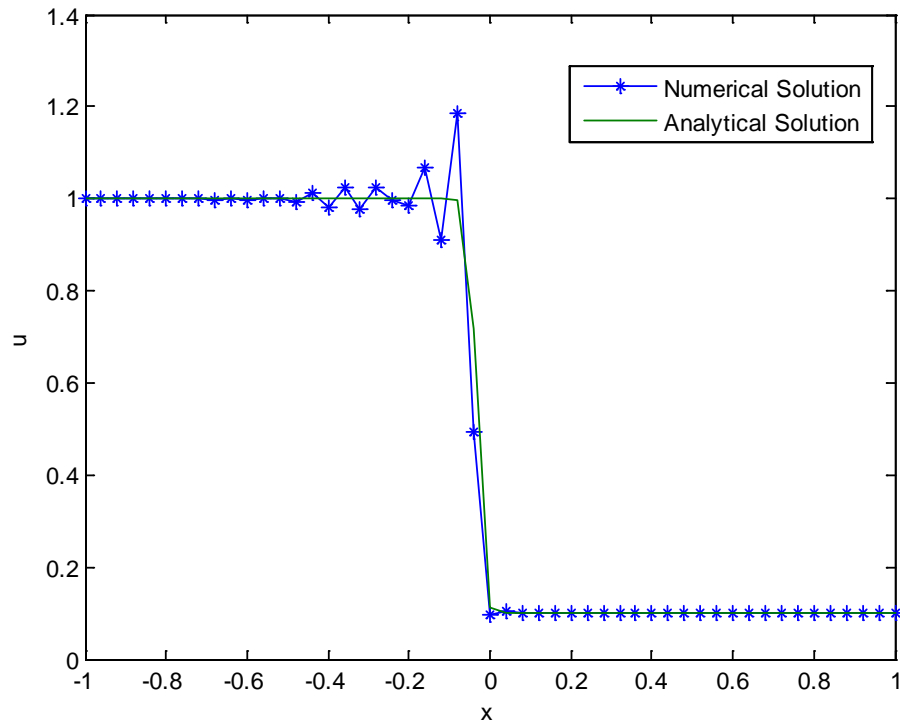


Figure 5.12. TPS-RBF, $m = 4$, $N = 51$, $dt = 0.0001$, $t = 1.1$ s, $RMS = 8.9000e-03$

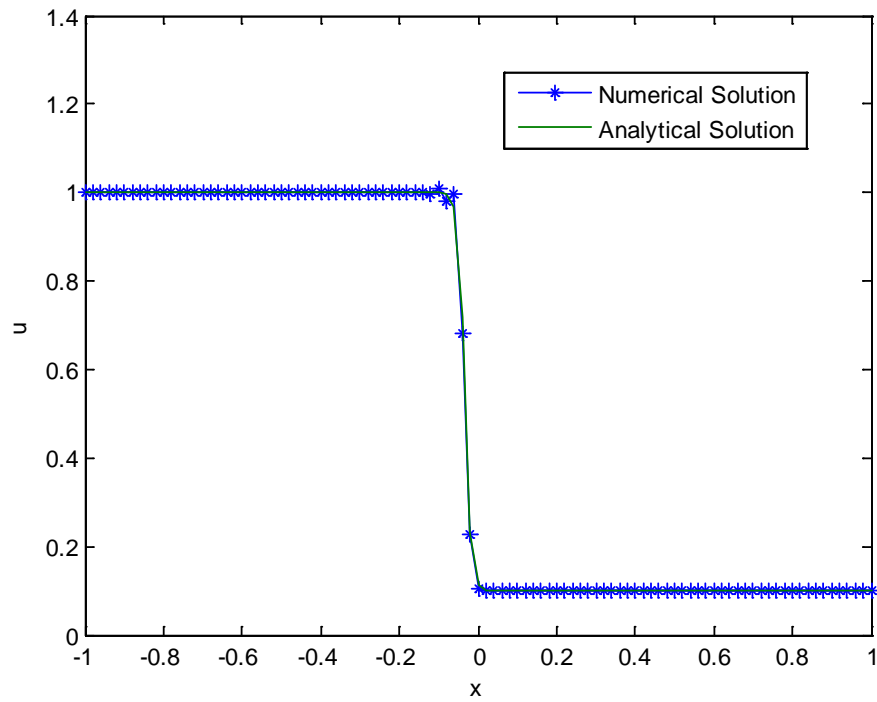


Figure 5.13. TPS-RBF, $m = 4$, $N = 101$, $dt = 0.0001$, $t = 1.1$ s, $RMS = 7.0384e-03$

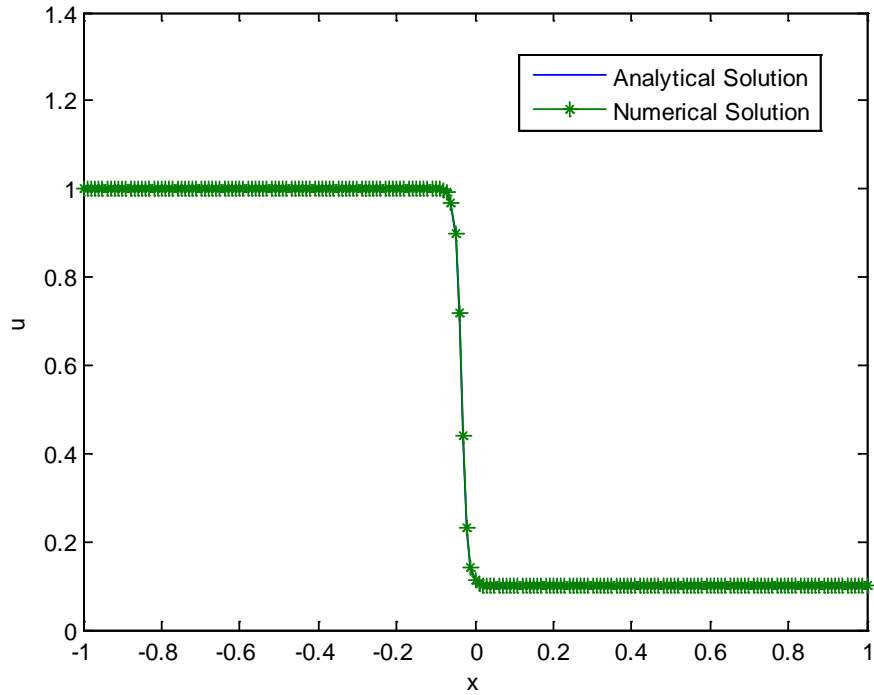


Figure 5.14. TPS-RBF, $m = 4$, $N = 201$, $dt = 0.0001$, $t = 1.1$ s, $RMS = 1.8529e-04$

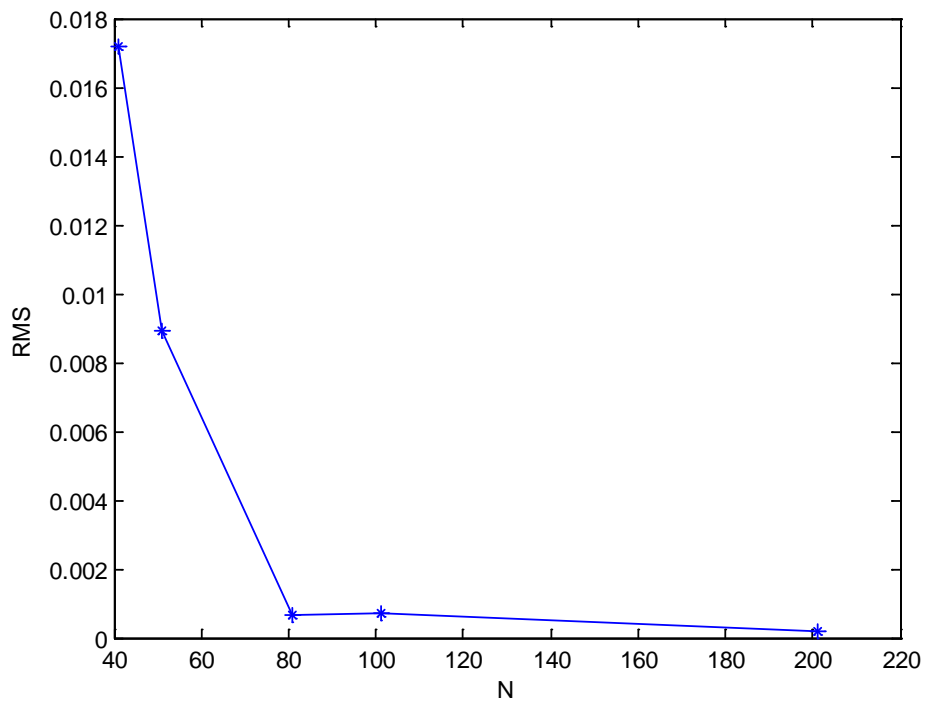


Figure 5.15. TPS-RBF, RMS vs. N , $m = 4$, $dt = 0.0001$, $t = 1.1$ s

Table 5.3. MQ-RBF Solution of Problem 2, RMS errors

Problem 2					
RBF	Features of RBF optimum "c" or order of the TPS	Number of Nodes	Time Step	Time	RMS error
MQ	c = 0.006	41	0.01	t = 1.1 s	1,6300E-02
	c = 0.006		0.001	t = 1.1 s	1,3100E-02
	c = 0.006	51	0.01	t = 1.1 s	1,2100E-02
	c = 0.006		0.001	t = 1.1 s	7,9000E-03
	c = 0.009		0.0001	t = 1.1 s	6,0000E-03
	c = 0.004	81	0.01	t = 1.1 s	9,3000E-03
	c = 0.080		0.001	t = 1.1 s	2,9000E-03
	c = 0.070		0.0001	t = 1.1 s	5,2135E-04
	c = 0.0032	101	0.01	t = 1.1 s	8,2000E-03
	c = 0.010		0.001	t = 1.1 s	2,6000E-03
	c = 0.005	201	0.001	t = 1.1 s	1,6000E-03
	c = 0.010		0.0001	t = 1.1 s	2,2391E-04

Table 5.4. TPS-RBF Solution of Problem 2, RMS errors

Problem 2					
RBF	Features of RBF optimum "c" or order of the TPS	Number of Nodes	Time Step	Time	RMS error
TPS	m = 2	41	0.001	t = 1.1 s	*
	m = 4		0.001	t = 1.1 s	1,7200E-02
	m = 6		0.001	t = 1.1 s	1,7800E-02
	m = 8		0.001	t = 1.1 s	*
	m = 2	51	0.001	t = 1.1 s	*
	m = 4		0.0001	t = 1.1 s	8,9000E-03
	m = 6		0.0001	t = 1.1 s	9,8000E-03
	m = 8		0.001	t = 1.1 s	*
	m = 2	81	0.01	t = 1.1 s	*
	m = 4		0.0001	t = 1.1 s	6,7592E-04
	m = 6		0.0001	t = 1.1 s	4,7470E-04
	m = 8		0.01	t = 1.1 s	*
	m = 2	101	0.01	t = 1.1 s	*
	m = 4		0.0001	t = 1.1 s	7,0384E-04
m = 6	0.001		t = 1.1 s	*	
m = 4	201	0.001	t = 1.1 s	1,8000E-03	
		0.0001	t = 1.1 s	1,8529E-04	

5.3. The Nonlinear Advection-Diffusion Problem in 1-D

The nonlinear advection-diffusion problem is solved using radial basis functions collocation method as an example of a highly nonlinear advection-diffusion case.

The governing equation (4.14) is again discretized using radial basis functions. The system matrix of the problem is carefully constructed considering the nonlinear terms. As the problem is nonlinear, the solution is iterative.

The initial condition which is defined in Equation (4.17) shows sharp variation in the vicinity of coordinate $x = 0$. The boundary conditions are determined according to this condition. Different source strengths which are applied at this location lead to different solutions. The curves for the sources are shown in figures 4.1, 4.2 and 4.3.

For multiquadric solution in 1-D, with $\beta = 0$ and $\beta = -1/4$, the domain is,

$$x = [-10 , x_1] \quad (5.1)$$

where the x vector is defined in terms of the x_1 vector given as,

$$x_1 = [-1 \quad 130] \quad (5.2)$$

The shape parameter is accepted as $c = 1$, and time step is taken as $dt = 0.04$. This is not the optimum shape parameter, but satisfies the solutions given in [53]. Using these, results which are in good agreement are obtained when compared with the results given in [53]. Providing those minimum conditions, great computational time decrease and efficiency has been found. But when $\beta = 1/10$, $N = 656$, time difference $dt = 0.005$ are considered. To eliminate the stability problem and to obtain more smooth curve, the number of nodes can be increased and time step can be decreased.

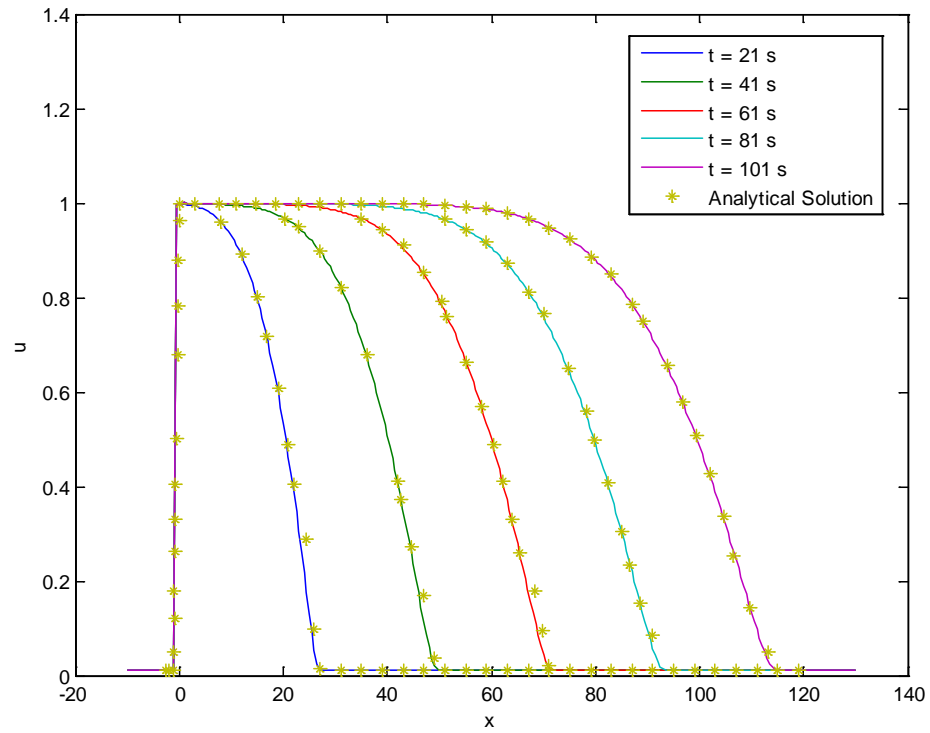
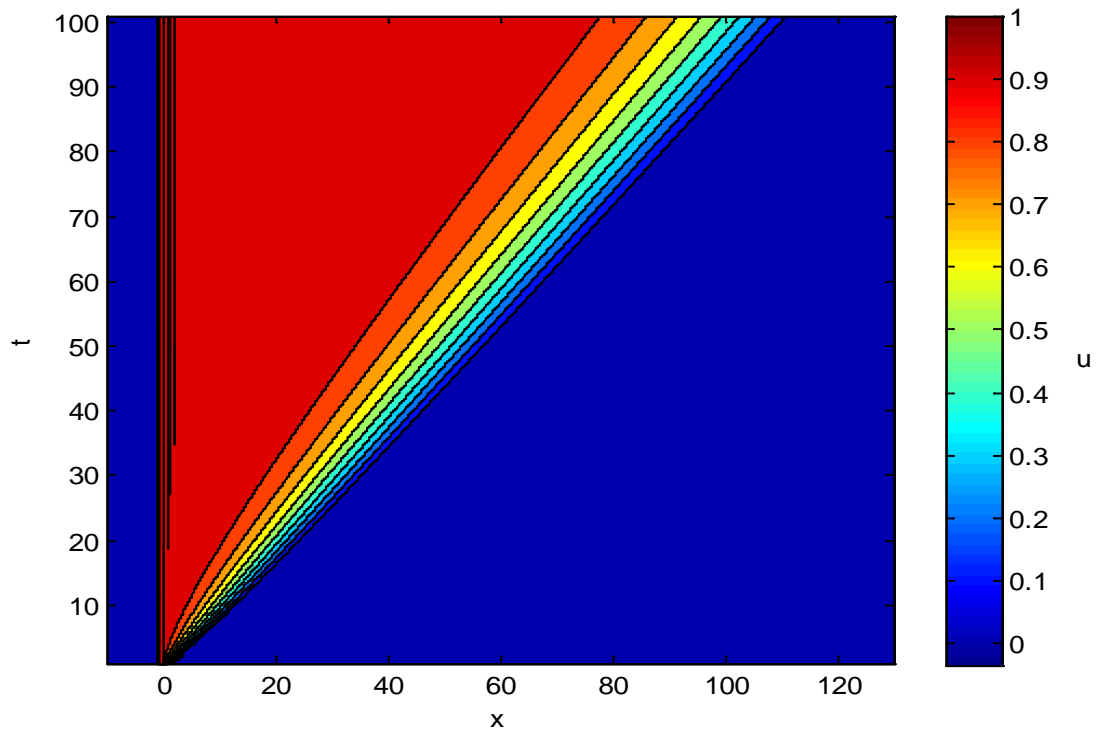


Figure 5.16. MQ-RBF solution, for $\beta = 0$, $N = 264$, $dt = 0.04$, $c = 1$



5.17. Time and spatial evolution of u , $\beta = 0$

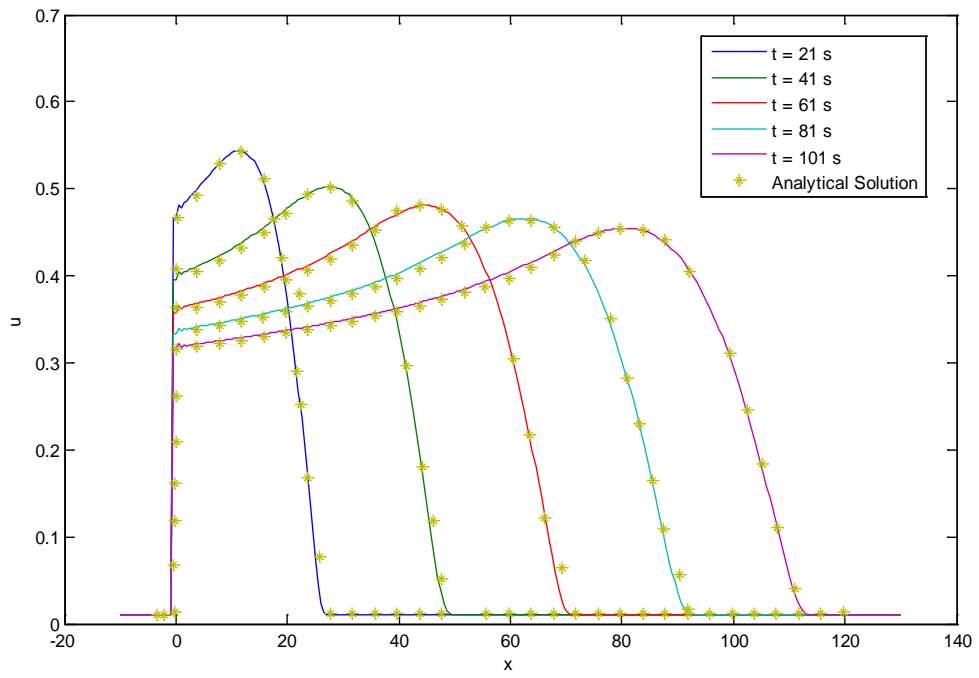
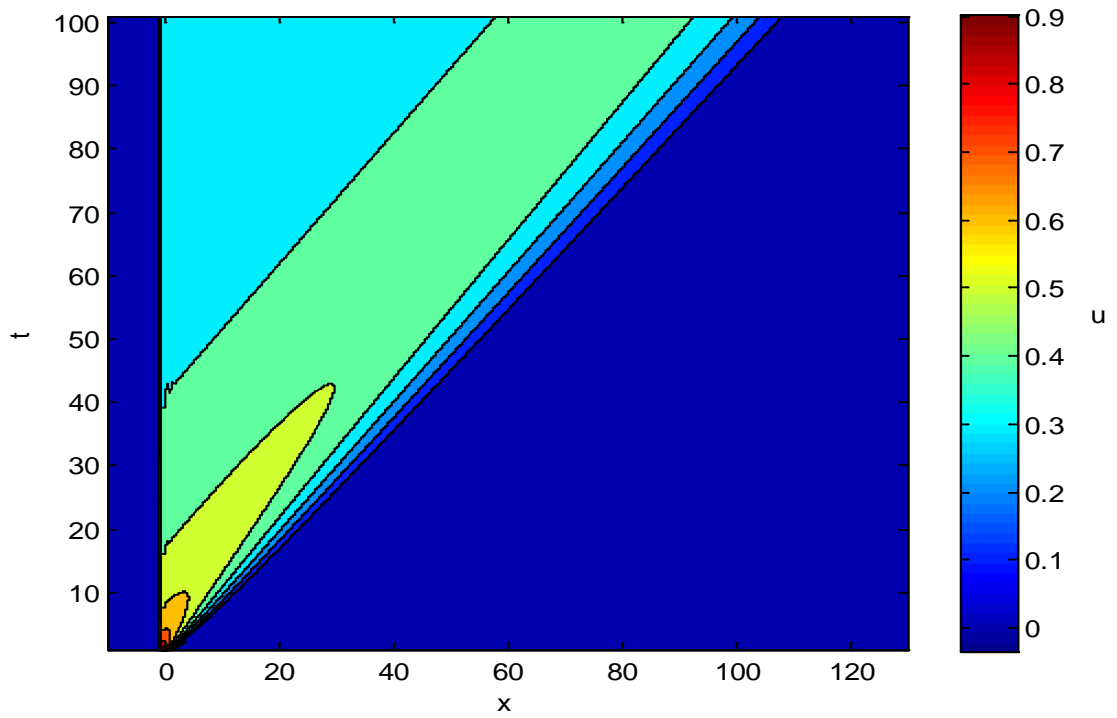


Figure 5.18. MQ-RBF solution, for $\beta = -1/4$, $N = 264$, $dt = 0.04$, $c = 1$



5.19. Time and spatial evolution of u , $\beta = -1/4$

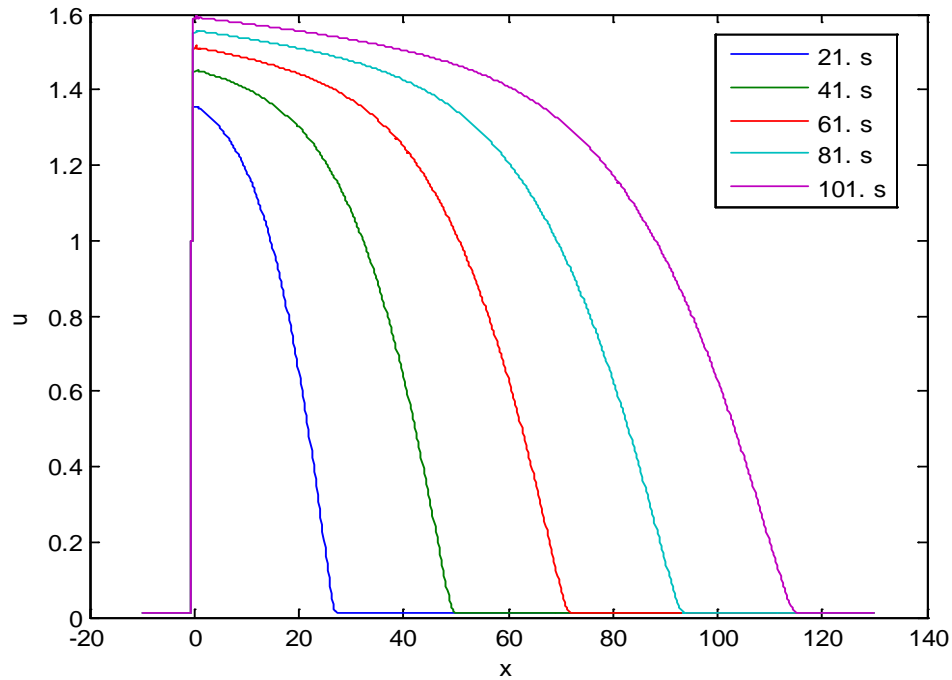


Figure 5.20. MQ-RBF solution, for $\beta = 1/10$, $N = 656$, $dt = 0.005$, $c = 0.2$

5.4. The Viscoelastic Flow Problem

The numerical solutions of two constitutive Equations 4.24 and 4.28 governing viscoelastic fluids using MQ-RBF and TPS-RBF method are investigated. These two equations are handled for one mode to simplify the solution. The momentum equation only consists of velocity as a dependent variable. This equation is considered with those parameters which are defined in [54].

The governing equation includes the second order time derivative. To approximate it, the popular and robust Houbolt method for the second order time integration was used. To start the procedure the first three steps must be determined. To this end, the dependent variables and their derivatives were written in the radial basis function discretization, then reduced with finite difference method to eliminate the terms with second order with respect to time. Finally, the first three initial vectors were obtained with Heaviside step function loading to the upper moving plate, the other values of vector were taken to be zero, after that, those vectors were substituted into Houbolt procedure to continue time marching process.

The important thing is that the initial vector must be prepared carefully because the shock disturbance could violate the solution. Step function loading contains the elements smaller than 1 at the initial vector then it is adjusted to satisfy the real initial step function loading. So, results are parallel with the results given in the related paper [54]. A few studies have been carried out to overcome the solution of this type of problem and different techniques have been used. Similar results are obtained which have same characteristics in agreement with the results in [54] for the centerline velocity profile.

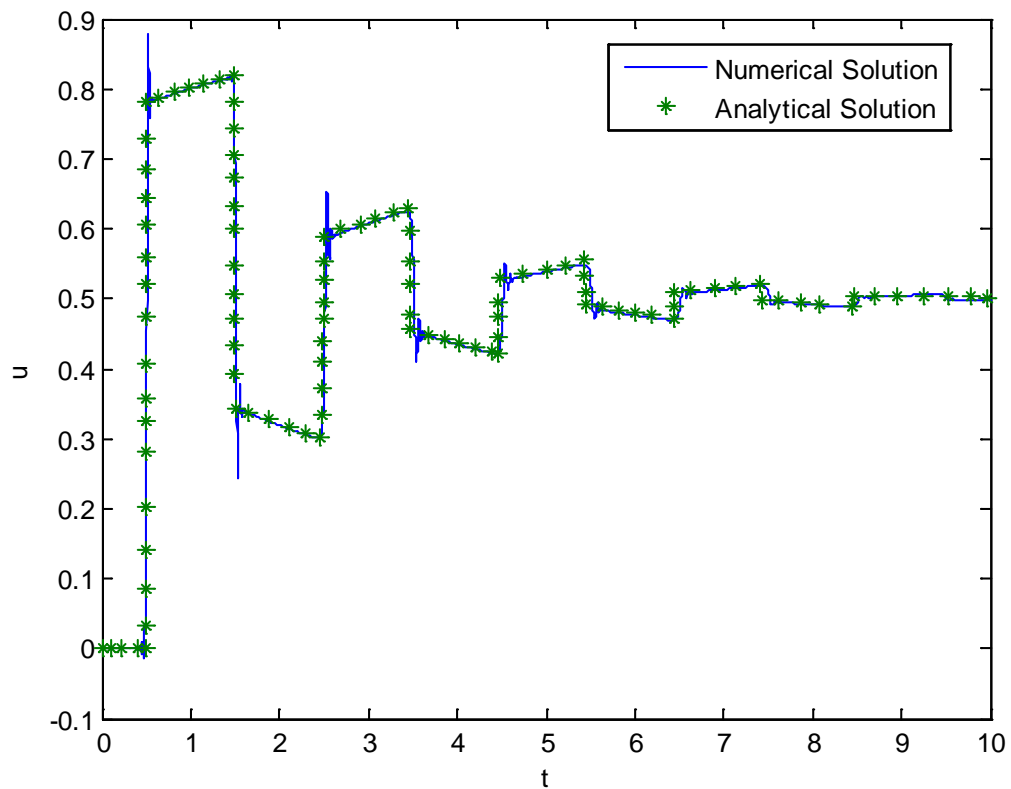


Figure 5.21. UCM Fluid, MQ-RBF solution, $\gamma = 0.5$, $N = 101$, $dt = 0.001$, $c = 0.02$, $E = 1$

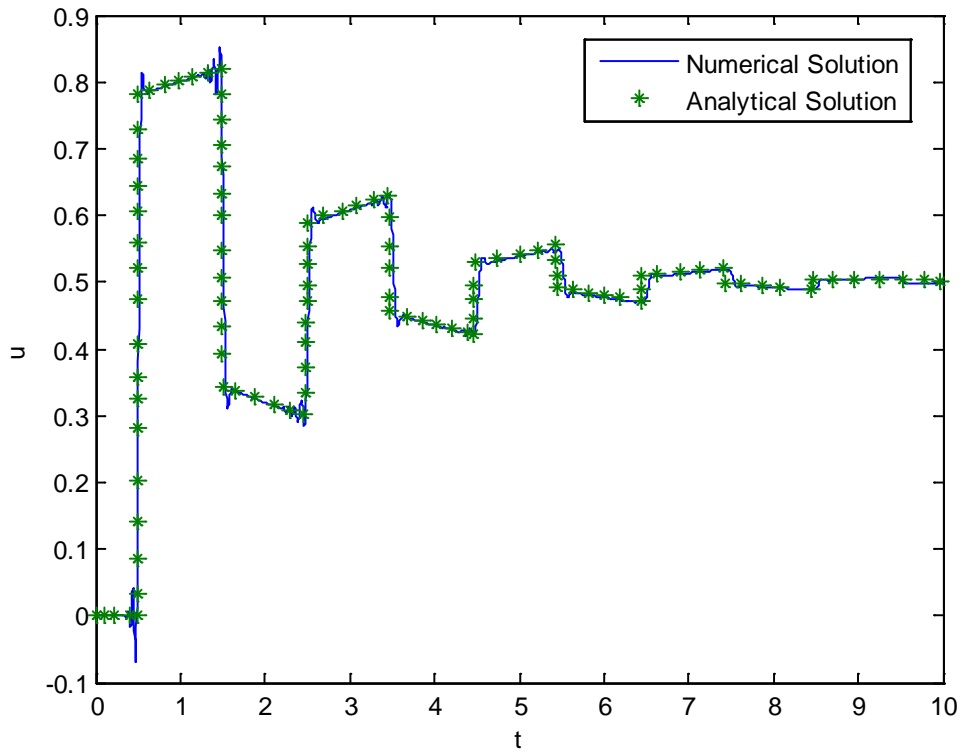


Figure 5.22. UCM Fluid, TPS-RBF (Augmented Approximation) solution, for $y = 0.5$,
 $N = 51$, $dt = 0.0025$, $m = 4$, $E = 1$

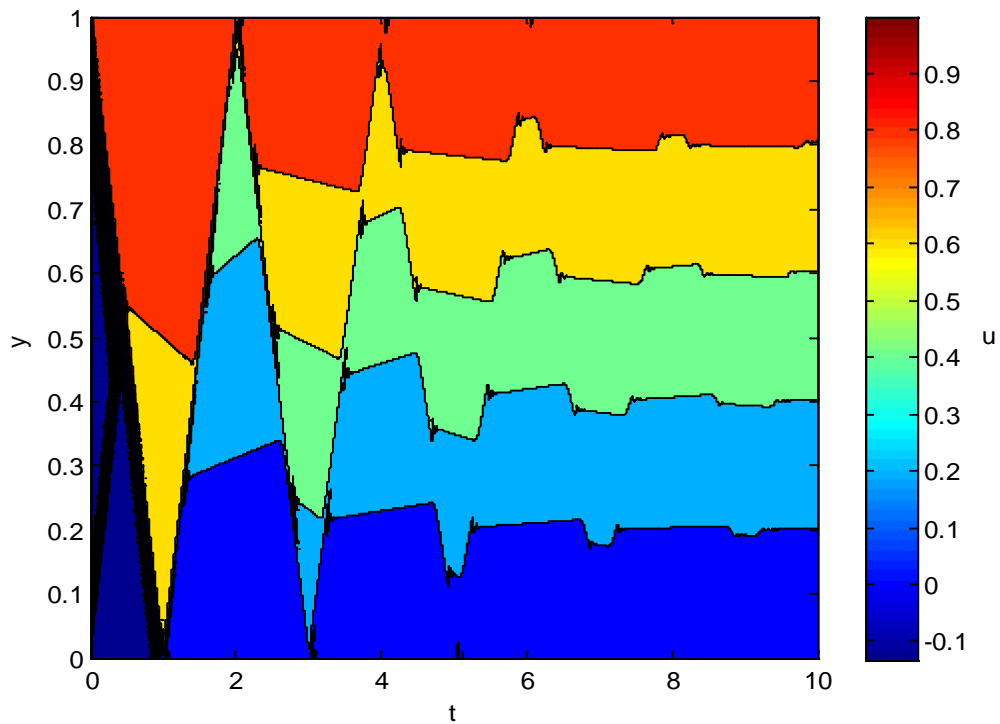


Figure 5.23 Time and spatial evolution of u , $N = 101$, $c = 0.02$

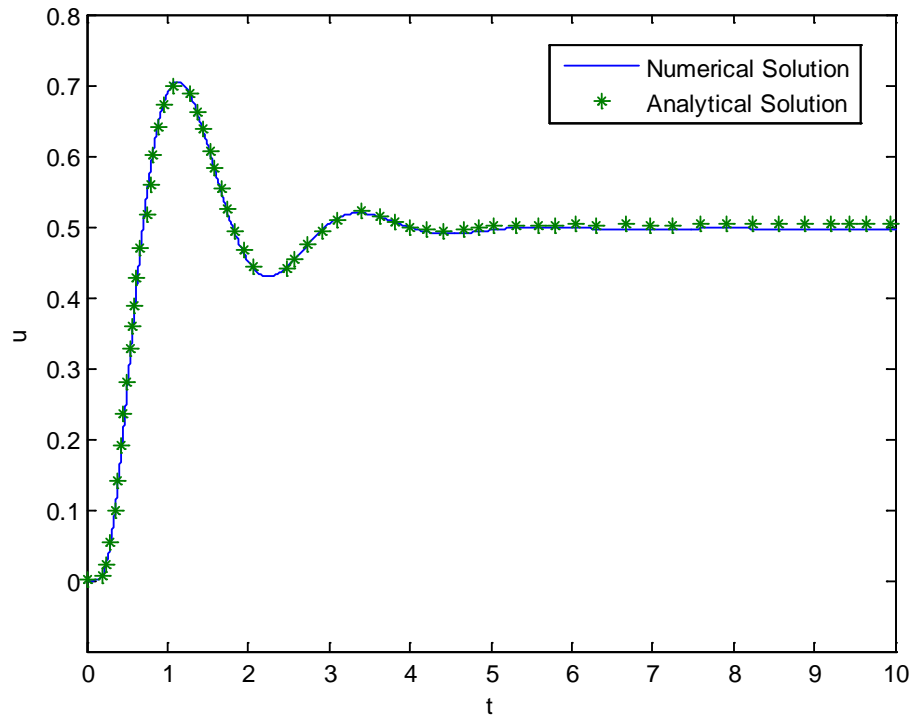


Figure 5.24. Oldroyd-B Fluid, TPS-RBF solution, for $y = 0.5$, $N = 101$, $dt = 0.001$,
 $m = 4$, $E = 1$

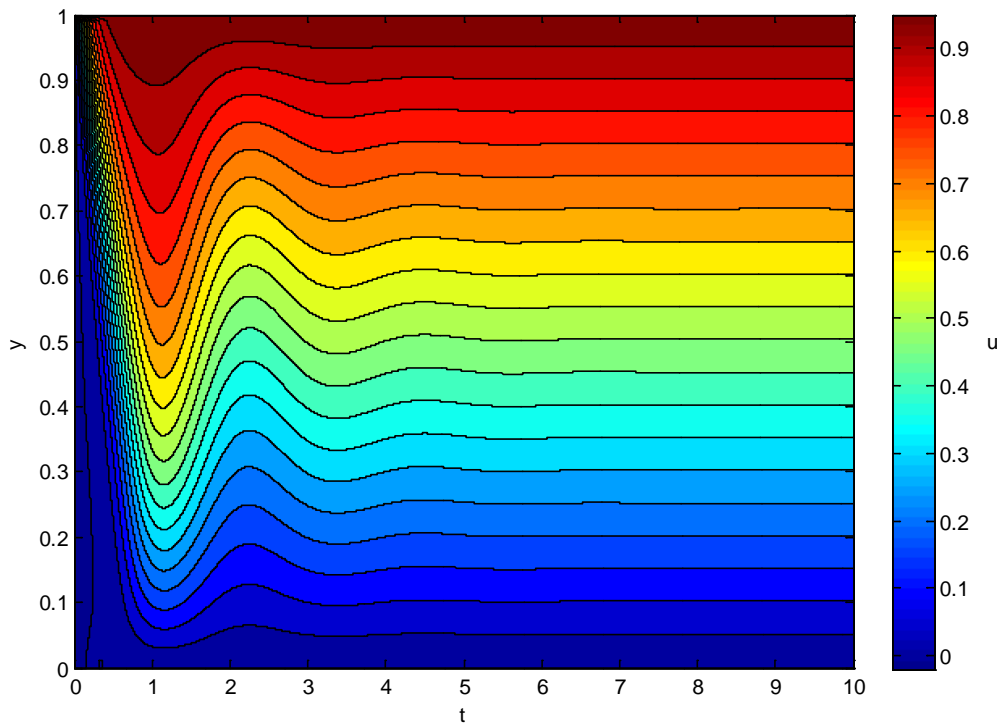


Figure 5.25 Time and spatial evolution of u , $N = 101$, $m = 4$

In Figures 5.23 and 5.25, time and spatial evolutions of velocity profiles are shown. The number of nodes used and the order of thin-plate spline are given below the figure. The analytical solutions are taken from the related papers using Data Analysis program and the data has been matched to the numerical solution. The numerical results are in good agreement with analytical results. It has shown that this meshless radial basis function collocation method is still providing very good accuracy and robustness for viscoelastic equations governing Upper-Convected Maxwell fluid model and Oldroyd-B fluid model.

6. CONCLUSION

In the present study, an application of the meshless radial basis functions method to the advection-diffusion and viscoelastic fluid problem is demonstrated. Numerical experiments show that this meshless method has many advantages over traditional methods.

Meshless methods do not require mesh generation which is a cumbersome work and need to be done carefully. Severe interaction problems between meshes may occur. Distorsion of the mesh may cause serious obstacles in solution of the problems. Obviously, meshless methods have an advantage. Nodes are assigned to the related domain and radial basis functions are defined radially between the nodes. Radial basis functions method is based on the collocation scheme. The approximation function is the product of radial basis functions with unknown coefficients.

We approximated to the solution with pure approximation functions, say, without augmentation except thin-plate spline solution for Oldroyd-B fluid. At every time, coefficients vary and have different values. Time vector is multiplied by system matrix. As far as the system matrix is considered, this has elements which the distances are calculated radially between the all nodes on the domain. This gives an $N \times N$ matrix. For example, the first row of the matrix possesses values of distances which are calculated with respect to the first numbered node. The others are determined using assigned nodes with the same logic. The most important thing is to construct the elements of the system matrix carefully for which node is related to which boundary conditions such as Dirichlet, Neumann or Robin.

After the coefficient matrix for geometry and numbers in vector for time space are prepared, the right side of the equation has to be assigned with respect to the initial and boudary conditions. The unknown coefficients for every time can then be completed easily. Once these are found, the values of the dependent variables may be copmleted.

As we can see from the procedure above, this meshless method has great advantages of being dimension independent. Coding is easy, only assigning the boundary conditions is a delicate work. Inversion of the coefficient matrix is important to consider. Mostly the singularity of the so-called matrix may be overcome with an addition of a polynomial term, adaptive node method or by applying symmetric version of the method called the symmetric collocation method.

Multiquadrics and thin-plate spline radial basis functions were used. Multiquadrics have a free-parameter and thin-plate spline has parameter-free feature. The accuracy of the multiquadric approximation is adjusted with the parameter called shape parameter. The MQ-RBF is purely geometric. But from the tables 5.1, 5.2, 5.3 and 5.4, the optimum shape parameter varies according to number of nodes and time step. For the linear advection-diffusion problem and one dimensional time dependent Burgers' equation, we obtain shape parameter optimization curves for specific time steps. The optimum shape parameter is determined for minimum RMS error. The shape parameter variations for different number of nodes and time differences are also tabulated. It can be observed that the RMS error and the solution accuracy of the problem are affected by those parameters. RMS error decreases when the number of nodes increase. But it does not mean there is less or more error difference in comparison with the thin-plate spline approximation, because it differs from one problem to another.

It is observed that the thin-plate spline functions are more sensitive to the number of nodes. It does not include a free parameter like multiquadrics. But it shows stability in small time step sizes. The order of thin-plate splines are investigated from first order to fourth. We can't obtain any results for the first order say $r^2 \ln r$ and fourth order $r^8 \ln r$ most of the time. Whereas the first order TPS favors a sparser node distribution, the higher order splines favor dense node distribution. But $r^4 \ln r$ and $r^6 \ln r$ have always been more reliable than the others. They provide stable solutions and non-singular coefficient matrices. Singularity may be overcome with augmented approximation using additional polynomial terms. It has claimed by Karur [20] that the augmented form results in a slight decrease in the error.

When multiquadrics and thin-plate spline function approximations are compared, we can not attain an accurate judgement. For some solution of problems, MQ-RBF gives less error in comparison with the TPS-RBF solutions, for some TPS-RBF provides less error. This can be thought to be due to the nature of the partial differential equation. Errors may vary according to the domination of advection/diffusion terms or nonlinearity nature.

If we consider the viscoelastic fluid problems, some obstacles are encountered during the numerical solution. The need for second order time integration diverted us to handle with the Houbolt method. Houbolt method has reliability and robustness for the integration. It gives satisfactory results with the curves obtained in the related papers. At the beginning, adjusting the initial vector causes problems in the solution of the problem, then we amortize the shock input effect. Finally more accurate results similar to the solution given in the papers are obtained.

To sum up, all observations and investigations done throughout the study, it can be inferred that the meshless radial basis functions collocation method is quite easy to code and very convenient to implement both linear and nonlinear type of partial differential equations. In addition to all advantages of radial basis functions collocation method, the most important side is that this method is entirely information based method. How much information you have about the nodes on the domain, you will obtain more accurate and reliable results. With this method, you can easily find value of a function that you haven't assign an coefficient to be determined using interpolation property of approximation function. The advantage of being dimension independent and only being in conjunction with regular or irregular node distribution may render the method possible to apply everywhere in science and engineering problems. The efficiency increases when the method is applied to high dimension of problems. I hope the method will become more widespread and popular in the following years with more possible investigations.

The CPU times may give an insight about run time of the codes. These calculations are done with HP workstation having a random 8 GB random access memory including dual core. It is quite fast and simple to obtain the results and MATLAB programming was used in this study.

Table 6.1. CPU times of the problems

Problems	RBF Type	N	Time Step	RMS Error	CPU Time
The Linear Advection-Diffusion Equation in 1-D	MQ	81	0.01	0.00007878	10.818 s
The Linear Advection-Diffusion Equation in 1-D	TPS	81	0.01	0.000083804	11.528 s
The Burgers' Equation in 1-D	MQ	81	0.0001	0.00052135	23.745 s
The Burgers' Equation in 1-D	TPS	81	0.0001	0.00067592	241.121 s
The Nonlinear Advection-Diffusion Equation in 1-D	MQ	264	0.04	0.000009647	2114.358 s
The UCM Fluid Model	MQ	101	0.001	0.07184	10.293 s
The UCM Fluid Model	TPS	51	0.0025	0.09342	1.087 s
The Oldroyd-B Fluid Model	TPS	101	0.001	0.00564	11.077 s
The Linear Advection-Diffusion Equation in 2-D	MQ	121	0.0001	0.00000092563	6.554 s
The Linear Advection-Diffusion Equation in 2-D	TPS	121	0.0001	0.00002334	5.404 s
The Burgers' Equation in 2-D	MQ	121	0.005	0.00086575	9.259 s
The Burgers' Equation in 2-D	MQ	441	0.005	0.00049388	310.118 s
The Burgers' Equation in 2-D	TPS	121	0.005	0.0278	310.198 s

APPENDIX A : SOLUTION PROCEDURE

A.1. Construction of the Coefficient Matrix

Radial Basis Functions Collocation Method approximates to a solution by a linear combination of radial basis functions. It does not require any connectivity between the nodes or the collocation points since it's a truly meshless method. Using uniformly distributed or scattered data points approximation is a great advantage of this method. We can describe the approximation as following ;

$$u_i^b = \phi_{ij} \cdot \lambda_j^b \quad (\text{A.1})$$

Here ϕ_{ij} refers to radial basis function, i and j denotes the entire number of collocation points, so we can derive that this means the distances between every nodes can be defined using this radially expressed functions which are truly smooth and infinitely differentiable shown in table. And b is used to denote at which time step the procedure undergoes. It facilitates the work ,so we can easily obtain the curves using the time step at what time we need to.

For instance, we will scatter the data points uniformly, Δx is equal between two nodes, and also time will march with Δt time difference. N is the number of collocation points, obviously ; $i=1,2,3,\dots,N, j=1,2,3,\dots,N, t_i = \text{initial time}, t_f = \text{final time}, T: \text{number of time steps}, T = (t_f - t_i) / \Delta t + 1$. So, $b=1,2,3,\dots,T$. The following matrices show in an explicit way in the solution procedure. For $b=1$, generally expresses the initial condition for $t=0.s$

For $b = 1$,

$$\begin{bmatrix} \phi_{11} & \phi_{12} & \cdot & \cdot & \cdot & \phi_{1N} \\ \phi_{21} & \phi_{22} & \cdot & \cdot & & \\ \cdot & & & & & \\ \cdot & & & & & \\ \cdot & & & & & \\ \phi_{N1} & \cdot & \cdot & \cdot & & \phi_{NN} \end{bmatrix} \begin{bmatrix} \lambda_1^1 \\ \lambda_2^1 \\ \lambda_3^1 \\ \cdot \\ \cdot \\ \lambda_N^1 \end{bmatrix} = \begin{bmatrix} u_1^1 \\ u_2^1 \\ \cdot \\ \cdot \\ \cdot \\ u_N^1 \end{bmatrix} \quad (\text{A.2})$$

For $b = 2$,

$$\begin{bmatrix} \phi_{11} & \phi_{12} & \cdot & \cdot & \cdot & \phi_{1N} \\ \phi_{21} & \phi_{22} & \cdot & \cdot & & \\ \cdot & & & & & \\ \cdot & & & & & \\ \cdot & & & & & \\ \phi_{N1} & \cdot & \cdot & \cdot & & \phi_{NN} \end{bmatrix} \begin{bmatrix} \lambda_1^2 \\ \lambda_2^2 \\ \lambda_3^2 \\ \cdot \\ \cdot \\ \lambda_N^2 \end{bmatrix} = \begin{bmatrix} u_1^2 \\ u_2^2 \\ \cdot \\ \cdot \\ \cdot \\ u_N^2 \end{bmatrix} \quad (\text{A.3})$$

For $b = 3$,

$$\begin{bmatrix} \phi_{11} & \phi_{12} & \cdot & \cdot & \cdot & \phi_{1N} \\ \phi_{21} & \phi_{22} & \cdot & \cdot & & \\ \cdot & & & & & \\ \cdot & & & & & \\ \cdot & & & & & \\ \phi_{N1} & \cdot & \cdot & \cdot & & \phi_{NN} \end{bmatrix} \begin{bmatrix} \lambda_1^3 \\ \lambda_2^3 \\ \lambda_3^3 \\ \cdot \\ \cdot \\ \lambda_N^3 \end{bmatrix} = \begin{bmatrix} u_1^3 \\ u_2^3 \\ \cdot \\ \cdot \\ \cdot \\ u_N^3 \end{bmatrix} \quad (\text{A.4})$$

For $b = T$,

$$\begin{bmatrix} \phi_{11} & \phi_{12} & \cdot & \cdot & \cdot & \phi_{1N} \\ \phi_{21} & \phi_{22} & \cdot & \cdot & & \\ \cdot & & & & & \\ \cdot & & & & & \\ \cdot & & & & & \\ \phi_{N1} & \cdot & \cdot & \cdot & & \phi_{NN} \end{bmatrix} \begin{bmatrix} \lambda_1^T \\ \lambda_2^T \\ \lambda_3^T \\ \cdot \\ \cdot \\ \lambda_N^T \end{bmatrix} = \begin{bmatrix} u_1^T \\ u_2^T \\ \cdot \\ \cdot \\ \cdot \\ u_N^T \end{bmatrix} \quad (\text{A.5})$$

In the governing equation, the approximation function is also suited to its space and time derivatives to construct the system matrix involving the boundary conditions and the initial conditions.

$$(u_x)_i^b = \phi_{ij}^x \cdot \lambda_j^b \quad (\text{A.6})$$

For $b = 1$, generally expresses the initial condition for $t=0$.

$$\begin{bmatrix} \phi_{11}^x & \phi_{12}^x & \cdot & \cdot & \cdot & \phi_{1N}^x \\ \phi_{21}^x & \phi_{22}^x & \cdot & \cdot & & \\ \cdot & & & & & \\ \cdot & & & & & \\ \cdot & & & & & \\ \phi_{N1}^x & \cdot & \cdot & \cdot & & \phi_{NN}^x \end{bmatrix} \begin{bmatrix} \lambda_1^1 \\ \lambda_2^1 \\ \lambda_3^1 \\ \cdot \\ \cdot \\ \lambda_N^1 \end{bmatrix} = \begin{bmatrix} (u_x)_1^1 \\ (u_x)_2^1 \\ \cdot \\ \cdot \\ \cdot \\ (u_x)_N^1 \end{bmatrix} \quad (\text{A.7})$$

For $b = 2$,

$$\begin{bmatrix} \phi_{11}^x & \phi_{12}^x & \cdot & \cdot & \cdot & \phi_{1N}^x \\ \phi_{21}^x & \phi_{22}^x & \cdot & \cdot & \cdot & \cdot \\ \cdot & \cdot & \cdot & \cdot & \cdot & \cdot \\ \cdot & \cdot & \cdot & \cdot & \cdot & \cdot \\ \phi_{N1}^x & \cdot & \cdot & \cdot & \cdot & \phi_{NN}^x \end{bmatrix} \begin{bmatrix} \lambda_1^2 \\ \lambda_2^2 \\ \lambda_3^2 \\ \cdot \\ \cdot \\ \lambda_N^2 \end{bmatrix} = \begin{bmatrix} (u_x)_1^2 \\ (u_x)_2^2 \\ \cdot \\ \cdot \\ \cdot \\ (u_x)_N^2 \end{bmatrix} \quad (\text{A.8})$$

For $b = 3$,

$$\begin{bmatrix} \phi_{11}^x & \phi_{12}^x & \cdot & \cdot & \cdot & \phi_{1N}^x \\ \phi_{21}^x & \phi_{22}^x & \cdot & \cdot & \cdot & \cdot \\ \cdot & \cdot & \cdot & \cdot & \cdot & \cdot \\ \cdot & \cdot & \cdot & \cdot & \cdot & \cdot \\ \phi_{N1}^x & \cdot & \cdot & \cdot & \cdot & \phi_{NN}^x \end{bmatrix} \begin{bmatrix} \lambda_1^3 \\ \lambda_2^3 \\ \lambda_3^2 \\ \cdot \\ \cdot \\ \lambda_N^3 \end{bmatrix} = \begin{bmatrix} (u_x)_1^3 \\ (u_x)_2^3 \\ \cdot \\ \cdot \\ \cdot \\ (u_x)_N^3 \end{bmatrix} \quad (\text{A.9})$$

For $b = T$,

$$\begin{bmatrix} \phi_{11}^x & \phi_{12}^x & \cdot & \cdot & \cdot & \phi_{1N}^x \\ \phi_{21}^x & \phi_{22}^x & \cdot & \cdot & \cdot & \cdot \\ \cdot & \cdot & \cdot & \cdot & \cdot & \cdot \\ \cdot & \cdot & \cdot & \cdot & \cdot & \cdot \\ \phi_{N1}^x & \cdot & \cdot & \cdot & \cdot & \phi_{NN}^x \end{bmatrix} \begin{bmatrix} \lambda_1^T \\ \lambda_2^T \\ \lambda_3^T \\ \cdot \\ \cdot \\ \lambda_N^T \end{bmatrix} = \begin{bmatrix} (u_x)_1^T \\ (u_x)_2^T \\ \cdot \\ \cdot \\ \cdot \\ (u_x)_N^T \end{bmatrix} \quad (\text{A.10})$$

Second derivative of approximation function,

$$(u_{xx})_i^b = \phi_{ij}^{xx} \cdot \lambda_j^b \quad (\text{A.11})$$

For $b=1$,

$$\begin{bmatrix} \phi_{11}^{xx} & \phi_{12}^{xx} & \cdot & \cdot & \cdot & \phi_{1N}^{xx} \\ \phi_{21}^{xx} & \phi_{22}^{xx} & \cdot & \cdot & \cdot & \cdot \\ \cdot & \cdot & \cdot & \cdot & \cdot & \cdot \\ \cdot & \cdot & \cdot & \cdot & \cdot & \cdot \\ \phi_{N1}^{xx} & \cdot & \cdot & \cdot & \cdot & \phi_{NN}^{xx} \end{bmatrix} \begin{bmatrix} \lambda_1^1 \\ \lambda_2^1 \\ \lambda_3^1 \\ \cdot \\ \cdot \\ \lambda_N^1 \end{bmatrix} = \begin{bmatrix} (u_{xx})_1^1 \\ (u_{xx})_2^1 \\ \cdot \\ \cdot \\ \cdot \\ (u_{xx})_N^1 \end{bmatrix} \quad (\text{A.12})$$

For $b = 2$,

$$\begin{bmatrix} \phi_{11}^{xx} & \phi_{12}^{xx} & \cdot & \cdot & \cdot & \phi_{1N}^{xx} \\ \phi_{21}^{xx} & \phi_{22}^{xx} & \cdot & \cdot & \cdot & \cdot \\ \cdot & \cdot & \cdot & \cdot & \cdot & \cdot \\ \cdot & \cdot & \cdot & \cdot & \cdot & \cdot \\ \phi_{N1}^{xx} & \cdot & \cdot & \cdot & \cdot & \phi_{NN}^{xx} \end{bmatrix} \begin{bmatrix} \lambda_1^2 \\ \lambda_2^2 \\ \lambda_3^2 \\ \cdot \\ \cdot \\ \lambda_N^2 \end{bmatrix} = \begin{bmatrix} (u_{xx})_1^2 \\ (u_{xx})_2^2 \\ \cdot \\ \cdot \\ \cdot \\ (u_{xx})_N^2 \end{bmatrix} \quad (\text{A.13})$$

For $b = 3$,

$$\begin{bmatrix} \phi_{11}^{xx} & \phi_{12}^{xx} & \cdot & \cdot & \cdot & \phi_{1N}^{xx} \\ \phi_{21}^{xx} & \phi_{22}^{xx} & \cdot & \cdot & \cdot & \cdot \\ \cdot & \cdot & \cdot & \cdot & \cdot & \cdot \\ \cdot & \cdot & \cdot & \cdot & \cdot & \cdot \\ \phi_{N1}^{xx} & \cdot & \cdot & \cdot & \cdot & \phi_{NN}^{xx} \end{bmatrix} \begin{bmatrix} \lambda_1^3 \\ \lambda_2^3 \\ \lambda_3^3 \\ \cdot \\ \cdot \\ \lambda_N^3 \end{bmatrix} = \begin{bmatrix} (u_{xx})_1^3 \\ (u_{xx})_2^3 \\ \cdot \\ \cdot \\ \cdot \\ (u_{xx})_N^3 \end{bmatrix} \quad (\text{A.14})$$

For $b=T$,

$$\begin{bmatrix} \phi^{xx}_{11} & \phi^{xx}_{12} & \cdot & \cdot & \cdot & \phi^{xx}_{1N} \\ \phi^{xx}_{21} & \phi^{xx}_{22} & \cdot & \cdot & & \\ \cdot & & & & & \\ \cdot & & & & & \\ \cdot & & & & & \\ \phi^{xx}_{N1} & \cdot & \cdot & \cdot & \cdot & \phi^{xx}_{NN} \end{bmatrix} \begin{bmatrix} \lambda_1^T \\ \lambda_2^T \\ \lambda_3^T \\ \cdot \\ \cdot \\ \lambda_N^T \end{bmatrix} = \begin{bmatrix} (u_{xx})_1^T \\ (u_{xx})_2^T \\ \cdot \\ \cdot \\ \cdot \\ (u_{xx})_N^T \end{bmatrix} \tag{A.15}$$

In one dimensional case ;

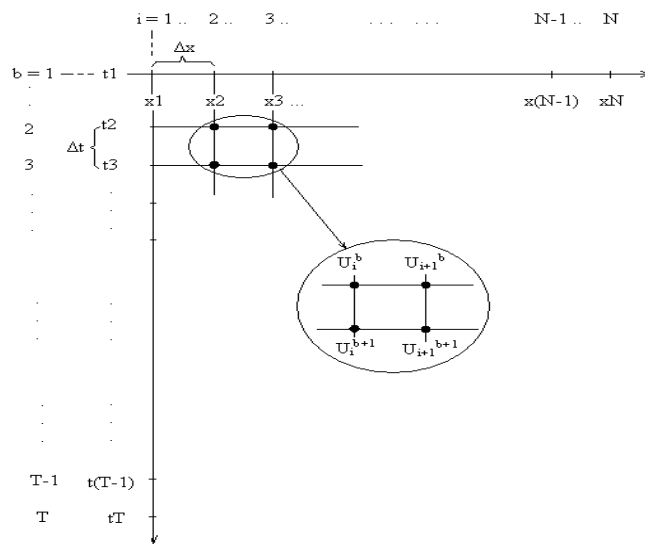


Figure A.1. One Dimensional Domain - Space and Time

Boundary Conditions ;

$$\begin{aligned}
 x=x_i ; t > 0 \quad u(x_i,t) &= u_b \\
 x=x_f ; t > 0 \quad u(x_f,t) &= u_f
 \end{aligned}$$

Here u_b and u_f are the functions defined on the boundary . In vector notation; the left side of the domain,

$$\begin{aligned}
\phi_{11} \cdot \lambda_1^1 + \phi_{12} \cdot \lambda_2^1 + \phi_{13} \cdot \lambda_3^1 + \dots + \phi_{1N} \cdot \lambda_N^1 &= u_1^1 \\
\phi_{11} \cdot \lambda_1^2 + \phi_{12} \cdot \lambda_2^2 + \phi_{13} \cdot \lambda_3^2 + \dots + \phi_{1N} \cdot \lambda_N^2 &= u_1^2 \\
\phi_{11} \cdot \lambda_1^3 + \phi_{12} \cdot \lambda_2^3 + \phi_{13} \cdot \lambda_3^3 + \dots + \phi_{1N} \cdot \lambda_N^3 &= u_1^3 \\
&\cdot \\
&\cdot \\
&\cdot \\
\phi_{11} \cdot \lambda_1^T + \phi_{12} \cdot \lambda_2^T + \phi_{13} \cdot \lambda_3^T + \dots + \phi_{1N} \cdot \lambda_N^T &= u_1^T
\end{aligned}$$

The right side of the domain,

$$\begin{aligned}
\phi_{N1} \cdot \lambda_1^1 + \phi_{N2} \cdot \lambda_2^1 + \phi_{N3} \cdot \lambda_3^1 + \dots + \phi_{NN} \cdot \lambda_N^1 &= u_N^1 \\
\phi_{N1} \cdot \lambda_1^2 + \phi_{N2} \cdot \lambda_2^2 + \phi_{N3} \cdot \lambda_3^2 + \dots + \phi_{NN} \cdot \lambda_N^2 &= u_N^2 \\
\phi_{N1} \cdot \lambda_1^3 + \phi_{N2} \cdot \lambda_2^3 + \phi_{N3} \cdot \lambda_3^3 + \dots + \phi_{NN} \cdot \lambda_N^3 &= u_N^3 \\
&\cdot \\
&\cdot \\
&\cdot \\
\phi_{N1} \cdot \lambda_1^T + \phi_{N2} \cdot \lambda_2^T + \phi_{N3} \cdot \lambda_3^T + \dots + \phi_{NN} \cdot \lambda_N^T &= u_N^T
\end{aligned}$$

If there exists any boundary conditions in derivatives of the function, the coefficient matrices should be obtained like the procedure above.

Let's now write the first time derivate of the approximation function, here λ pulls the effect of time derivations on itself. So,

$$(u_t)_i^b = \phi_{ij} \cdot (\lambda_j^t)^b \quad (\text{A.16})$$

Initial conditions are given to start a time marching procedure with a convenient method chosen according to easy implementation or efficiency for accurate solution.

A.2. Obtaining The System of Matrix

Governing equations are valid on entire domain and collocation points. Using governing equations and boundary conditions every information, except initial conditions or relations involving time derivatives, should be put in a general matrix form. So we can understand that the coefficient matrix of the general system of matrix is constant, we proceed and calculate the λ or u unknown values according to right hand side vector of the system of matrix. It is very simple since the coefficient matrix is constant, it means that it defines this meshless methods only take into consideration node arrangement in/over the domain. As time marches we calculate the unknown values using the right hand side vectors involving the known values from the governing equations and boundary conditions.

APPENDIX B: DERIVATION OF GOVERNING EQUATIONS FOR UPPER-CONVECTED MAXWELL AND OLDROYD-B FLUID MODEL

From the reference paper [54] in order to compare centerline velocity profile results using the basic equations, we should derive a partial differential equation for the velocity field. For this unidirectional flow, the equation of motion simplifies to following equation,

$$\rho \frac{\partial U}{\partial t} = -\frac{\partial \tau_{xy}}{\partial y} \quad (\text{B.1})$$

in which U and τ_{xy} are the velocity in the x-direction and the shear stress respectively. The constitutive equations used in the study are the single mode UCM (Upper-Convected Maxwell) and the Oldroyd-B models. The total stress can be expressed as a superposition of N quasi-linear modes,

$$\tau = \sum_{i=1}^N \tau_i \quad (\text{B.2})$$

where N is the number of modes. The relationship between stress and strain rate for each mode can be described by;

$$\tau_i + \lambda_i \tau_i^\nabla = -\eta_i (A + \lambda_{2i} A^\nabla) \quad (\text{B.3})$$

Here A is the rate of strain tensor, and A^∇ is the upper-convected time derivative of a tensor,

$$A^\nabla = \frac{D}{Dt} A - (\nabla \mathbf{v})^T \cdot A - A \cdot (\nabla \mathbf{v}) \quad (\text{B.4})$$

where $D(\cdot)/Dt$ is known substantial or material derivative and defined,

$$\frac{D(\cdot)}{Dt} = \frac{\partial(\cdot)}{\partial t} + \mathbf{U} \cdot \nabla(\cdot) \quad (\text{B.5})$$

where ∇ is the gradient operator,

$$\nabla = \mathbf{i} \frac{\partial}{\partial x} + \mathbf{j} \frac{\partial}{\partial y} + \mathbf{k} \frac{\partial}{\partial z} \quad (\text{B.6})$$

and rate of strain tensor A is equal to,

$$A \equiv \frac{1}{2} [\nabla \mathbf{U} + (\nabla \mathbf{U})^T] \quad (\text{B.7})$$

In Equation (B.3), η_i is the viscosity, λ_{1i} and λ_{2i} are the relaxation and the retardation time of each mode. If λ_{2i} is set to zero then one obtains the multimode version of UCM model while if it is not zero the multimode version of the Oldroyd-B model is obtained. Given that the velocity $\mathbf{U}=\mathbf{U}(y,t)$ which is in x-direction, the stress tensor can be written as,

$$\boldsymbol{\tau} = \sum_{i=1}^N \tau_i = - \sum_{i=1}^N \frac{\eta_i (1 + \lambda_{2i} P)}{(1 + \lambda_{1i} P)} A \quad (\text{B.8})$$

where P is the upper-convected differential operator. For one mode $N=1$,

$$\boldsymbol{\tau} = \tau_1 = - \frac{\eta_1 (1 + \lambda_{21} P)}{(1 + \lambda_{11} P)} A \quad (\text{B.9})$$

and the equation becomes for mode one,

$$\tau_1 + \lambda_{11} P \tau_1 = -\eta_1 (A + \lambda_{21} P A) \quad (\text{B.10})$$

The stress constitutive equations can be easily derived from the notations given in the appendix in the paper [54], then once the stress equations are found in Equation (B.7) and (B.8) the expression for the shear stress is substituted into the equation of motion (B.1) resulting in a partial differential equation for the velocity field as Equation (B.9),

$$\Lambda_0 \tau_{xy} + \Lambda_1 \frac{\partial \tau_{xy}}{\partial t} = - \left(K_1 \dot{\gamma}_{xy} + K_2 \frac{\partial \dot{\gamma}_{xy}}{\partial t} \right) \quad (\text{B.11})$$

$$\Lambda_0 \tau_{xx} + \Lambda_1 \frac{\partial \tau_{xx}}{\partial t} = 2K_2 \dot{\gamma}_{xy}^2 + 2\Lambda_1 \dot{\gamma}_{xy} \tau_{xy} \quad (\text{B.12})$$

$$\left\{ \sum_{i=1}^{N+1} K_i \frac{\partial^{(i-1)}}{\partial t^{(i-1)}} \right\} \frac{\partial^2 U}{\partial y^2} - \rho \left\{ \sum_{i=0}^N \Lambda_i \frac{\partial^{(i+1)}}{\partial t^{(i+1)}} \right\} U = 0 \quad (\text{B.13})$$

where K_i and Λ_i are constants which depend on η_i , λ_{1i} , λ_{2i} and N is the number of modes. The provided expressions for K_i and Λ_i are directly taken from the appendix of the paper [54].

For mode one,

$$K_1 = \eta_1 / K_2 = \eta_1 \lambda_{21} / \Lambda_0 = 1 / \Lambda_1 = \lambda_{11} \quad (\text{B.14})$$

If we construct the Equation (B.10) for mode one, $N = 1$

$$\left\{ \sum_{i=1}^2 K_i \frac{\partial^{(i-1)}}{\partial t^{(i-1)}} \right\} \frac{\partial^2 U}{\partial y^2} - \rho \left\{ \sum_{i=0}^1 \Lambda_i \frac{\partial^{(i+1)}}{\partial t^{(i+1)}} \right\} U = 0 \quad (\text{B.15})$$

$$\left\{ K_1 \frac{\partial^{(0)}}{\partial t^{(0)}} + K_2 \frac{\partial}{\partial t} \right\} \frac{\partial^2 U}{\partial y^2} - \rho \left\{ \Lambda_0 \frac{\partial}{\partial t} + \Lambda_1 \frac{\partial^2}{\partial t^2} \right\} U = 0 \quad (\text{B.16})$$

$$K_1 \frac{\partial^2 U}{\partial y^2} + K_2 \frac{\partial}{\partial t} \left(\frac{\partial^2 U}{\partial y^2} \right) - \rho \Lambda_0 \frac{\partial U}{\partial t} - \rho \Lambda_1 \frac{\partial^2 U}{\partial t^2} = 0 \quad (\text{B.17})$$

Let's substitute the expressions for K_i and Λ_i into the Equation (B.11),

$$\eta_1 \frac{\partial^2 U}{\partial y^2} + \eta_1 \lambda_{21} \frac{\partial}{\partial t} \left(\frac{\partial^2 U}{\partial y^2} \right) - \rho \frac{\partial U}{\partial t} - \rho \lambda_{11} \frac{\partial^2 U}{\partial t^2} = 0 \quad (\text{B.18})$$

This is the general equation governing both UCM and the Oldroyd-B fluid flow model. If we set to $\lambda_{21} = 0$ then UCM model is obtained otherwise the Oldroyd-B model is obtained.

Upper-Convected Maxwell Model - Mode 1

Setting $\lambda_{21} = 0$, the additional criteria used are equivalence of shear and normal stress at steady state which result in the following constraints when selecting a viscosity and relaxation time spectra,

$$\eta_0 = \sum_{i=1}^N \eta_i \quad (\text{B.19})$$

$$\eta_0 \lambda_0 = \sum_{i=1}^N \eta_i \lambda_i \quad (\text{B.20})$$

where η_0 and λ_0 are the viscosity and the relaxation time for the 1-mode Maxwell model and N is the number of modes.

$$\eta_1 \frac{\partial^2 U}{\partial y^2} - \rho \frac{\partial U}{\partial t} - \rho \lambda_{11} \frac{\partial^2 U}{\partial t^2} = 0 \quad (\text{B.21})$$

if $N=1$,

$$\eta_0 = \eta_1 \quad (\text{B.22})$$

$$\eta_0 \lambda_0 = \eta_1 \lambda_{11} \quad (\text{B.23})$$

so it is found that,

$$\lambda_0 = \lambda_{11} \quad (\text{B.24})$$

Substituting into the Equation (B.13),

$$\eta_0 \frac{\partial^2 U}{\partial y^2} - \rho \frac{\partial U}{\partial t} - \rho \lambda_0 \frac{\partial^2 U}{\partial t^2} = 0 \quad (\text{B.25})$$

We nondimensionalize using,

$$U^* = \frac{U}{V_0}, \quad y^* = \frac{y}{h}, \quad t^* = \frac{t}{(h/V_0)} \quad (\text{B.26})$$

We assign U^* , y^* and t^* as the dimensionless velocity, distance and the time respectively. Curves will be obtained using dimensionless scales.

$$U = V_0 U^*, \quad y = h y^*, \quad t = \frac{h}{V_0} t^* \quad (\text{B.27})$$

$$\eta_0 \frac{\partial^2 (V_0 U^*)}{\partial (h y^*)^2} - \rho \frac{\partial (V_0 U^*)}{\partial \left(\frac{h}{V_0} t^* \right)} - \rho \lambda_0 \frac{\partial^2 (V_0 U^*)}{\partial \left(\frac{h}{V_0} t^* \right)^2} = 0 \quad (\text{B.28})$$

$$\frac{V_0 \eta_0}{h^2} \frac{\partial^2 (U^*)}{\partial (y^*)^2} - \frac{\rho V_0^2}{h} \frac{\partial (U^*)}{\partial (t^*)} - \frac{\rho \lambda_0 V_0^3}{h^2} \frac{\partial^2 (U^*)}{\partial (t^*)^2} = 0 \quad (\text{B.29})$$

if we multiply the last equation by $\frac{h}{V_0^2 \rho}$,

$$\frac{\eta_0}{V_0 \rho h} \frac{\partial^2 (U^*)}{\partial (y^*)^2} - \frac{\partial (U^*)}{\partial (t^*)} - \frac{\lambda_0 V_0}{h} \frac{\partial^2 (U^*)}{\partial (t^*)^2} = 0 \quad (\text{B.30})$$

Dimensionless Numbers are,

$$\text{Weissenberg number,} \quad We = \frac{\lambda_0 V_0}{h} \quad (\text{B.31})$$

$$\text{Reynolds number,} \quad Re = \frac{\rho V_0 h}{\eta_0} \quad (\text{B.32})$$

Since we are considering inertial viscoelastic flows the elasticity number can be conveniently used to analyze the results. This dimensionless group can be defined,

$$\text{Elasticity number,} \quad E = \frac{We}{Re} = \frac{\lambda_0 \eta_0}{\rho h^2} \quad (\text{B.33})$$

Finally, the governing equation becomes from Equation (B.15),

$$\frac{1}{Re} \frac{\partial^2(U^*)}{\partial(y^*)^2} - \frac{\partial(U^*)}{\partial(t^*)} - We \frac{\partial^2(U^*)}{\partial(t^*)^2} = 0 \quad (\text{B.34})$$

multiplying the Equation (B.16) by We ,

$$E \frac{\partial^2(U^*)}{\partial(y^*)^2} - We \frac{\partial(U^*)}{\partial(t^*)} - We^2 \frac{\partial^2(U^*)}{\partial(t^*)^2} = 0 \quad (\text{B.35})$$

and getting rid of the notations for nondimensional variables, the equation becomes

$$E \frac{\partial^2 U}{\partial y^2} - We \frac{\partial U}{\partial t} - We^2 \frac{\partial^2 U}{\partial t^2} = 0 \quad (\text{B.36})$$

Oldroyd-B Fluid Model - Mode 1

Setting $\lambda_{21} \neq 0$,

The additional criteria used are equivalence of shear and normal stress at steady state which result in the following constraints when selecting a viscosity and relaxation time spectra, for Oldroyd-B fluid,

$$\eta_0 = \sum_{i=1}^N \eta_i \quad (\text{B.37})$$

$$\eta_0 \lambda_0 = \eta_1 (\lambda_{11} - \lambda_{21}) \quad (\text{B.38})$$

where η_0 and λ_0 are the viscosity and the relaxation time for the 1-mode Maxwell model and N is the number of modes.

$$\eta_1 \frac{\partial^2 U}{\partial y^2} + \eta_1 \lambda_{21} \frac{\partial}{\partial t} \left(\frac{\partial^2 U}{\partial y^2} \right) - \rho \frac{\partial U}{\partial t} - \rho \lambda_{11} \frac{\partial^2 U}{\partial t^2} = 0 \quad (\text{B.39})$$

for $N=1$,

$$\eta_0 = \eta_1 \quad (\text{B.40})$$

so it is found that,

$$\lambda_0 = \lambda_{11} - \lambda_{21} \quad (\text{B.41})$$

An equivalent Oldroyd-B model is obtained by setting

$$\lambda_{11} = 1.125 \lambda_0 \quad (\text{B.42})$$

$$\lambda_{21} = 0.125\lambda_0 \quad (\text{B.43})$$

and putting them into the Equation (B.18),

$$\eta_0 \frac{\partial^2 U}{\partial y^2} + 0.125\lambda_0 \eta_0 \frac{\partial}{\partial t} \left(\frac{\partial^2 U}{\partial y^2} \right) - \rho \frac{\partial U}{\partial t} - 1.125\lambda_0 \rho \frac{\partial^2 U}{\partial t^2} = 0 \quad (\text{B.44})$$

Nondimensionalizing,

$$U^* = \frac{U}{V_0}, \quad y^* = \frac{y}{h}, \quad t^* = \frac{t}{(h/V_0)} \quad (\text{B.45})$$

we assign U^* , y^* and t^* as the dimensionless velocity, distance and the time respectively.

Curves will be obtained using dimensionless scales.

$$U = V_0 U^*, \quad y = h y^*, \quad t = \frac{h}{V_0} t^* \quad (\text{B.46})$$

$$\eta_0 \frac{\partial^2 (V_0 U^*)}{\partial (h y^*)^2} + 0.125\eta_0 \lambda_0 \frac{\partial}{\partial \left(\frac{h}{V_0} t^* \right)} \left(\frac{\partial^2 (V_0 U^*)}{\partial (h y^*)^2} \right) - \rho \frac{\partial (V_0 U^*)}{\partial \left(\frac{h}{V_0} t^* \right)} - 1.125\rho \lambda_0 \frac{\partial^2 (V_0 U^*)}{\partial \left(\frac{h}{V_0} t^* \right)^2} = 0 \quad (\text{B.47})$$

$$\frac{\eta_0 V_0}{h^2} \frac{\partial^2 (U^*)}{\partial (y^*)^2} + \frac{0.125\eta_0 \lambda_0 V_0^2}{h^3} \frac{\partial}{\partial (t^*)} \frac{\partial^2 (U^*)}{\partial (y^*)^2} - \frac{V_0^2}{h} \rho \frac{\partial (U^*)}{\partial (t^*)} - \frac{1.125\rho \lambda_0 V_0^3}{h^2} \frac{\partial^2 (U^*)}{\partial (t^*)^2} = 0 \quad (\text{B.48})$$

if we multiply the last equation by $\frac{h^2}{V_0 \eta_0}$,

$$\frac{\partial^2 (U^*)}{\partial (y^*)^2} + \frac{0.125\lambda_0 V_0}{h} \frac{\partial}{\partial (t^*)} \left(\frac{\partial^2 (U^*)}{\partial (y^*)^2} \right) - \frac{\rho V_0 h}{\eta_0} \frac{\partial (U^*)}{\partial (t^*)} - \frac{1.125\rho \lambda_0 V_0^2}{\eta_0} \frac{\partial^2 (U^*)}{\partial (t^*)^2} = 0 \quad (\text{B.49})$$

Finally, the governing equation becomes from Equation (B.21),

$$\frac{\partial^2(U^*)}{\partial(y^*)^2} + 0.125We \frac{\partial}{\partial(t^*)} \left(\frac{\partial^2(U^*)}{\partial(y^*)^2} \right) - Re \frac{\partial(U^*)}{\partial(t^*)} - 1.125ReWe \frac{\partial^2(U^*)}{\partial(t^*)^2} = 0 \quad (\text{B.50})$$

multiplying the Equation (B.22) by $1/Re$,

$$\frac{1}{Re} \frac{\partial^2(U^*)}{\partial(y^*)^2} + 0.125E \frac{\partial}{\partial(t^*)} \left(\frac{\partial^2(U^*)}{\partial(y^*)^2} \right) - \frac{\partial(U^*)}{\partial(t^*)} - 1.125We \frac{\partial^2(U^*)}{\partial(t^*)^2} = 0 \quad (\text{B.51})$$

and getting rid of the notations for nondimensional variables, the governing equation is obtained as the following.

$$\frac{1}{Re} \frac{\partial^2 U}{\partial y^2} + 0.125E \frac{\partial}{\partial t} \left(\frac{\partial^2 U}{\partial y^2} \right) - \frac{\partial U}{\partial t} - 1.125We \frac{\partial^2 U}{\partial t^2} = 0 \quad (\text{B.52})$$

**APPENDIX C: ADDITIONAL PROBLEMS – THE LINEAR
ADVECTION-DIFFUSION EQUATION IN 2-D AND THE TIME
DEPENDENT BURGERS' EQUATION IN 2-D**

C.1. The Linear Advection-Diffusion Equation in 2-D

This problem presents an application of radial basis functions method to linear advection-diffusion equation in two dimension. In Boztosun's paper [6] only thin-plate spline of functions is investigated and the solutions are compared with the analytical and the finite difference method solutions. The governing equation involves the linear advection-diffusion problem in two dimension as follows,

$$\frac{\partial u}{\partial t} = \kappa_x \frac{\partial^2 u}{\partial x^2} + \kappa_y \frac{\partial^2 u}{\partial y^2} + v_x \frac{\partial u}{\partial x} + v_y \frac{\partial u}{\partial y} \quad (\text{C.1})$$

where u is the temperature at position (x,y) at time t , κ_x and κ_y are the diffusion coefficients and v_x, v_y are the velocity vectors or the advection coefficients which are in x and y direction, respectively. The following gives the Dirichlet Boundary and the Initial Conditions as,

$$u(0, y, t) = a \exp(bt) [1 + \exp(-c_y y)] \quad (\text{C.2})$$

$$u(1, y, t) = a \exp(bt) [\exp(-c_x) + \exp(-c_y y)] \quad (\text{C.3})$$

$$u(x, 0, t) = a \exp(bt) [\exp(-c_x x) + 1] \quad (\text{C.4})$$

$$u(x, 1, t) = a \exp(bt) [\exp(-c_x x) + \exp(-c_y)] \quad (\text{C.5})$$

$$u(x, y, 0) = a \left[\exp(-c_x x) + \exp(-c_y y) \right] \quad (\text{C.6})$$

The analytical solution is given by,

$$u(x, y, t) = a \exp(bt) \left[\exp(-c_x x) + \exp(-c_y y) \right] \quad (\text{C.7})$$

After substitution of the analytical solution to the Governing Equation (C.1), the following equivalentents are obtained for c_x and c_y ,

$$c_x = \frac{v_x + \sqrt{v_x^2 + 4b\kappa_x}}{2\kappa_x} \quad \text{and} \quad c_y = \frac{v_y + \sqrt{v_y^2 + 4b\kappa_y}}{2\kappa_y} \quad (\text{C.8})$$

The domain of the problem will be on $0 \leq x \leq 1$, $0 \leq y \leq 1$ and the time interval tested is $0 \leq t \leq 1$. The constants are $a = 100$, $b = 0.2$, $\kappa_x = 1.4$, $\kappa_y = 1.7$, $v_x = 1$ and $v_y = 1$. It can be found from the given constants $c_x = 0.8771507$ and $c_y = 0.7459497$. This problem is considered for different number of nodes, such as $N = 36$, 121 , 441 and 676 . For each time step sizes, a new shape parameter has been found which satisfies minimum RMS error at time $t = 1$ s. Thin-plate spline solutions are again investigated from the first order to fourth order. Those solutions for multiquadric and thin-plate splines functions are given on the tables C.1 and C.2.

Table C.1. MQ-RBF Solution of Problem, RMS errors

Problem C.1					
RBF	Features of RBF optimum "c" or order of the TPS	Number of Nodes	Time Step	Time	RMS error
MQ	c = 2.06	36	0.001	t = 1 s	8,7226E-07
	c = 1.9		0.0001	t = 1 s	1,2746E-06
	c = 0.62	121	0.001	t = 1 s	6,4868E-07
	c = 0.68		0.0005	t = 1 s	3,8899E-07
	c = 0.68		0.0001	t = 1 s	9,2563E-07
	c = 0.25	441	0.0002	t = 1 s	1,8024E-07
	c = 0.25		0.0001	t = 1 s	5,2769E-07
	c = 0.18	676	0.0001	t = 1 s	1,2724E-07

Table C.2. TPS-RBF Solution of Problem, RMS errors

Problem C.1					
RBF	Features of RBF optimum "c" or order of the TPS	Number of Nodes	Time Step	Time	RMS error
TPS	m = 2	36	0.001	t = 1 s	*
	m = 4		0.001	t = 1 s	9,3369E-04
	m = 6		0.001	t = 1 s	3,4000E-03
	m = 8		0.001	t = 1 s	*
	m = 2	121	0.001	t = 1 s	*
	m = 4		0.0001	t = 1 s	2,3340E-05
	m = 6		0.0001	t = 1 s	7,3342E-05
	m = 8		0.0001	t = 1 s	1,3615E-04
	m = 2	441	0.0001	t = 1 s	*
	m = 4		0.0001	t = 1 s	1,0337E-06
	m = 6		0.0001	t = 1 s	6,9802E-07
	m = 8		0.0001	t = 1 s	*
	m = 2	676	0.0001	t = 1 s	*
	m = 4		0.0001	t = 1 s	3,6076E-07
	m = 6		0.0001	t = 1 s	6,9209E-06
	m = 8		0.0001	t = 1 s	*

C.2. The Time Dependent Burgers' Equation in 2-D

Apart from the one dimensional test case time dependent Burgers's equation given in the fourth chapter, it can be useful to validate the radial basis functions method in two dimensional nonlinear problem. From Jichun's paper [16], the governing equation for time dependent Burgers' equation in two dimension is taken as,

$$\frac{\partial u}{\partial t} = \alpha \left(\frac{\partial^2 u}{\partial x^2} + \frac{\partial^2 u}{\partial y^2} \right) - \left(u \frac{\partial u}{\partial x} + u \frac{\partial u}{\partial y} \right) \quad (\text{C.9})$$

And the analytical solution is given as the following,

$$u(x, y, t) = \frac{1}{1 + \exp\left(\frac{x + y - t}{2\alpha}\right)} \quad (\text{C.10})$$

The Boundary and the Initial Conditions will be obtained from the given analytical solution (C.10). The domain in two dimension can be chosen as which the intervals are,

$$0 \leq x \leq 1 \text{ and } 0 \leq y \leq 1 \quad (\text{C.11})$$

and α is given as $\alpha = 0.05$, the time will be between $0 \leq t \leq 1.25$ s with different time steps as shown in the table. This nonlinear problem is solved for different number of nodes on the domain and time step sizes. For each time step sizes, the optimum shape parameter is evaluated which provides the minimum RMS error at time $t = 1.25$ s. Again all RMS errors are tabulated in the tables for different number of nodes, shape parameters and time step sizes.

For thin-plate spline solutions, different order of spline functions are tried to investigate RMS errors. It has been checked for several time step sizes in order to get approximate solutions. The star sign "*" in the boxes means no solution with pure thin-plate spline approximation is obtained. It can be interpreted as the coefficient matrix becomes singular or very close to singular for that node density and time difference. If

such a thing has been encountered, the methods for reducing the ill-conditioning of the coefficient matrix must be resorted to as partially explained in the chapter three.

Table C.3. MQ-RBF Solution of Problem, RMS errors

Problem C.2					
RBF	Features of RBF optimum "c" or order of the TPS	Number of Nodes	Time Step	Time	RMS error
MQ	c = 0.14	9	0.05	t = 1.25 s	3,1900E-02
	c = 0.16		0.001	t = 1.25 s	2,6900E-02
	c = 0.3	36	0.005	t = 1.25 s	1,9000E-03
	c = 0.37		0.001	t = 1.25 s	1,2000E-03
	c = 0.08	121	0.01	t = 1.25 s	1,8550E-03
	c = 0.1		0.005	t = 1.25 s	8,6575E-04
	c = 0.18		0.001	t = 1.25 s	1,6947E-04
	c = 0.3	441	0.005	t = 1.25 s	4,9388E-04
	c = 0.06		0.001	t = 1.25 s	8,8304E-05
	c = 0.16	676	0.005	t = 1.25 s	4,5080E-04
	c = 0.04		0.001	t = 1.25 s	7,6887E-05

Table C.4. TPS-RBF Solution of Problem, RMS errors

Problem C.2					
RBF	Features of RBF optimum "c" or order of the TPS	Number of Nodes	Time Step	Time	RMS error
TPS	m = 2	36	0.005	t = 1.25 s	*
	m = 4		0.005	t = 1.25 s	1,9000E-03
	m = 6		0.005	t = 1.25 s	8,2000E-03
	m = 8		0.005	t = 1.25 s	*
	m = 2	121	0.005	t = 1.25 s	*
	m = 4		0.005	t = 1.25 s	2,7800E-02
	m = 6		0.005	t = 1.25 s	1,1000E-03
	m = 8		0.005	t = 1.25 s	5,5000E-03
	m = 2	441	0.005	t = 1.25 s	*
	m = 4		0.005	t = 1.25 s	4,4616E-04
	m = 6		0.005	t = 1.25 s	5,7199E-04
	m = 8		0.005	t = 1.25 s	*
	m = 2	676	0.005	t = 1.25 s	*
	m = 4		0.005	t = 1.25 s	*
	m = 6		0.005	t = 1.25 s	2,6000E-03
	m = 8		0.001	t = 1.25 s	*

REFERENCES

1. Jianyu, L., L. Siwei, Q. Yingjian and H. Yaping, "Numerical Solution of Elliptic Partial Differential Equation by Growing Radial Basis Function Neural Networks", Proceedings of the International Joint Conference on Neural Networks 2003, Vol.1, pp. 85-90, Northern Jiatong University, China, 2003
2. Chinchapatnam, P.P., K. Djidjeli and P.B. Nair , "Domain Decomposition For Time-Dependent Problems Using Radial Based Meshless Methods", Inc. Numerical Methods in Partial Differential Equations, Vol.23, pp. 38-59, University of Southampton, U.K., 2006
3. Gomez, J.A.M., P.G. Casanova and G.G. Rodriguez , "Domain Decomposition by Radial Basis Functions for Time Dependent Partial Differential Equations", Proceedings of the IASTED International Conference on Advances in Computer Science and Technology, pp.105-109, 2006
4. Lui, Y., Z. Xin and M. Lu, "A meshless method based on least-squares approach for steady- and unsteady-state heat conduction problems", An International Journal of Computation and Methodology - Numerical Heat Transfer, Part B, Fundamentals, Vol. 47:3, pp. 257-275, Tsinghua University, 2005
5. Chantasiriwan, S., "Multiquadric Collocation Method for Time-Dependent Heat Conduction Problems with Temperature-Dependent Thermal Properties", Journal of Heat Transfer, Vol. 129, No. 2, pp. 109-113, February 2007
6. Boztosun, I., A. Charafi, M. Zerroukat and K. Djidjeli, "Thin-Plate Spline Radial Basis Function Scheme for Advection-Diffusion Problems", Electronic Journals of Boundary Elements ,Vol. Beteq , No.2, pp. 267-282, 2002
7. Shu, C., H. Ding and K.S. Yeo, "Solution of partial differential equations by a global radial basis function-based differential quadrature method", Engineering Analysis with Boundary Elements, Vol. 28, No. 10, pp. 1217-26, Singapore, 2004

8. Sarra, S.A., "Adaptive radial basis function methods for time dependent partial differential equations", *Applied Numerical Mathematics*, Vol. 54, No.1, pp. 79-94, June 2005, Marshall University, Huntington, 2004
9. Williams, H.A. and E. Jensen, "Two-Dimensional Nonlinear Advection-Diffusion in a Model of Surfactant Spreading on a Thin Liquid Film", *Journal of Applied Mathematics*, Vol. 66, pp. 55-82, University of Cambridge, 2000
10. Soroushian, A. and J. Farjoodi, "A unified starting procedure for the Houbolt method", *Communications in Numerical Methods in Engineering*, Vol.23, pp. 1-13, Iran, 2006
11. Fasshauer, G.E., "Solving Partial Differential Equations by Collocation with Radial Basis Functions", Northwestern University, Evanston, 1996
12. Li, Q., "Effects of Adaptive Discretization on Numerical Computation using Meshless Method with Live-object Handling Applications", Ph.D. Thesis, Georgia Institute of Technology, 2007
13. Li, J., C.S. Chen and D. Pepper, "Meshfree method for groundwater modeling", University of Nevada, USA
14. Li, J. and C.S. Chen, "Some Observations on Unsymmetric Radial Basis Function Collocation Methods for Convection-Diffusion Problems", Vol. 57, pp. 1085-1094, University of Nevada, Las Vegas, USA, 2002
15. Perko, J., B. Sarler and G. Kuhn, "Natural Convection in Porous Media - a meshless solution of the Brinkman extended Darcy model", *Proc. Appl. Math. Mech.*, Vol. 2, pp. 511-512, Slovenia, 2003
16. Hon, Y.C., K. Cheung, X.Z. Mao and E.J.Kansa , "Multiquadric Solution for Shallow Water Equations", *Journal of Hydraulic Engineering*, 1999

17. Singh, I.V., "Application of meshless EFG method in fluid flow problems", *Sadhana*, Vol. 29, Part 3, pp. 285–296., Birla Institute of Technology and Science, India, 2004
18. Chen, W., "Symmetric boundary knot method", Simula Research Laboratory, Norway, 2002
19. E.J. Kansa, "Multiquadrics - A Scattered Data Approximation Scheme with Applications to Computational Fluid-Dynamics - Solutions to Parabolic, Hyperbolic and Elliptic Partial Differential Equations", *Computers Math. Applic.*, Vol. 19, No. 8/9, pp. 147-161, 1990
20. Karur, S.R. and P.A. Ramachandran, "Augmented Thin Plate Spline Approximation in DRM", *Boundary Elements Communications*, Vol. 6, No. 2, pp. 55-58, March 1995
21. Wang, J.G. and G.R. Liu, "A Point Interpolation Meshless Method on Radial Basis Function", *International Journal of Numerical Methods In Engineering*, Vol.54, pp.1623-1648, National University of Singapore, Singapore, 2001
22. Munoz-Gomez, J.A., P. Gonzalez and G. Rodriguez, "Adaptive Node Refinement Collocation Method for Partial Differential Equations", *Seventh Mexican International Conference on Computer Science*, Mexico, 2006
23. Heryudono, A. and T. Driscoll, "Adaptive Radial Basis Function Methods with Residual Subsampling Technique for Interpolation and Collocation Problems", *Computers and Mathematics with Applications*, Vol. 53, No. 6, pp. 927-939, March 2007
24. Iske, A. and Martin K., "Two-Phase Flow Simulation by AMMoC, an Adaptive Meshfree Method of Characteristics", University of Leicester, 2005
25. Boztosun, I. and A. Charafi, "An Analysis of the Linear Advection-Diffusion Equation Using Mesh-Free and Mesh-Dependent Methods", *Engineering Analysis with Boundary Elements*, Vol.26, pp. 889-895, 2002

26. Zerroukat, M., K. Djidjeli and A.Charafi, “Explicit and Implicit Meshless Methods for Linear Advection-Diffusion Type Partial Differential Equations”, *International Journal For Numerical Methods in Engineering*, Vol. 48, pp. 19-35, U.K., 2000
27. Li,C., Y.Chen and D. Pepper, “Radial Basis Function Method for 1-D and 2-D Groundwater Contaminant Transport Modelling”, *Computational Mechanics*, Vol. 32, pp. 10-15, Las Vegas, USA, 2003
28. David, I., “A New Linearization Technique of the Advection-Diffusion Equation for Modelling free-Phase Napl Spreading in Groundwater”, *Geophysical Research Abstracts*, Vol.7, European Geosciences Union, 2005
29. Thiffeault, J.L. ,“Advection–Diffusion in Lagrangian Coordinates”, *Physics Letters A*, Vol. 309, No. 5-6, pp. 415-22, New York , 31 March 2003
30. Chantasiriwan, S. , “Cartesian grid methods using radial basis functions for solving Poisson, Helmholtz, and diffusion–convection equations”, *Engineering Analysis with Boundary Elements*, Vol. 28, No. 12, pp. 1417-1425, Thailand, 2004
31. Hernandez, J.A., “High-order Finite Volume Schemes For the Advection-Diffusion Equations”, *International Journal For Numerical Methods in Engineering*, Vol. 53, pp. 1211-1234, Madrid, Spain, 2001
32. Wan, X., D. Xiu and G. Karniadakis, “Stochastic Solutions for the Two-Dimensional Advection-Diffusion Equation”, *Society for Industrial and Applied Mathematics*, Vol.26, No. 2, pp. 578-590, Brown University, 2004
33. Zhang, L., *Runge-Kutta-Chebyshev Methods for Advection-Diffusion-Reaction Problems*, M.S.Thesis in Numerical Analysis, Stockholm, Sweden, 2004
34. Hundsdorfer, W.H., *Numerical Solution of Advection-Diffusion-Reaction Equations*, Department of Numerical Mathematics, Lecture Notes, Amsterdam, Netherlands, 1996

35. Mehra, M. and B.V. Kumar, "Time-accurate Solution of Advection-Diffusion Problems by wavelet - Taylor-Galerkin Method", *Communications in Numerical Methods in Engineering*, Vol. 21, pp. 313-326, Kanpur, India, 2005
36. Chen, W., "Analytical solution of transient scalar wave and diffusion problems of arbitrary dimensionality and geometry by RBF wavelet series", University of Oslo, Norway, 2002
37. Lastdrager, B., B. Koren and J.G. Verwer, "Solution of Time-Dependent Advection-Diffusion Problems with Sparse-Grid Combination Technique and a Rosenbrock Solver, Modelling, Analysis and Simulation", research report with The Netherlands Organization for Scientific Research (NOW), Amsterdam, Netherlands, 2000
38. Lesnic, D., "The Decomposition Method for Cauchy Advection-Diffusion Problems", *An International Journal of Computers and Mathematics with Applications*, Vol. 49, pp. 525-537, University of Leeds, U.K., 2005
39. James, T., *Numerical Solution of Advection-Diffusion Equations for Radial Flow*, M.S. Thesis, Wedham College, University of Oxford, 2002
40. Hon, Y.C. and W. Chen, "Boundary knot method for 2D and 3D Helmholtz and convection-diffusion problems under complicated geometry", City University of Hong Kong, China
41. Xin, L., "Radial point collocation method (RPCM) for solving convection-diffusion problems", *Journal of Zhejiang University Science A*, Vol. 6, pp. 1061-1067, Zhejiang University, China, 2006
42. Tadmor, E., "High Resolution Methods for Time Dependent Problems with Piecewise Smooth Solutions", *ICM*, Vol. 3, pp. 1-3, 2002

43. Ferreira, A.J.M., P.A.L.S. Martins and C.M.C. Roque, "Solving Time-Dependent Engineering Problems with Multiquadrics", *Journal of Sound and Vibration*, Vol. 280, pp. 595-610, Portugal, 2005
44. Larsson, E. and Fornberg, B., "A Numerical Study of some Radial Basis Function based Solution Methods for Elliptic PDEs", Uppsala University, Sweden, 2003
45. Börekçi ,O., *The Radial Basis Function Collocation Method: A Meshless Method for the Solution of Boundary Value Problems*, Department of Civil Engineering, Lecture notes, Boğaziçi University, 2005
46. Iske, A., "Radial Basis Functions:Basics, Advanced Topics and Meshfree Methods for Transport Problems", *Rem. Sem. Mat. University Pol. Torino*, Vol. 63, Lecture notes from workshop *Spline Functions and Radial Functions*, University of Turin, 2003
47. Ellero, M. and R.I. Tanner, "SPH simulations of transient viscoelastic flows at low Reynolds Number", *J. Non-Newtonian Fluid Mech.*, Vol. 132, pp. 61-72, Australia, 2005
48. Kansa E.J. and Hon Y.C., "Circumventing the Ill-Conditioning Problem with Multiquadric Radial Basis Functions: Applications to Elliptic Partial Differential Equations", *Computers and Mathematics with Applications*, Vol. 39, pp. 123-137, 2000
49. Hornberger and Wiberg, "Numerical Methods for Solving First-Order Ordinary Differential Equations", notes, *Numerical Methods in the Hydrological Sciences*, 2005
50. Fetecau, C., Corina Fetecau, "Decay of a potential vortex in an Oldroyd-B fluid", *International Journal of Engineering Science*, Vol. 43, pp. 340-351, Technical University of Iasi, Romaina, 2005
51. Boger, D.V., and K. Walters, "Experimental dilemmas in non-Newtonian fluid mechanics and their theoretical resolution", *Korea-Australia Rheology Journal*, Vol. 12, No. 1, pp. 27-38, 2000

52. Beraudo, C., and A. Fortin, "A finite element method for computing the flow of multi-mode viscoelastic fluids: comparison with experiments", *J. Non-Newtonian Fluid Mech.*, Vol. 75, pp. 1–23, 1998
53. Doa, C. and F.T. Pinho, "Fully-Developed Pipe and Planar Flows of Multimode Viscoelastic Fluids", *J. Non-Newtonian Fluid Mech.*, Vol. 141, pp. 85–98, 2006
54. Damasky, P.A.S. and B. Khomami, "A Note on Start-up and Large Amplitude Oscillatory Shear Flow of Multimode Viscoelastic Fluids", *Rheologica Acta*, Vol. 35, No. 3, pp. 211-224, 1995
55. Lancaster, P. and Salkauskas K., "Surfaces generated by moving least squares methods", *Mathematics of Computation*, Vol. 37, pp.141-158, 1981
56. T. Belytschko, Y.Y. Lu and L. Gu, "Element-Free Galerkin Methods," *International Journal for Numerical Methods in Engineering*, Vol. 37, pp. 229-256, 1994
57. R.L. Hardy, "Multiquadric equations of topography and other irregular surfaces", *Journal of Geophys. Res.*, Vol. 76, pp. 1905-1915, 1971
58. Buhmann, M.D., *Radial Basis Functions – Theory and Implementations*, Cambridge University Press, Cambridge, UK, 2003
59. Trebotich, D., P. Colella, G. Miller and D. Liepmann, "A Numerical Model of Viscoelastic Flow in Microchannels", Lawrence Livermore National Laboratory, University of California, 2002
60. Somfai, E., A.N. Morozov and W.v. Saarloos, "Modeling viscoelastic flow with discrete methods", *Elsevier Science*, Lieden University, Netherlands, 2006
61. Tran-Cong, T., N. Mai-Duy and N. Phan-Thien, "BEM-RBF approach for viscoelastic flow analysis", *Engineering Analysis with Boundary Elements*, Vol. 26, pp. 757-762, Australia, 2002

62. Tan, W. and T. Masuoka, "Stokes' First Problem for an Oldroyd-B fluid in a porous half space", *Physics of Fluids*, Vol. 17, pp. 023101/1-7, Japan, 2005

63. Hosseini, S.M., M.T. Manzari and S.K. Hannani, "A fully explicit three-step SPH algorithm for simulation of Non-Newtonian fluid flow", *International Journal of Numerical Methods for Heat and Fluid Flow*, Vol. 17, No.7, pp. 715-735, Iran, 2006

64. Tran-Canh, D. and T. Tran-Cong, "Computation of viscoelastic flow using neural networks and stochastic simulation", *Korea-Australia Rheology Journal*, Vol. 14, No. 4, pp. 161-174, Australia, 2002